EXPERIMENTAL AND NUMERICAL INVESTIGATIONS ON EFFICACY OF SINGLY CURVED THIN PIEZO TRANSDUCERS FOR ENERGY HARVESTING AND STRUCTURAL HEALTH MONITORING

ALEENA V K

DEPARTMENT OF CIVIL ENGINEERING
INDIAN INSTITUTE OF TECHNOLOGY DELHI (IIT DELHI)

JUNE 2022

EXPERIMENTAL AND NUMERICAL INVESTIGATIONS ON EFFICACY OF SINGLY CURVED THIN PIEZO TRANSDUCERS FOR ENERGY HARVESTING AND STRUCTURAL HEALTH MONITORING

Submitted in partial fulfilment of the requirement of the award of the degree of

MASTER OF TECHNOLOGY

in

STRUCTURAL ENGINEERING

Submitted by

ALEENA V K
(2020CES7581)

Under the guidance of

Prof. Suresh Bhalla
&
Dr Naveet Kaur, Scientist, CSIR-CRRI

DEPARTMENT OF CIVIL ENGINEERING

INDIAN INSTITUTE OF TECHNOLOGY DELHI (IIT DELHI)

JUNE 2022

DEDICATED TO MY FAMILY AND FRIENDS

CERTIFICATE

This is to certify that the thesis entitled **"EXPERIMENTAL AND NUMERICAL INVESTIGATIONS ON EFFICACY OF SINGLY CURVED THIN PIEZO TRANSDUCERS FOR ENERGY HARVESTING AND STRUCTURAL HEALTH MONITORING"** is a bonafide record of the research work carried out by **ALEENA V K** towards the partial fulfilment of the requirements for the degree of **MASTER OF TECHNOLOGY** in **STRUCTURAL ENGINEERING**. She had worked under our supervision and guidance at the **INDIAN INSTITUTE OF TECHNOLOGY DELHI**. The thesis has not been submitted in part or full to any other Institution or University for the award of any degree.

Prof. SURESH BHALLA
Professor
IIT Delhi

Dr NAVEET KAUR
Scientist
CSIR-Central Road Research Institute

June 2022
New Delhi

ACKNOWLEDGEMENTS

I would like to express my immense gratitude to my supervisor **Prof. Suresh Bhalla** for his invaluable supervision, inspiration, and unconditional support throughout my life at IIT Delhi. I've benefited greatly from your wealth of knowledge and meticulous guidance. I would also like to extend my sincere gratitude to **Dr Naveet Kaur** for all her guidance throughout my thesis work. You've always lent me a hand whenever I lost myself at the crossroads of my research.

I would like to gratify all the faculty members of the **Structural Engineering** program for giving me an insight into various fields of structural engineering.

I would also like to thank the staff of **Smart Structures and Dynamics Laboratory (SSDL)** for their kind help and cooperation throughout the project.

I am indebted to my parents, my in-laws and my husband for continuous motivation and understanding of my work life. I am thankful to my friends and batchmates who have willingly helped me out with their abilities.

ALEENA V K

(2020CES7581)

Department of Civil Engineering

Indian Institute of Technology (IIT DELHI)

ABSTRACT

Structural health monitoring (SHM) is an advancing engineering field that integrates leading sensor technologies with brilliant scientific codes to assess the state of "health" of structures, thereby improving their durability and performance in the safest manner. It is invariably accompanied by the installation of several sensors and other electronic gadgets that demand power throughout their life cycle. Therefore, it is time to think about energy harvesting methods to run these devices. Kaur and Bhalla, (2015) proposed that the same piezoelectric ceramic (PZT) material in a specific form can be utilised for both SHM and harvesting the power required for running the sensors.

Piezoelectric materials have now secured a significant position in the fields of SHM and energy harvesting. These materials are available in several forms and configurations, but their efficacy in these realms for most of the unconventional configurations is still unexplored. The study aims at analysing the potential of the singly curved configuration of thin piezo transducers in the fields of energy harvesting and SHM. Several experimental investigations have been conducted on an RC beam embedded with a concrete vibration sensor (CVS), the straight piezo transducer, and a concrete vibration energy harvester (CVEH), the curved piezo transducer at the mid-span. The study includes the analysis of open-circuit voltage generated across the piezo transducers, the power achieved under impedance matching conditions and the capability of power storage into capacitors for both the configurations. The CVEH is found to generate 1.6 times higher voltage and around 10 times higher power than the CVS when excited at one-third and one-fourth of the span respectively. The CVEH could harvest energy at the rates of 5.42 μW and 8.65 μW corresponding to 3.82 μW and 5.14 μW of CVS for average mid-point accelerations of 4.9 m/s^2 and 8.8 m/s^2 respectively, proving that the CVEH can store an average of 55% higher power than the CVS.

The research also experimentally scrutinises the improved damage detection capability of the curved piezo transducers (originally conceived for energy harvesting only) over the straight configurations by the method of the electro-mechanical impedance (EMI) technique. The beam is electrically excited at two frequency ranges, 1 kHz to 1000 kHz and 100 kHz to 300 kHz. The former range of frequencies provided more reliable results than the latter range. The root mean square deviation (RMSD) with respect to baseline signature is calculated after each damage and is found to have a maximum value after the

second damage. The RMSD indices of conductance and susceptance signatures after second damage are found to be 77% and 91% respectively for CVEH, whereas they have reduced to 33% and 37% respectively for CVS when excited at a frequency range of 1 kHz to 1000 kHz. The experimental results clearly prove the suitability of curved piezo transducers for structural health monitoring.

In order to analyse the various parameters of CVEH for energy harvesting, 3-D models of the RC beam with curved piezo transducers embedded inside are developed and analysed using commercially available finite element (FE) software, COMSOL Multiphysics version 4.4, MEMS module. It is found that the transducer with a sector angle of 145 degrees has the maximum voltage generation capability, with 1.6 times the output of the straight transducer. It has maximum efficiency when placed towards the top or bottom surface of the beam cross-section. An increase in the thickness of the patch is also found to have a positive impact on voltage generation.

As a preliminary step towards the analytical analysis of curved piezo transducers for energy harvesting, a 2-D skeletal analytical model of an RC beam embedded with a curved piezo transducer is developed by formulating a MATLAB code based on the direct stiffness approach. The effect of the curvature and thickness of the transducer is also analysed and compared with the findings of the numerical investigations. The optimum curvature as per the analytical model is 196 degrees, while the 3-D numerical model predicts it as 145 degrees. Also, contrary to the numerical investigation results, the thickness of the curved transducer is found to have barely any effect on the terminal voltage generated across it. This is because the 3-D effects of the structure and strain variation across the thickness of the transducer are not considered in the analytical model where each element is considered as a 1-D element. Hence, it is recommended to extend the research to 3-D analytical models.

In a nutshell, the results of the experimental and numerical investigations summarise the suitability of singly curved thin piezo transducers embedded in RC structures for energy harvesting and SHM.

TABLE OF CONTENTS

LIST OF FIGURES

LIST OF TABLES

LIST OF ACRONYMS

AC	Alternating Current
CC	Pearson Correlation Coefficient
CCD	Correlation Coefficient Deviation
CVEH	Concrete Vibration Energy Harvester
CVS	Concrete Vibration Sensor
DC	Direct Current
EMI	Electro-Mechanical Impedance
FE	Finite Element
FFT	Fast Fourier Transform
FRF	Frequency Response Function
LCR	Inductance(L) Capacitance (C) Resistor (R) (Circuit)
MFC	Macro Fibre Composite
NASA	National Aeronautics and Space Administration
NDT	Non-Destructive Testing
PCR	Piezoelectric Ceramic Rings
PVDF	Polyvinylidene Fluoride
PZT	Lead Zirconate Titanate
RC	Reinforced Concrete
RMSD	Root Mean Square Deviation
SHM	Structural Health Monitoring
SSDL	Smart Structures and Dynamics Laboratory

LIST OF SYMBOLS

a	Distance to the load from the nearest support
b	Distance to the load from the farthest support
B	Breadth
C	Capacitance
C_r	Curvature of the beam
$[C]$	Damping matrix
D	Depth of the beam
D_1, D_2, D_3, D_4	Diodes
D_3	Charge density or electric displacement across the surface normal to axis 3
$\{D\}$	Global displacement vector
d_{31}	Piezoelectric strain coefficient of piezo transducer corresponding to axes 3and 1
$[d^E]$	Coupling matrix
dl	Length of element
E	Modulus of elasticity
E_3	Electric field along axis 3 of piezo transducer
E_T	Total Energy stored in the capacitor
EI	Flexural rigidity
f	Frequency
f_i	Internal force on the i^{th} element
f_n	Natural frequency
$\{f\}$	Internal force vector
F_1	Real part of force vector
F_2	Imaginary part of force vector
$\overline{[F]}$	Complex force vector
g	Acceleration due to gravity
h	Thickness of element
h_p	Thickness of the piezoelectric material

i	Current
I	Moment of inertia
$[K]$	Total stiffness matrix
$[K]_L$	Local stiffness matrix
$[K]_G$	Global stiffness matrix
l	Length of the curved piezo transducer
L	Length
m	Mass per unit length
$[M]$	Mass matrix
n	Sample size
P	Concentrated load
P_{avg}	Average power
P_{CVEH}	Power generated by CVEH
P_{CVS}	Power generated by CVS
Q	Charge
R	Radius of curvature
R_1, R_2	Resistances used in power measuring circuit
S	Strain
S_1	Mechanical strain along axis 1
$[S^E]$	Compliance matrix
T_1	Mechanical stress along axis 1 of the piezo transducer
T_c	Total charging time
$[T]$	Transformation matrix
u	Deflection
$\ddot{u}$	Acceleration
$\overline{[u]}$	Complex displacement vector
u_1	Real part of displacement vector
u_2	Imaginary part of displacement vector
V	Voltage

V_1	Voltage across piezo transducer in power measuring circuit
V_2	Voltage across Resistance R_2 in power measuring circuit
V_c	Output voltage of the rectifier circuit
V_{CVEH}	Voltage generated across the CVEH
V_{CVS}	Voltage generated across the CVS
x_{di}	i^{th} value in the damaged signature
x_{hi}	i^{th} value in the healthy signature
y	Vertical deflection of the beam at any section x
$y_{L/2}$	Vertical deflection of the beam at the centre
Y	Young's modulus of elasticity
$\overline{Y^E}$	Complex Young's modulus of elasticity at a constant electric field
δ_{ES}	Dielectric loss factor
ε_{33}	Electric permittivity of piezo transducer along axis 3
$\overline{\varepsilon_{33}^T}$	Complex electric permittivity of piezo transducer along axis 3 at a constant stress
η	Mechanical loss factor
η_{CE}	Compliance Matrix loss factor
θ	Angle of bend
μ	Dipole moment
μ_r	Poisson's ratio
ξ_{r}	Relative permittivity
ω	Angular frequency
ρ	Density

CHAPTER 1

INTRODUCTION

1.1 BACKGROUND

Structural health monitoring (SHM) is a field of eminent importance and promising potential for copious inventions. Day by day, the cost of preservation and maintenance of our existing structures is a matter of critical concern. SHM has mitigated this by introducing 'as-needed maintenance' instead of the 'scheduled maintenance', thereby saving the cost of inessential or additional maintenance. Damage can be defined as a modification in a system or a structure that can affect its capability to wholly perform its proposed function most safely. SHM expedites the detection or identification of such damages at the earliest feasible event so that necessary remedial measures can be taken to reduce the operational and maintenance cost, failure of a structure, or its components. SHM of large structures is always allied with positioning a wide range of sensors on the structure. Though the quantity of power required to run these sensors is in the micro to milliwatts range, powering these sensors needs further installations using wires or exhaustible batteries, making the whole process more complicated and uneconomical. The idea of energy harvesting plays a prominent role in this scenario.

Energy harvesting or energy scavenging is the process of converting the energy present in natural or man-made sources into usable forms for powering electronic devices or circuits (Beeby et al., 2013). It works on the principle that the ambient energy available in the environment can be converted or harvested in real-time by certain devices and can be used immediately. This reduces the requirement for numerous batteries as the energy needs to be stored only temporarily. It also allows the devices to acquire a lifetime that is theoretically infinite, restrained only by the life span of their constituent units. Piezoelectric energy harvesters are one of the advanced scientific know-how that gratifies the aforesaid demand to a significant extent. It stands at the leading edge among various mechanical energy harvesting techniques by virtue of its high piezoelectric strain coefficients, electro-mechanical coupling factors, etc. in comparison with that of electrostatic/magnetic, thermoelectric, or triboelectric transductions. Thus, the mechanism of piezoelectric energy harvesting is gaining paramount attention among research scholars.

1.2 MOTIVATION

With the advancement of globalisation and modern construction techniques, infrastructural development has witnessed rapid growth across the world. As the economic and social welfares of a country are very well linked to its transportation facilities, a significant rise is evident in the field of transportation infrastructure as well. Bridges, tunnels, flyovers, metro rails, airports, etc. have therefore become the backbone of our economic growth. However, these structures are subjected to either prolonged vibrations or impact forces all through their service life. These vibrations have the potential to deteriorate the structure, leading to its collapse, interruption of services, or even loss of life and property. As a result, the regular maintenance or structural health monitoring of these structures is inevitable. The detrimental vibrations of these structures can further be utilised as a source of energy for powering the electronic devices required for their health monitoring. Piezoelectric materials, which are considered as smart materials, have the ability to function as energy harvesters as well as sensors for SHM. Structural data recorded by these piezo materials can be employed for the monitoring and detection of damage in these structures, and it also offers the flexibility of installing them at inaccessible locations as it eliminates the need for a complex network of wires. Kaur and Bhalla (2015) proposed that the same piezoelectric ceramic (PZT) patches in the form of surface-bonded sensors as well as concrete vibration sensors (CVS) can be utilised for SHM as well as energy harvesting of concrete structures. Nowadays, piezo patches are available in various forms such as macro fibre composites (MFC), DuraAct, quick pack, etc. as well as in various configurations such as disks, plates, rings, tubes, spheres, and so on. However, the potential of various configurations of piezo transducers in the field of SHM and energy harvesting needs to be explored.

1.3 OBJECTIVES AND SCOPE

The primary objective of the research is to evaluate the performance of the single curved configuration of thin piezoelectric transducers relative to their straight configuration in the realm of energy harvesting and SHM. The first focus of the research is to experimentally analyse the relative energy harvesting potential of CVEH (curved configuration) over CVS (straight configuration). The investigations include a comparative study of the terminal voltage, power, and energy generated by the piezo transducers under periodic loadings, and the capability of their power storage into capacitors. Secondly, the study experimentally

scrutinises the effect of the curved configuration of piezo transducers in the field of SHM by using the EMI technique for damage detection.

Thirdly, the research aims at analysing the various parameters of the CVEH that can affect its relative energy harvesting potential through numerical investigations. For this purpose, 3-D models of an RC beam with CVEH and CVS embedded at its mid-span are developed in COMSOL Multiphysics version 4.4 FE software. The parametric study includes the effect of curvature, thickness, and the position of placement of CVEH across the depth of the beam. The study also looks at the impact of model refinement. Finally, the research has also been extended to analytical modelling to study the effects of curved piezo transducers for energy harvesting. The effect of the curvature and thickness of the piezo transducers on energy harvesting as determined by the analytical model is compared with the results of the numerical investigations as well.

1.4 ORGANISATION OF THESIS

The thesis is categorised into six chapters, one of which is the current introduction chapter. Essential figures and tables have been depicted wherever admissible. The essence of each chapter is explained below:

Chapter 1: Introduction

This chapter briefly describes the background and motivation behind the selection of this topic for the thesis followed by the objectives and scope of the work.

Chapter 2: Literature Review

This chapter provides a short description of SHM, piezoelectricity, commercial piezo variants, and so on followed by a detailed literature review on the EMI technique for damage diagnosis in SHM and the advances in piezoelectric energy harvesting.

Chapter 3: Experimental Evaluation of CVEH for Energy Harvesting

This chapter presents the experimental investigations conducted on an RC beam with CVEH and CVS embedded at its mid-span. It includes comparative studies of the terminal voltage, power, and energy generated by CVEH relative to CVS under various loading conditions and the capability of their power storage into capacitors.

Chapter 4: Damage Detection Potential of CVEH for Structural Health Monitoring

This chapter deals with the experimental investigations undertaken to assess the suitability of CVEH for SHM. The chapter provides a comparative study of the damage detection potential of CVEH and CVS using the EMI technique. The effect of the curvature of CVEH on the EMI signatures is also analysed in this chapter.

Chapter 5: Numerical and Analytical Investigations of CVEH for Energy Harvesting

This chapter covers the numerical investigations to analyse the influence of various parameters of CVEH for energy harvesting. 3-D models of CVEH and CVS embedded inside an RC beam are developed in COMSOL Multiphysics version 4.4 FE software. The FE analysis is validated experimentally by conducting an impact hammer test. A detailed parametric study of the curvature, thickness and position of placement of the curved piezo transducer for energy harvesting and the effect of model refinement are covered in this chapter. The chapter also presents the analytical investigations of CVEH for energy harvesting based on the direct stiffness approach. The effect of the curvature and thickness of the curved piezo transducer is also assessed based on the analytical model.

Chapter 6: Conclusions and Future Recommendations

This chapter summarises the major findings of the investigative research and also specifies the recommendations for further investigations in this field.

CHAPTER 2

LITERATURE REVIEW

2.1 INTRODUCTION

Structural health monitoring (SHM) is an advancing technology that couples the foremost sensor technologies with brilliant algorithms to figure out the state of "health" of structures thereby improving their safety, reliability, designated performance, and reducing the life-cycle cost. The past few decades have witnessed an upsurge in the use of piezoelectric materials for damage diagnosis and SHM. Nowadays, more research works are being conducted to determine the potentiality of these piezoelectric materials in energy harvesting. Despite the fact that the piezo patch generates electricity only in the micro to milliwatt range, it can be used to power low-power electronic devices and a variety of wireless sensors. This chapter provides a brief overview of the previous research work in piezoelectric energy harvesting and SHM with a focus on the EMI technique.

2.2 VIBRATION BASED SHM

In the field of SHM, vibration-based methods are gaining traction over static-based methods, which work on the concept that damage will alter the structure's static properties. As a result, a huge quantity of static force is required. Vibration-based SHM, on the other hand, is based on the idea that even minor defects will alter the structure's dynamic properties. Mode shapes, modal strain energy, frequency, structural response, and so on are examples. The structure is deliberately vibrated, and the above-mentioned parameters are recorded using a variety of sensors. Damages can be detected in real-time by carefully analysing their responses. Displacement, velocity, acceleration, strain, and other dynamic structural responses to be measured are chosen based on the specific objectives and monitoring conditions. Accordingly, the market offers a wide range of wireless sensors, including seismometers, velocity transducers, laser displacement sensors, strain gauges and piezoelectric accelerometers.

2.3 GLOBAL AND LOCAL SHM TECHNIQUES

The global and local SHM techniques have their own unique capabilities and drawbacks. In the case of the global SHM technique, the structure under inspection is subjected to low-frequency excitations and the structural response measured by various

sensors is deliberately analysed to obtain the initial modes of vibrations. The analysed values are then compared to those of a healthy structure in order to detect any structural deterioration. Harmonic and impulse excitations are commonly adopted in this technique with harmonic excitations being more precise than the latter. However, from a practical perspective, impulsive excitations are more comfortable (Giurgiutiu and Zagrai, 2002). Frequency response function (FRF) is an extensively used method in global damage detection. A change in the overall structure or a change that affects major portions of the structure is well identified by the method, but it falls behind in detecting the localised damage as it doesn't alter the global parameters significantly (Lin et al., 2014). Owing to that, the requirement of expensive hardware, intensive computations, etc. has led to the development of local SHM techniques which are specifically for the examination of localised parts of the structure.

As the local techniques specifically target the analysis of localised parts of a structure, more accuracy is achieved, with the EMI technique being the most precise one. Most of the non-destructive testing (NDT) methods, such as the ultrasonic pulse velocity method, dye penetration method, acoustic emission method, X-ray analysis, impact echo testing, etc. are the other widely used methods in this category. However, the need to move equipment, fixtures, probes and other items around the test specimen to capture data is a major disadvantage of these approaches, and it sometimes necessitates the removal of finishes, false ceilings and other items. These constraints can be addressed to some extent with the introduction of smart materials and ready-to-cast sensors.

2.4 PIEZOELECTRICITY AND PIEZOELECTRIC MATERIALS

Piezoelectricity, also known as the piezoelectric effect, is the phenomenon of developing an electric potential or voltage across the sides of a crystal when subjected to mechanical stress. It was discovered by Pierre and Paul-Jacques Curie in the year 1880. In Greek, the word *piezo* implies pressure. In short, piezoelectricity means electricity from pressure.

When non-centro symmetric crystals such as Lead Zirconate Titanate (PZT) ($Pb[Zr_xTi_{1-x}]O_3$), Lithium Niobate ($LiNbO_3$), quartz (SiO_2) and others are subjected to mechanical deformations, surface charges are produced due to electric dipoles. These crystals also exhibit the converse effect, in which they become mechanically strained in the

presence of an electric field, as illustrated in Figure 2.1. No dipole moments are induced in centro-symmetric crystals by the action of deformation.

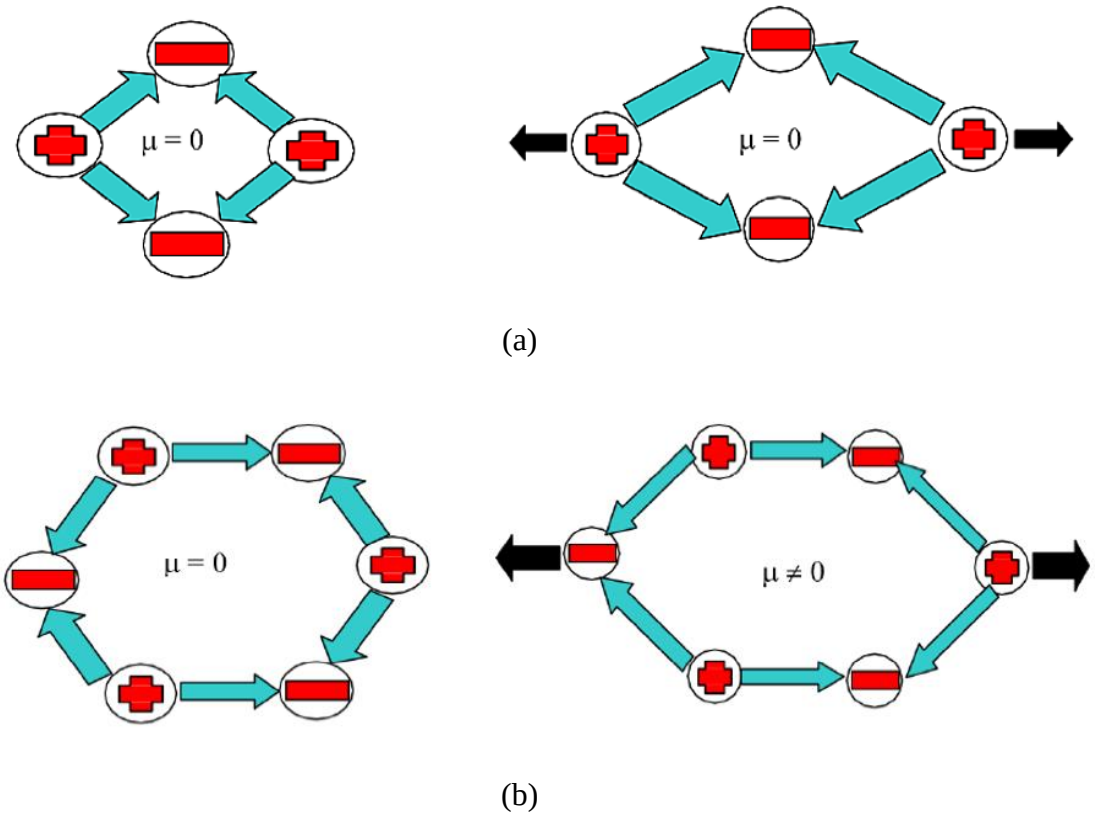

Figure 2.1: (a) Centro-symmetric crystals under deformation (μ = dipole moment) (Bhalla, 2004)

(b) Non centro-symmetric crystals under deformation (μ = dipole moment) (Bhalla, 2004)

2.4.1 Constitutive Relations

Under small field conditions, the constitutive relations for the piezoelectric materials are given by the following equations, where Eq. (2.1) represents the direct effect and Eq. (2.2) represents the converse effect (Bhalla et al., 2017).

$$D_3 = \overline{\varepsilon_{33}^T} E_3 + d_{31} T_1 \tag{2.1}$$

$$S_1 = \frac{T_1}{\overline{Y^E}} + d_{31} T_1 \tag{2.2}$$

where D_3 is the charge density or electric displacement vector in C/m^2, $\overline{\varepsilon_{33}^T}$ is the dynamic electric permittivity under constant or zero stress in F/m, E_3 is the applied external electric field along direction 3 in V/m, d_{31} is the piezoelectric strain coefficient in m/V or C/N, the

subscript 31 coveys that the electric field is applied along direction 3 and the strain is produced along the direction 1. T_1 is the stress tensor applied along direction 1 in N/m^2, S_1 is the strain tensor developed along direction 1 and $\overline{Y^E}$ is the dynamic Young's modulus of elasticity under zero or constant electric field. Figure 2.2 clearly explains the piezoelectric effects of the PZT patch.

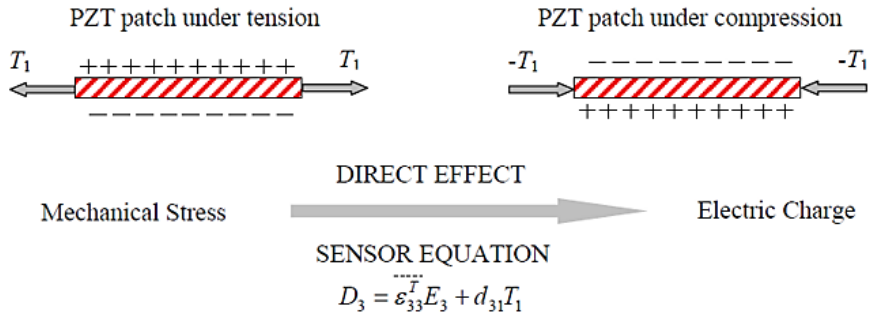

(a)

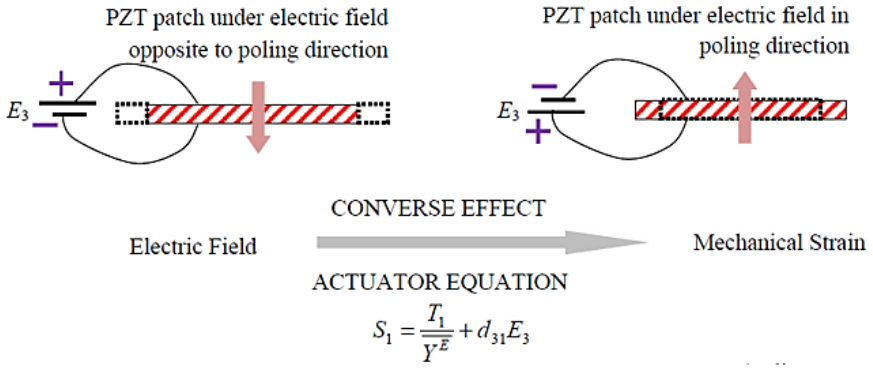

(b)

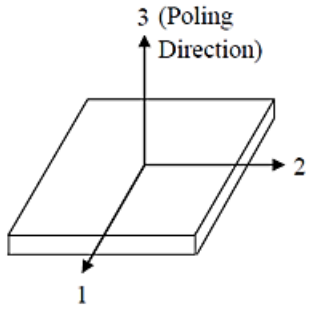

(c)

Figure 2.2: (a) Response of PZT patch under the direct effect (Kaur, 2015)
(b) Response of PZT patch under the converse effect (Kaur, 2015)
(c) Typical coordinate directions of the PZT patch

Based on the direct effect of piezoelectricity, the mechanical strain experienced by the piezoelectric material is related to the terminal voltage (V) developed across them by the following equation (Shanker et al., 2011).

$$V = \left(\frac{d_{31} h_p \overline{Y^E}}{\overline{\varepsilon_{33}^T}} \right) S_1 \tag{2.3}$$

where h_p is the thickness of the piezoelectric material.

2.5 COMMERCIAL PIEZO VARIANTS

Piezoelectric materials are widely available around us. However, for commercial purposes, these are available as piezoceramics and piezopolymers. Nowadays, several other forms of piezoelectric materials are also developed for specific uses. This section provides a brief overview of various piezo variants.

2.5.1 Piezoceramics

Piezoceramics are the most commonly used piezo products, both as sensors and actuators. They are a combination of a modified form of PZT and barium titanate and are generally brittle in nature. However, they are available in a variety of configurations, as shown in Figure 2.3.

Figure 2.3: Various piezoceramic products (PI Ceramic, 2021)

The piezoceramics are classified into ‘soft’ and ‘hard’ categories, based on the mobility of dipoles and their ability to polarise and depolarise. Soft piezoceramics are used for actuator applications that have field strengths with low polarity reversal, i.e., they can be polarised very easily at lower field strengths due to their high domain mobility. Soft PZT patches have high coupling factors, moderate permittivities and high piezoelectric charge

coefficients. High-power acoustic applications utilise hard PZT materials. Apart from high coupling factors and moderate permittivities, hard PZT patches are known for their good stability and high mechanical properties. Currently, lead-free piezoceramics are also available on the market, and are widely used as ultrasonic transducers (PI Ceramic, 2021).

2.5.2 Piezopolymers

Unlike piezoceramics, piezoelectric polymers are mechanically flexible, and can withstand a large amount of strain. These materials also have numerous applications in the field of piezoelectric energy harvesting. Light-weighted nature, non-toxicity, biodegradability and ductility are the other major highlights of piezopolymers. They have less power density, electro-mechanical coupling and stiffness compared to piezoceramics. However, they can withstand large driving fields, and have a high dielectric breakdown and good functional field strength (Covaci et al., 2020). Therefore, they are suitable as sensors but not as actuators. Polyvinylidene Fluoride (PVDF) is the most commonly used piezopolymer.

2.5.3 Macro Fiber Composite (MFC)

National Aeronautics and Space Administration (NASA) developed a very flexible and high-performance smart material known as Macro-Fiber Composite (MFC), as shown in Figure 2.4.

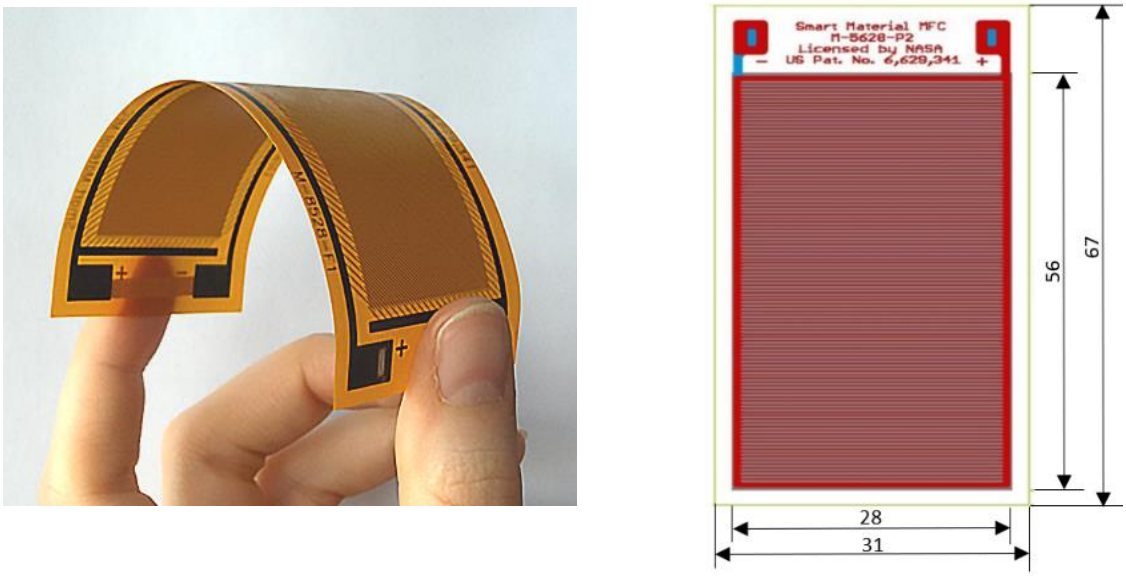

(a) (b)

Figure 2.4: (a) Macro fiber composite (MFC) (Smart Materials, 2021)
(b) M5628-P2 model – a type of MFC (Smart Materials, 2021)

It is prepared by sandwiching piezo ceramic rods between interdigitated electrodes, layers of adhesives and polyimide film. The carefully designed assembly of MFC enables sensing, actuation and in-plane poling in a durable, sealed and ready-to-use manner. It acts as an actuator on the application of electric potential, and therefore, it either distorts or bends the materials or either generates or counteracts the vibrations. It also acts as a sensitive strain gauge when no potential is applied, and will sense the deformations, vibrations and noises. It also has an excellent capacity to harvest energy from vibrations. It is readily available in d_{33} and d_{31} modes depending on its function.

2.6 CONCRETE VIBRATION SENSOR

A concrete vibration sensor (CVS) is a ready-to-cast sensor developed in Smart Structures and Dynamics Laboratory (SSDL), IIT Delhi, specifically made for the structural health monitoring of concrete structures (patent filled by Bhalla and Gupta, 2007). Bare PZT patches cannot be installed in a concrete structure during construction as it gets deteriorated when contacted with wet concrete. In CVS, the PZT patch is carefully coated with a composite protective layer, and is then embedded in a concrete cylinder of dimensions 25 mm in diameter and 12 mm in thickness, as shown in Figure 2.5. The grade of the concrete cylinder will be the same as the grade of the concrete element in which it has to be installed. The strain compatibility of CVS is exceptionally good, and can easily acquire resonant frequency and curvature mode shapes.

Figure 2.5: Concrete vibration sensor (CVS) (SSDL, IIT Delhi)

Kaur (2015) experimentally proved that the same set of CVSs can be used for both SHM and energy harvesting by installing a layer of 19 CVS at the top as well as at the bottom of an RC beam, as depicted in Figure 2.6. In the idle stage, CVS will work as an

energy harvester, and the harvested energy will be utilised for carrying out SHM works. It was able to obtain an output power of 0.09 μW from the RC beam.

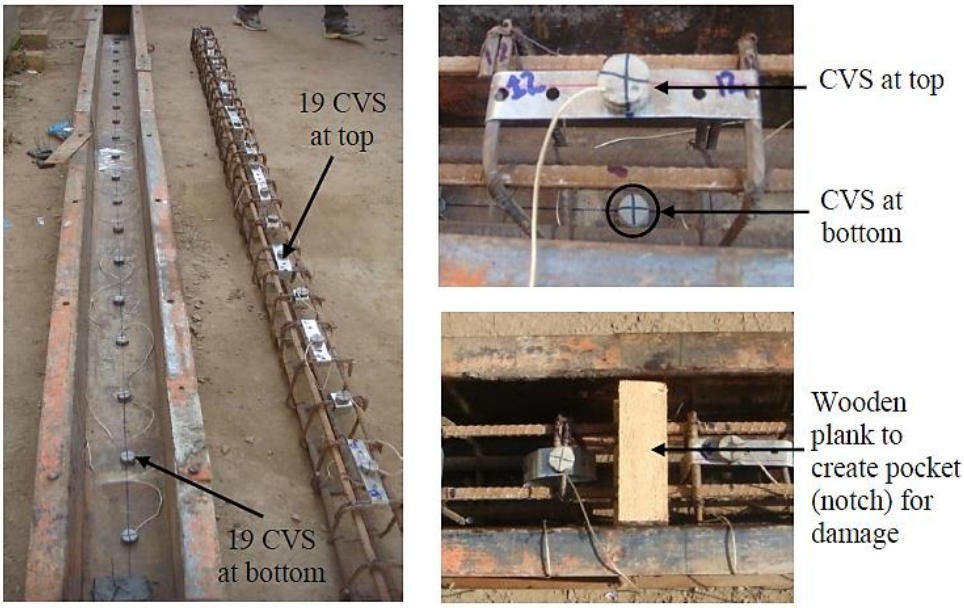

Figure 2.6: RC beam embedded with CVS before casting (Kaur, 2015)

2.7 CONCRETE VIBRATION ENERGY HARVESTER

The concrete vibration energy harvester (CVEH) is also a ready-to-cast sensor similar to CVS but the piezoelectric material is placed in a curved configuration, unlike the straight one in CVS. CVEH is also developed in SSDL, IIT Delhi, with a patent being filed by Kaur and Bhalla (2016a).

Due to the curved configuration, additional bending stress and bending strain will develop, resulting in the generation of higher voltage. However, all piezo patches cannot be used for developing CVEH as the piezoceramics are brittle in nature. Singh (2017) was successful in fabricating a CVEH using an MFC patch. The encapsulating cement mortar cylinder had a size of 100 mm diameter and 30 mm thickness. However, the dimensions can be altered based on the requirements and the size of the piezoelectric material installed in the CVEH.

Singh (2017) embedded CVS and CVEH at the mid-span of an RC beam, as shown in Figure 2.7, and experimentally proved that the CVEH has a far higher voltage generation capacity than CVS. The piezo element used for the fabrication of CVEH should be selected in such a way that it has only a d_{31} effect. The d_{33} effect can reduce the efficiency of CVEH.

The parametric study on the curvature and thickness of CVEH has not been explored so far.

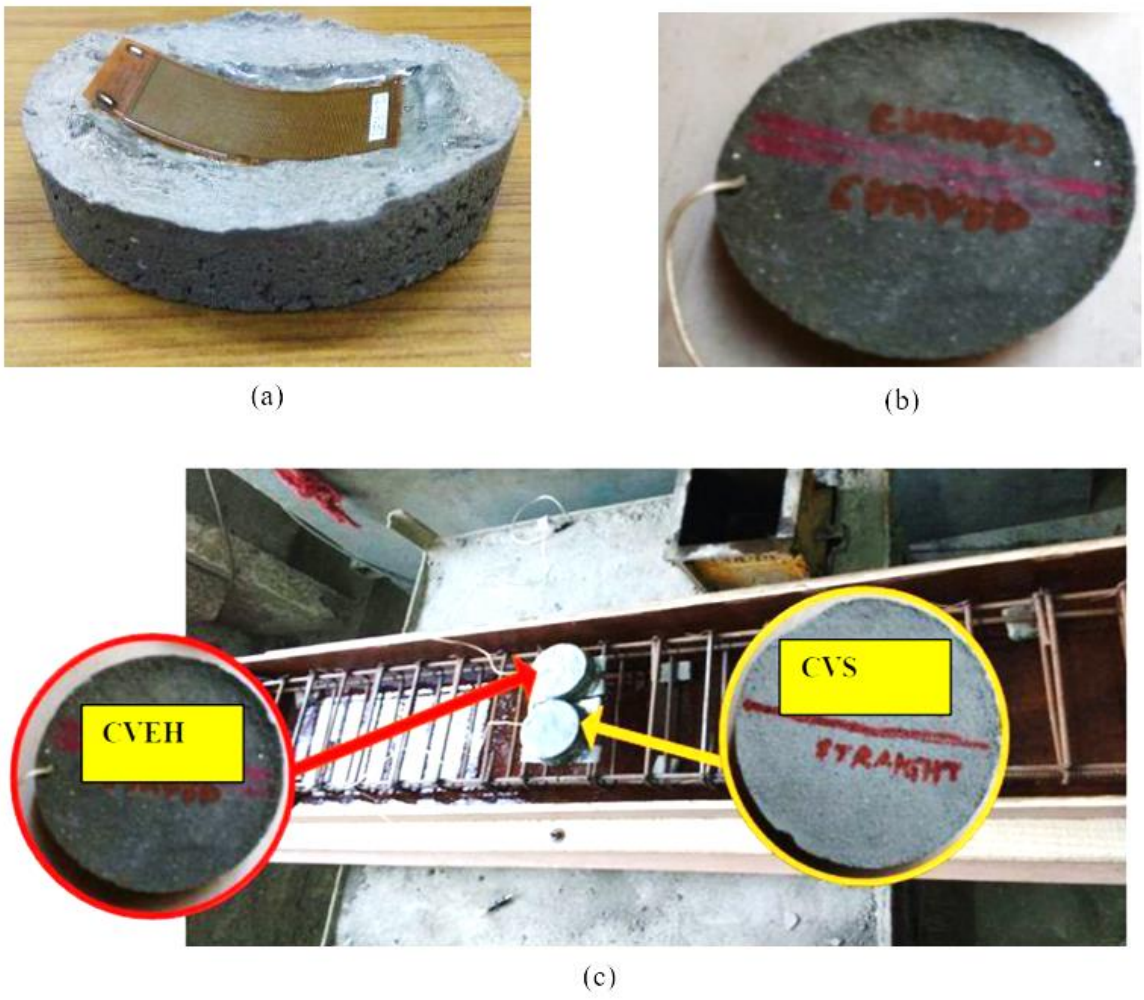

Figure 2.7: (a) Fabrication of CVEH using curved MFC (Singh, 2017)

(b) MFC based CVEH (Singh, 2017)

(c) MFC based CVEH and CVS placed in RC beam before casting (Singh, 2017)

2.8 EMI TECHNIQUE BASED STRUCTURAL HEALTH MONITORING

The electromechanical impedance (EMI) technique has been gaining wide popularity in the field of structural damage detection due to its non-destructive testing characteristics, easy implementation, cost-effective nature of piezoelectric (PZT) transducers installed on the structure and a reduction in manual inspection methods. The concept of the EMI technique was invented by Liang et al., (1994). The authors introduced a 1-D impedance model for SHM by considering the PZT transducer as a thin bar subjected to axial vibrations, as shown in Figure 2.8. Bhalla and Soh (2004a) and Baptista et al., (2014) have

thoroughly explained the installation and operation procedures of the EMI technique for structural damage diagnosis. Once the PZT sensors are installed, they are excited electrically by applying a harmonic electric potential across them by an impedance analyser or by an LCR meter (L stands for inductance, C for capacitance, and R for resistance) at high frequencies in sweep mode. As a result, an interaction takes place between the electrical impedance of the PZT sensor and the mechanical impedance of the host structure. The PZT transducers, which act as sensors and actuators simultaneously, generate the electrical impedance signature in the same frequency range as that of the excitation signal. These signatures are then compared with the baseline signature (the signature acquired during the healthy stage of the structure) for any anomalies or damages. Past studies have proved that the EMI technique is extremely delicate in detecting incipient damages.

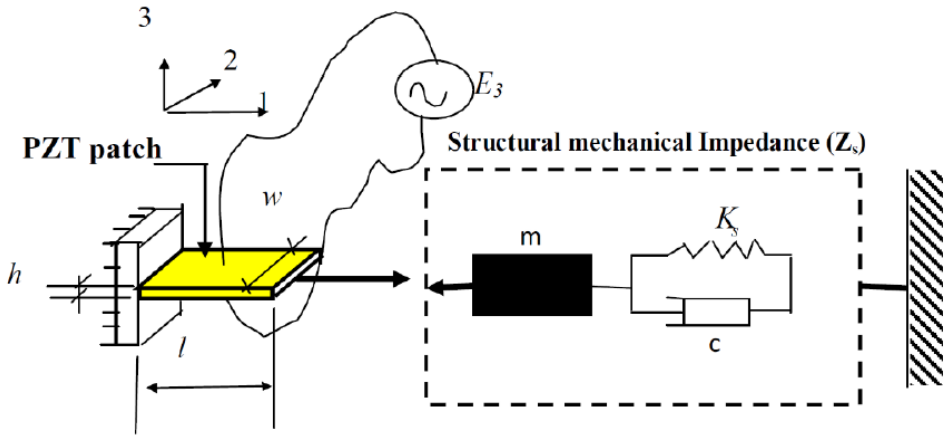

Figure 2.8: 1D impedance model for SHM (Liang et al., 1994)

Sun et al., (1995) described the details of a real-time SHM system based on the EMI technique, in which an array of PZT patches were bonded to a truss structure (test bed). Simple statistical algorithms were employed to identify the signature patterns. The author also reported that the localised sensing of PZT patches made the detection of damage location much easier. Park et al., (2004) investigated the suitability of the EMI technique for damage detection in lab sized steel bridges, and observed that the thickness mode of the PZTs resulted in more successful outcomes than the lateral mode-based method. The author proposed that the damages can be efficiently detected by monitoring the variations in the resonance frequencies if the damages occur near the piezo sensors. Giurgiutiu and Zagrai (2005) adopted the EMI technique for damage diagnosis on circular plates and aircraft panels, and observed that the damages had significantly modified the EMI signatures in terms of the shifts in frequency, splitting of peaks and the appearance of new harmonics.

Statistical parameters such as root mean square deviation (RMSD), correlation coefficient deviation (CCD) and mean absolute percentage deviation (MAPD) were used to quantify the severity of damages. Rosiek et al., (2010) utilised the EMI technique for incipient damage diagnosis in mechanical structures. In addition to the experimental investigations, FE analysis was also performed for damage detection based on the EMI plots, and suggested the use of this approach as a qualitative assessment method than a quantitative method.

So far, only conventional piezo sensors have been utilised for damage diagnosis. The suitability of various other configurations of piezo transducers is yet to be explored.

2.9 PIEZOELECTRIC ENERGY HARVESTING

Piezoelectric energy harvesting is based on the direct piezoelectric effect in which the mechanical strain due to human motion, seismic vibrations, flow-induced vibrations, acoustic noises, etc. are converted to electrical voltage. The harvested energy can be used to run low-power electronic devices like sensors, capacitors, electric watches, cellular phones, pagers, two-way communicators, global positioning system receivers and so on (Howells, 2009). Starner (1996) studied the energy generated or that can be harvested from human motion, by installing a piezoelectric device inside the shoe. It was found that by walking at an average pace, a human weighing 68 kg can produce 67 W of energy from piezo mounted shoes. Zhao et al., (2014) designed a piezo sandwiched thin structure that can be installed in shoes, as shown in Figure 2.9. Polyvinylidene difluoride (PVDF) was used as the piezoelectric material. During a normal walk, the harvester produced an average output power of 1 mW at a frequency of around 1 Hz.

Figure 2.9: PVDF film installed in the human shoe (Zhao et al., 2014)

Calio et al., (2014) conducted a study on various piezoelectric energy harvesting solutions. It was mainly emphasised on the operating modes of the material and the device configurations. d_{15} mode was found to be more efficient compared to other modes, though its fabrication seems to be quite complex. d_{33} mode and d_{31} were respectively found to be the superior ones in terms of the output voltage, and the simplest in terms of fabrication and performance.

Kaur and Bhalla (2014) researched the energy harvesting potential of surface-bonded thin piezo transducers in steel structures, and concluded that a power of 1.417 μW was generated against a peak displacement of 0.289 mm in d_{31} mode. Kaur and Bhalla (2016b) evaluated the energy harvesting potential of a concrete vibration sensor (CVS) which is a ready-to-cast sensor primarily developed as an SHM device by Bhalla and Gupta (2007). As the PZT patches are very delicate, durability is a major issue of the surface-bonded PZT patches. At this point, CVS plays a vital role as it can withstand extreme conditions as well. It was concluded that CVS was able to generate 60% energy as compared to the surface-bonded PZT patch. Singamsetty et al., (2014) experimentally analysed the output power generated from a PZT patch bonded to a parasitic steel structure, which is further attached to an RC beam. The beam was excited harmonically in a sweep mode, and the peak value of the voltage was generated when the excitation frequency matched the natural frequency of the external or parasitic structure. Numerical modelling and parametric study with respect to the size and shape of the parasitic structure were also conducted. A maximum power output of 2.2 μW was obtained at the fundamental frequency of the beam.

Singh (2017) fabricated a concrete vibration energy harvester (CVEH) using DuraAct and MFC. Though the former one was a failure, the latter one was successful, and was able to generate 1.96 times higher voltage than MFC based CVS. d_{31} mode was found to be more productive for the curved configurations. The effect of curvature and thickness of the CVEH are yet to be explored. Mittal (2017) performed a comparative study of the energy harvesting potential of piezoelectric ceramic rings (PCR), as depicted in Figure 2.9, and straight PZT patches. The author experimentally found that the PCR can generate a voltage output that is 5.5 times higher than the latter one. For PCR, the poling direction was taken normal to the plane of the ring. Higher voltage generation was obtained for d_{31} mode than d_{33} mode. A semi-circular-shaped piezo ring was able to generate a higher voltage than a PCR of the same arc length but a lesser angle than 180 degrees.

Kathpalia et al., (2017) experimentally investigated the application of curved piezo transducers for energy harvesting from smart paver tiles, which can harvest energy from human steps. The schematic diagram of the paver tile with the piezo transducer location is shown in Figure 2.11(a). THUNDER, a curved energy harvester developed by NASA Langley Research Center, as shown in Figure 2.11(b), was used as the piezo transducer, and observed that it can generate an average power in the range of 10 microwatts from very low dynamic force excitations.

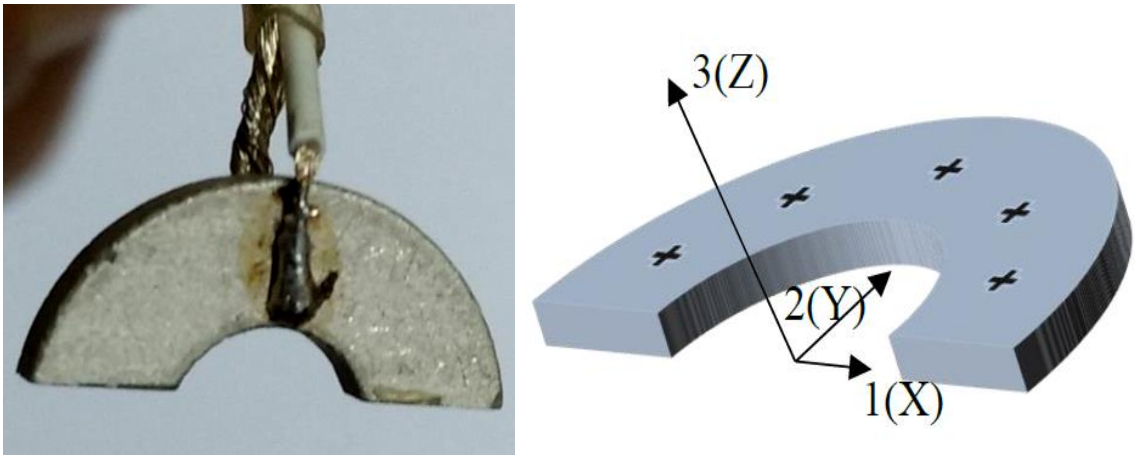

(a) (b)

Figure 2.10: (a) Piezoelectric ceramic rings (PCR) (Mittal, 2017)

(b) PCR with polarisation along 3(*Z*) direction (Mittal, 2017)

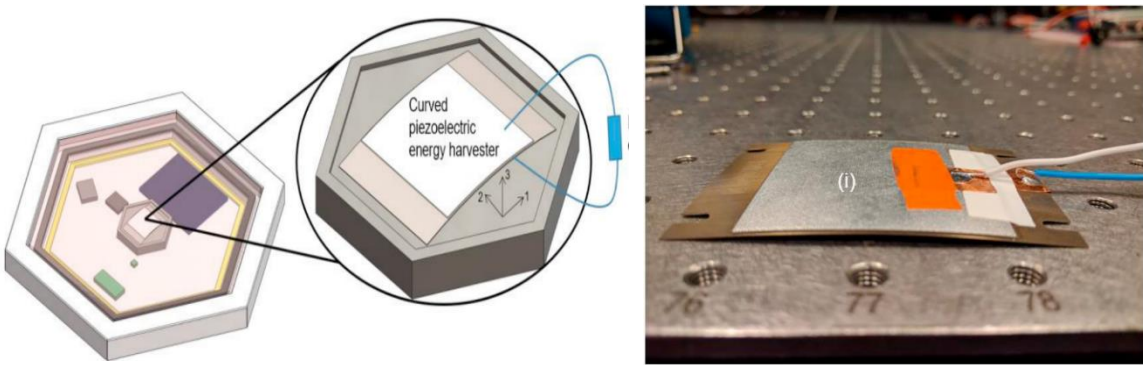

(a) (b)

Figure 2.11: (a) Schematic diagram of the paver tile showing the location of the energy harvester (Kathpalia et al., 2017)

(b) THUNDER - a curved energy harvester (Kathpalia et al., 2017)

Tanwar (2019) conducted a 1-D numerical analysis of the surface-bonded PZT transducers on a steel beam. The voltage generated by the curved configuration of PZT patches showed a decreasing trend with respect to an increase in the thickness of the patch. As per the 1-D study of the PZT patch on steel beams, the optimum radius of curvature was found to be 0.58 times the length of the PZT patch. The next section summarises the research gaps that are duly covered in this research work.

2.10 IDENTIFICATION OF RESEARCH GAPS

Although numerous studies have been conducted on SHM based on the EMI technique and piezoelectric energy harvesting in the past two decades, researches on curved piezo transducers are quite less. The following research gaps have been identified based on the detailed literature review presented in the previous sections.

i. Only experimental comparison of the voltage generated by curved and straight piezo patches by impact hammer test has been attempted. The comparison of power or energy generated by the curved configuration relative to straight configuration has not been undertaken

ii. The potential of power storage from curved piezo transducers has not been explored till date.

iii. The potential of CVEH in the field of SHM for damage detection has yet to be explored

iv. Numerical investigations (3-D modelling and FE analysis) to analyse the effect of curvature, thickness and the position of placement of the curved piezo transducers for energy harvesting have not been performed.

v. No closed-form solution of the voltage generated by the curved PZT patches has been derived. Also, the analytical modelling of CVEH embedded inside RC beams for SHM and piezoelectric energy harvesting has not been conducted so far.

2.11 AIM AND SCOPE OF THE RESEARCH

The study aims at analysing the potential of the curved piezo transducers in the field of structural health monitoring and energy harvesting. The curved configuration of piezo patches results in the development of additional bending stresses when excited externally.

Therefore, it is expected to have a higher voltage generation capacity. The specific aims and scope of the work are:

i. To experimentally analyse the relative response of CVEH and CVS embedded inside an RC beam under harmonic loading based on its terminal voltage.
ii. To experimentally measure the practical energy harvesting capability of CVEH and CVS in terms of the power and energy generated by them.
iii. To experimentally analyse the potential of CVEH and CVS for power storage into capacitors.
iv. To experimentally compare the performance of CVEH and CVS embedded in an RC beam for damage detection by EMI technique.
v. To develop a 3-D model of an RC beam embedded with CVEH and CVS and compare their output potential by finite element (FE) method, and validate the analysis experimentally.
vi. To analyse the influence of various parameters affecting the output potential such as curvature, thickness, and the position of placement of the curved piezo transducer for voltage generation by finite element method.
vii. To develop a 1-D analytical model of the RC beam embedded with a curved PZT patch by formulating a MATLAB code, and investigate its efficiency in voltage generation by the method of direct stiffness approach considering the effects of piezoelectricity.
viii. To perform a parametric study on the effect of thickness and curvature of the piezo transducer for voltage generation by the above method.

It is expected that the findings of this investigative research will lay the foundation for the implementation of curved piezo transducers in real-life RC structures for energy harvesting and structural health monitoring. The forthcoming chapter presents the experimental investigations undertaken to analyse energy harvesting potential of CVEH relative to CVS.

CHAPTER 3

EXPERIMENTAL EVALUATION OF CVEH FOR ENERGY HARVESTING

3.1 INTRODUCTION

In recent decades, several studies have been conducted to assess the energy harvesting capability of piezo transducers. However, there are relatively few experimental investigations on the efficiency of curved piezo transducers in this realm. This chapter presents the performance comparison of CVEH (curved configuration of the piezo transducer) with perpendicular poling direction to its curvature against the CVS (straight configuration of the piezo transducer) for energy harvesting. The experimental investigations are conducted on an RC beam with CVEH and CVS embedded at its mid-span. For both configurations, the study examines (i) the open-circuit voltage generated across the sensors, (ii) the power generated under the impedance matching conditions, and (iii) the feasibility of power storage in capacitors.

3.2 EXPERIMENTAL SETUP DETAILS

The experimental setup consists of an RC beam (1500 mm × 300 mm × 100 mm) of grade M30, with CVEH and CVS embedded at its mid-span, as shown in Figure 3.1 (Singh, 2017). Generally, piezoceramics, particularly PZT transducers, are widely preferred as sensors due to their high stiffness, strength and coupling factors. However, these materials are brittle, which restricts their suitability for curved surfaces. Therefore, the current study utilises a very flexible and high-performance smart material known as Macro-Fiber Composite (MFC) of model M5628-P2, a d_{31} variant, with a thickness of 300 μm. The CVS and CVEH are prepared by individually encapsulating M5628-P2 MFC patches in a 1:3 cement mortar cylinder of 100 mm diameter and 30 mm height in the straight and curved configurations respectively (refer chapter 2, Figure 2.7). The piezo transducers are installed in an RC beam in such a way that the top surface of the transducers and the beam coincide. The piezo transducers are tied to the compression reinforcement at the top surface while casting the beam. Singh (2017) provides a thorough explanation of the fabrication process of the beam and the piezo sensors. The RC beam with CVEH and CVS sensors embedded inside is placed in the simply supported condition with an effective span of 1100 mm.

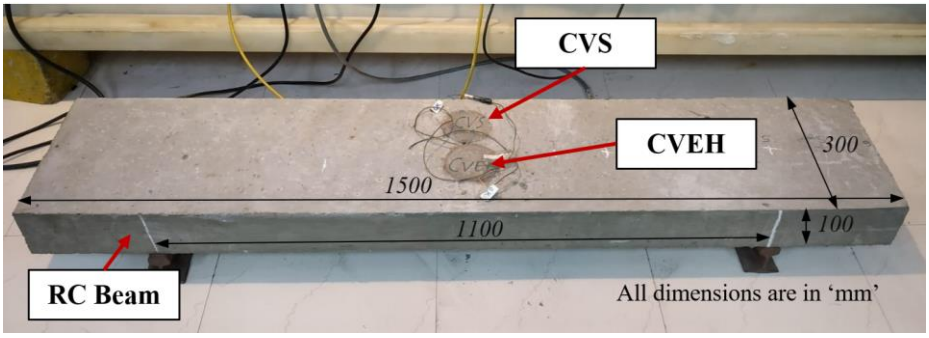

Figure 3.1: RC beam with CVEH and CVS embedded at its mid-span

3.3 COMPARISON OF OPEN-CIRCUIT VOLTAGE

To measure the open-circuit voltage generated across the sensors, the RC beam is excited harmonically using an LDS V406 series portable shaker placed at the mid-span of the beam, i.e., directly above the sensors. Electrical signals are generated using an Agilent 33210A function generator, which are amplified by an LDS PA500L power amplifier and transmitted to the portable shaker. The arrangement proposed by Kaur (2015) comprising of springs and a cover plate is used. The electrical signals are converted to mechanical force by the shaker. The CVEH and CVS sensors are connected to the first two channels of the TDS 2004B oscilloscope to measure the open-circuit voltage generated across the sensors. A PCB 352C34 accelerometer with a sensitivity of 100 mV per *g* is placed on the beam, closer to the shaker, and is connected to the PCB 482C Series ICP amplifier, which is further connected to the third channel of the oscilloscope (Figure 3.2). The beam is initially subjected to sweep excitations ranging from 10 Hz to 100 Hz for 2.5 seconds.

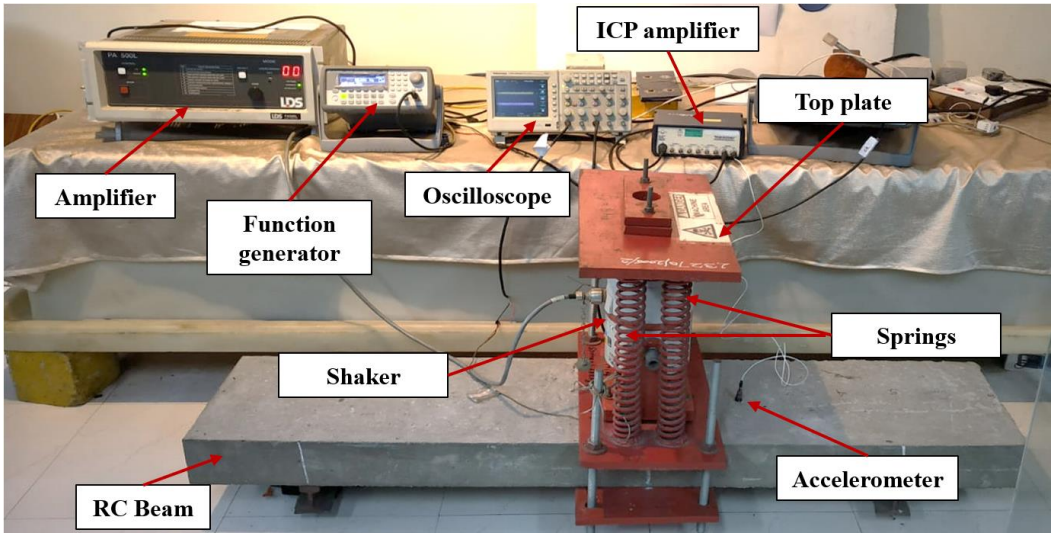

Figure 3.2: Experimental setup for open-circuit voltage measurement (shaker at midspan of the beam)

The beam's natural frequency equipped with the dynamic shaker at the mid-span is 55 Hz based on frequency domain analysis of the response recorded from piezo sensors and accelerometer (Figure 3.3). In comparison to the surface-mounted accelerometer, the embedded piezo sensors provided a substantially better signal to noise ratio.

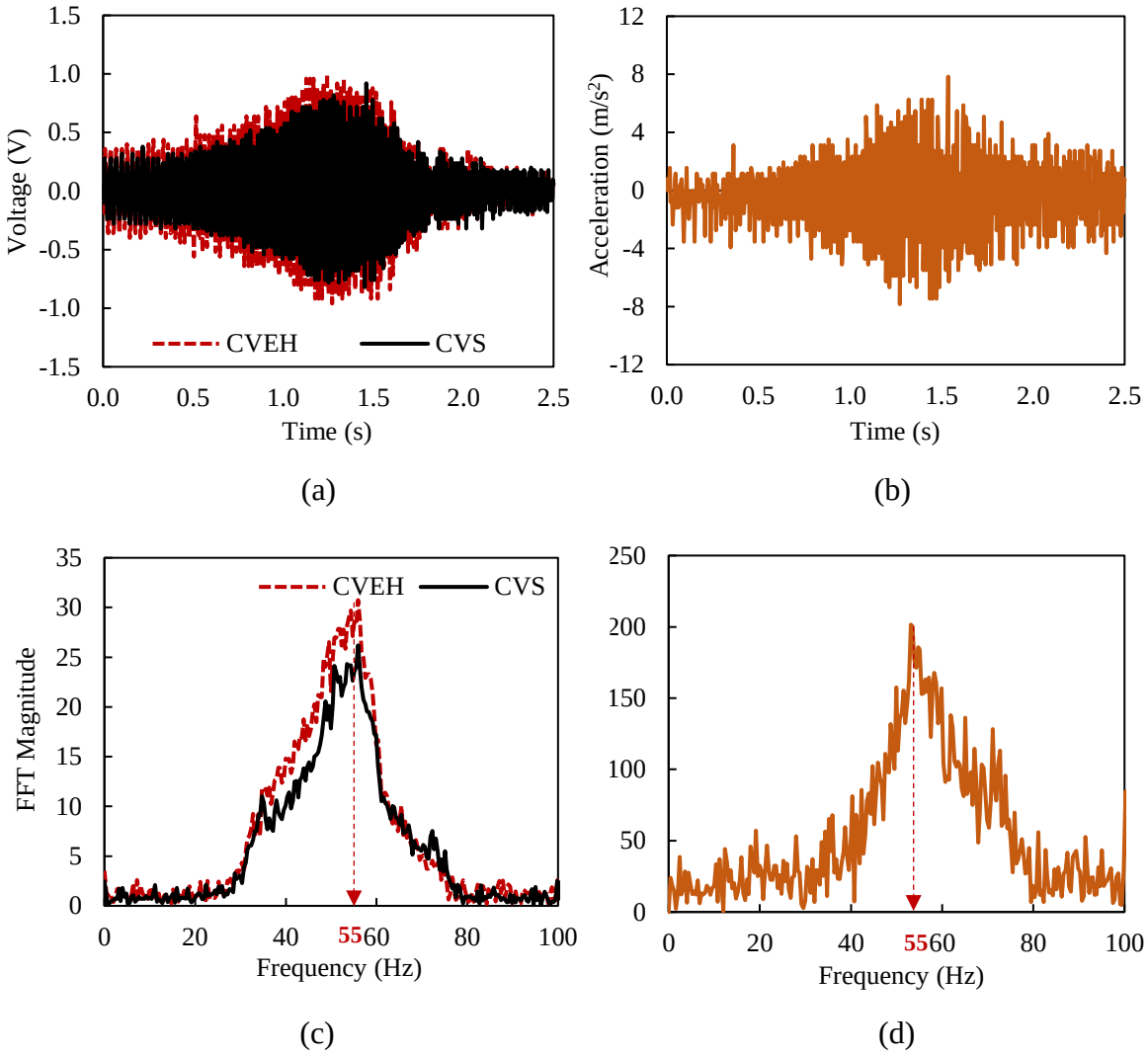

Figure 3.3: (a) Time-domain response of CVS and CVEH, subjected to sweep excitation
(b) Time-domain response of accelerometer, subjected to sweep excitation
(c) Frequency domain response of CVS and CVEH
(d) Frequency domain response of the accelerometer

For the comparison of open-circuit voltage generated by the piezo sensors for the same assembly of the beam shaker system, the beam is excited at designated frequencies ranging from 25 Hz to 85 Hz with a step interval of 15 Hz. The shaker is then shifted to positions at a distance of $L/3$ and $L/6$ from the left support. The open-circuit voltage generated by the

CVEH (curved configuration) and CVS (straight configuration) is compared for each scenario. Figure 3.4 (a) shows the typical response of CVEH and CVS when excited at 85 Hz at a distance of $L/3$ from the nearest support. The variation of the voltage ratio (V_{CVEH}/V_{CVS}) with respect to frequency is illustrated in Figure 3.4 (b). The full plots of the harmonic excitation test covering various frequencies and shaker positions are presented in Appendix A.

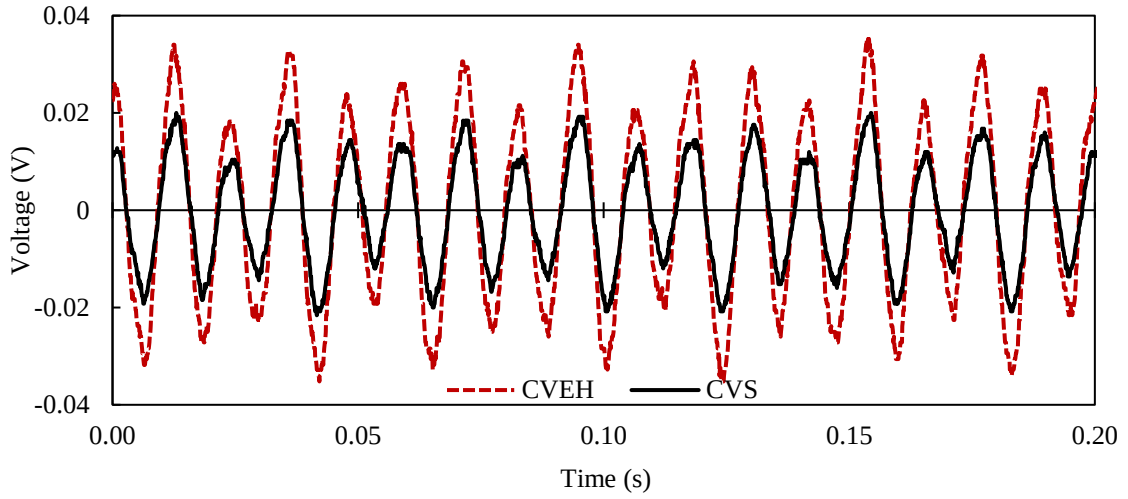

(a)

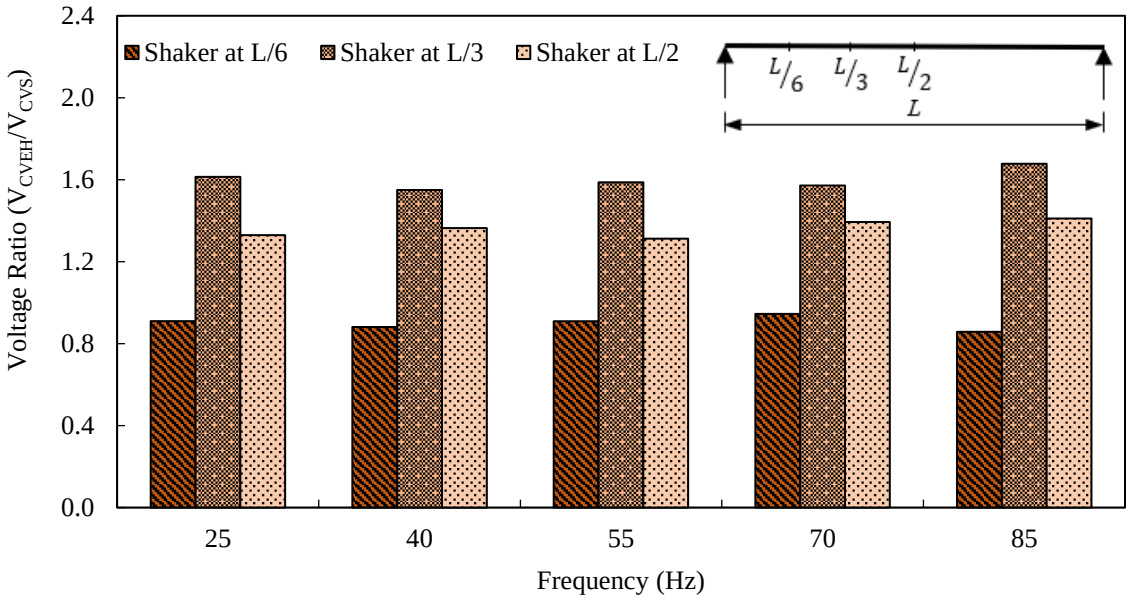

(b)

Figure 3.4: (a) Response of CVEH and CVS when excited at 85Hz at $L/3$ distance from the nearest support

(b) Variation of voltage ratio with respect to frequency for various positions of excitation

From the experimental results, it is observed that the voltage developed across CVEH is substantially higher than that of CVS in most cases. It is because of the additional strain developed due to the curved configuration in the former one. As per the direct effect of piezoelectricity, the voltage developed across the piezoelectric materials is directly proportional to the strain experienced by them. The CVEH is found to generate 1.6 times and 1.3 times higher voltage than CVS when excited at an *L*/3 and *L*/2 distance from the nearest support respectively. The slight drop in voltage ratio while exciting at *L*/2 distance might be due to the 3-D stress effects generated by the shaker's weight, which in this case is right above the sensors. The voltage ratio has decreased to around 0.9 when the shaker is positioned closer to the support, i.e., at an *L*/6 distance from the support. Though it is not fully explainable, it is possibly due to some support effects and the generation of certain complex stress situations. However, the first two excitation positions prove the superiority of CVEH in energy harvesting.

3.4 COMPARISON OF POWER GENERATED BY CVEH & CVS

This section compares the power generated across the two piezo transducers under the impedance matching conditions. The experimental setup consists of a Crompton Greaves XKF5577 crude shaker connected to a speed controller, and positioned at an *L*/4 distance from the nearest support. The voltage generated across the sensors as a result of the vibrations imparted by the shaker is measured using TDS 2004B oscilloscope. The crude shaker causes the beam to vibrate in a non-sinusoidal pattern, simulating a real-life situation. At the midpoint of the beam, a PCB 352C34 accelerometer with a sensitivity of 100 mV per *g*, is linked to a PCB 482C Series ICP amplifier, which is then connected to the oscilloscope's third channel. An additional circuit, as shown in Figure 3.5, is connected to the sensors for power measurement.

The voltage (V_1) generated across the sensors due to the vibrations is the input voltage to the circuit. Due to the high electrical impedance of the piezo transducer, the electric current (*i*) passing through the circuit will be very small, usually in the microampere range, making it almost impossible to measure. As a result, an Agilent 34411A digital multimeter is used to measure the circuit's output voltage (V_2), which is then linked to the laptop for data acquisition. The current flowing through the circuit is estimated as

$$i = V_2 / R_1 \tag{3.1}$$

The power generated by the sensors is thus given by

$$P = i^2\left(R_1 + R_2\right) \tag{3.2}$$

According to the maximum power transfer theorem, the source impedance (or resistance) must match the load impedance (or resistance) to generate the maximum amount of power (Kaur, 2015). Using an Agilent E4980A LCR meter, the impedance values of the CVEH and CVS are measured at various frequencies ranging from 20 Hz to 80 Hz with a step interval of 5 Hz, and are summarised in Table 3.1.

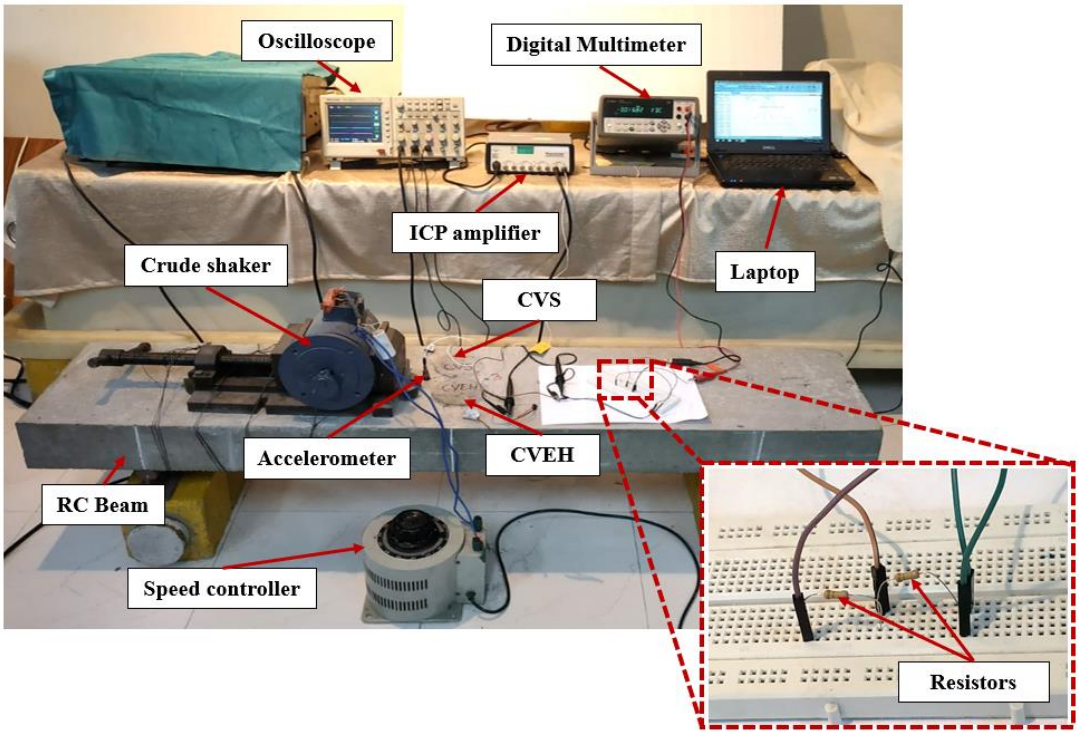

(a)

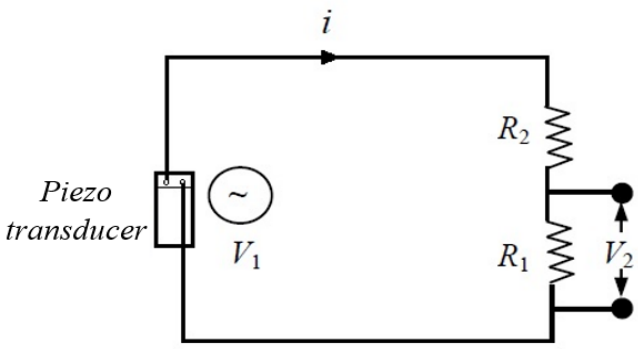

(b)

Figure 3.5: (a) Experimental setup for power measurement
(b) Circuit employed for power measurement

Based on the principle of impedance matching and the maximum power transfer theorem, the load resistors (R_1 = 335 kΩ and R_2 = 340 kΩ) are chosen such that they are in a similar range as that of the sensors. A highly unmatched system can lead to excessive loss of power and heat dissipation. It can even lead to circuit failure. Three sets of measurements are taken by varying the acceleration of the shaker to compare the power generated across the transducers (Figures 3.6 and 3.7). From the previous section, it is clear that the voltage developed across the CVEH is higher than the CVS, and therefore, the power developed across them is expected to be higher for CVEH. This is justified by the experimental results as the average power ratios (P_{CVEH}/P_{CVS}) of the three sets of measurements is about 10.36, implying that CVEH is 10 times more powerful than CVS in terms of power generation.

Table 3.1: Impedance of the CVEH and CVS for various frequencies

Sl No.	**Frequency (Hz)**	**Impedance (kΩ)**	
		CVEH	**CVS**
1	20	73	67
2	25	59	54
3	30	49	45
4	35	42	39
5	40	37	34
6	45	33	30
7	50	29	27
8	55	27	25
9	60	25	23
10	65	23	21
11	70	21	19.5
12	75	20	18
13	80	18.5	17
	Average	**35**	**32**

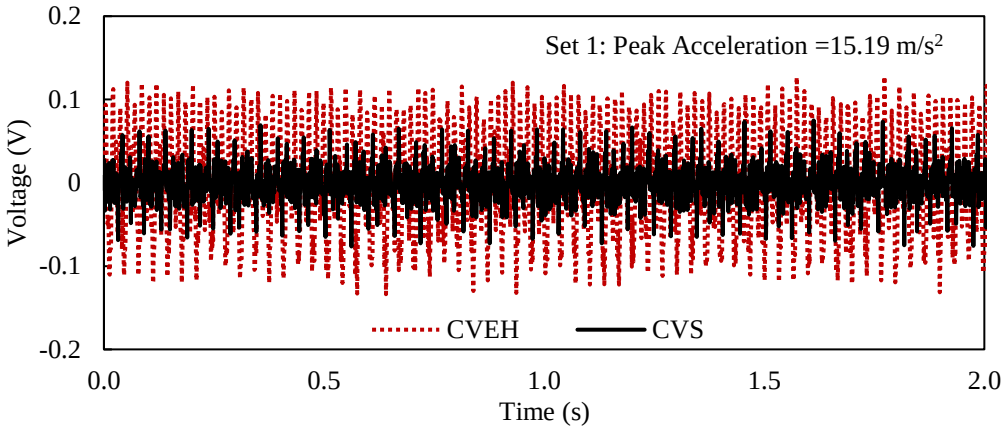

(a)

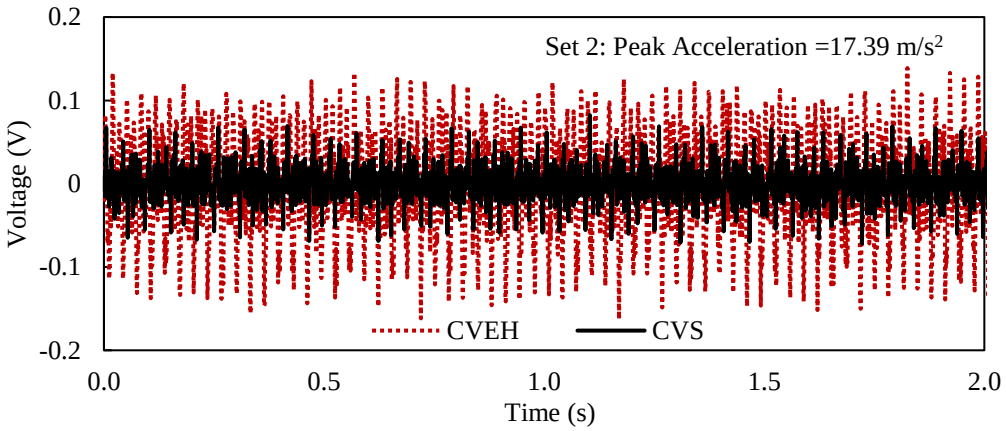

(b)

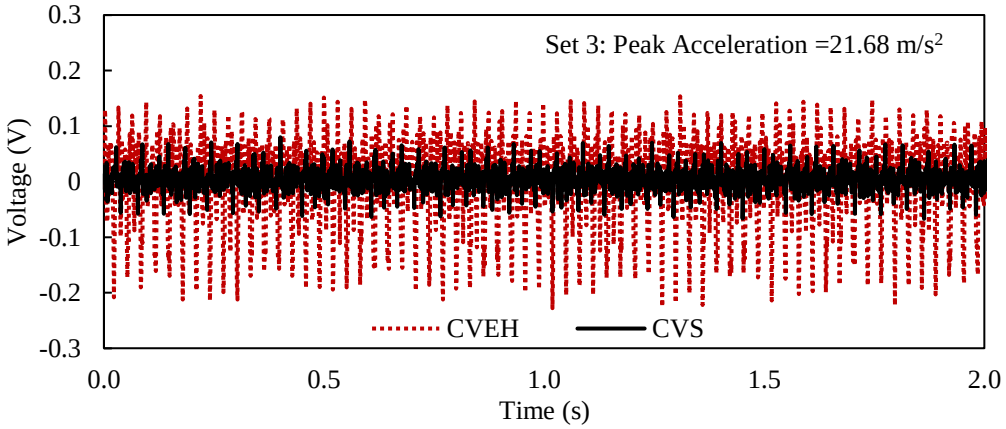

(c)

Figure 3.6: (c) Output voltage of the circuit for a peak acceleration of 15.19 m/s^2

(d) Output voltage of the circuit for a peak acceleration of 17.39 m/s^2

(e) Output voltage of the circuit for a peak acceleration of 21.68 m/s^2

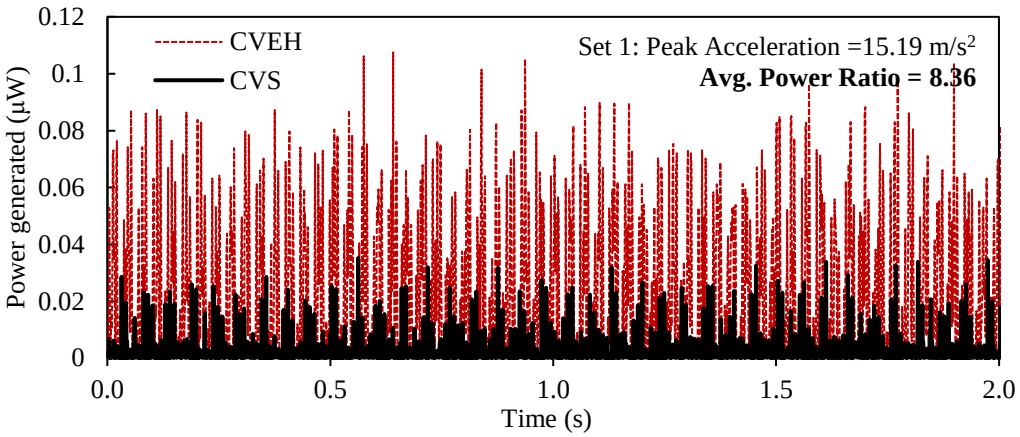

(a)

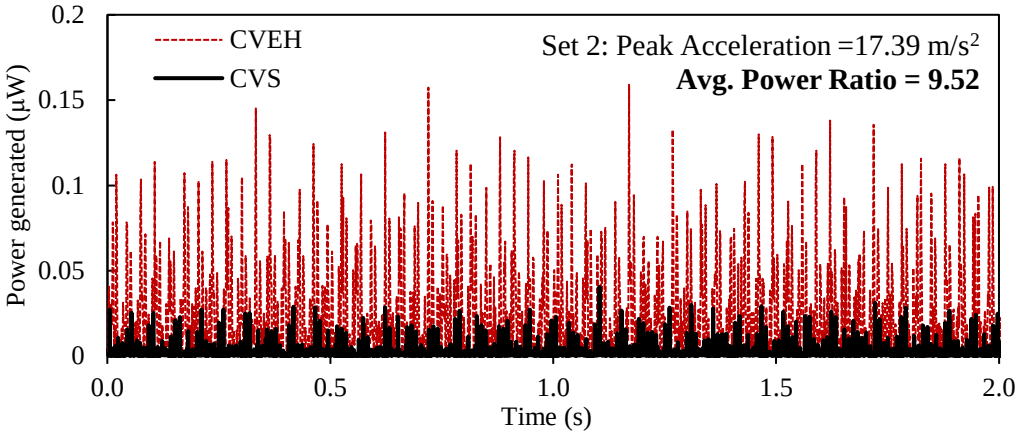

(b)

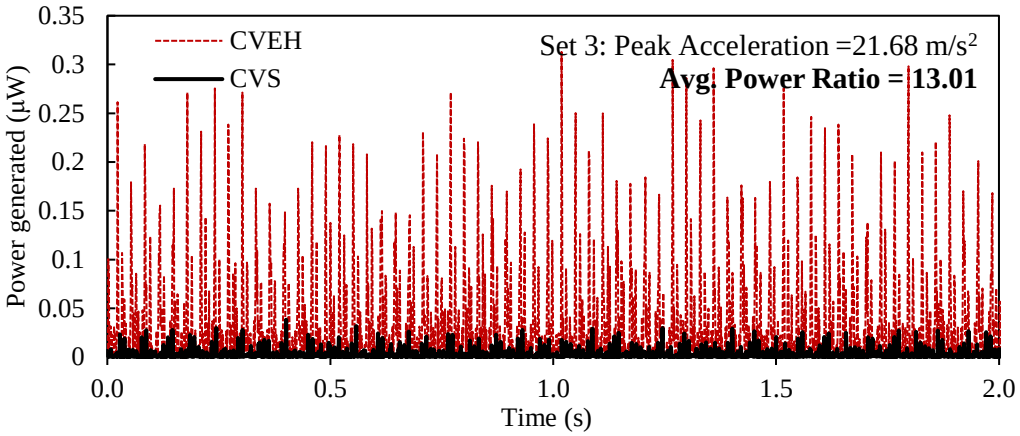

(c)

Figure 3.7: (a) Power developed across the transducers for a peak acceleration of 15.19 m/s^2

(b) Power developed across the transducers for a peak acceleration of 17.39 m/s^2

(c) Power developed across the transducers for a peak acceleration of 21.68 m/s^2

For periodic vibrations of frequency (f), the deflection (u) of the beam at the mid-span is related to the acceleration ($\ddot{u}$) of the beam by the following equation.

$$u = \frac{\ddot{u}}{(2\pi f)^2} \tag{3.3}$$

As per the fundamental bending theory of beams, the following equations can be derived for a simply supported beam of span L, with a concentrated load P acting a distance a from the nearest support and b from the farthest support, as shown in Figure 3.8.
The vertical deflection of the beam at the centre is given by

$$y_{L/2} = \frac{Pa}{48EI}\left[L^2 - 12b^2\right] \tag{3.4}$$

The vertical deflection of the beam at any section x is given by

$$y = \frac{8y_{L/2}}{L^3 - 12b^2L}\left[x^3 - 3b^2x\right] \tag{3.5}$$

The curvature of the beam is therefore derived as

$$C_r = \frac{d^2y}{dx^2} = \frac{48y_{L/2}x}{L^3 - 12b^2L} \tag{3.6}$$

where EI is the flexural rigidity of the beam.

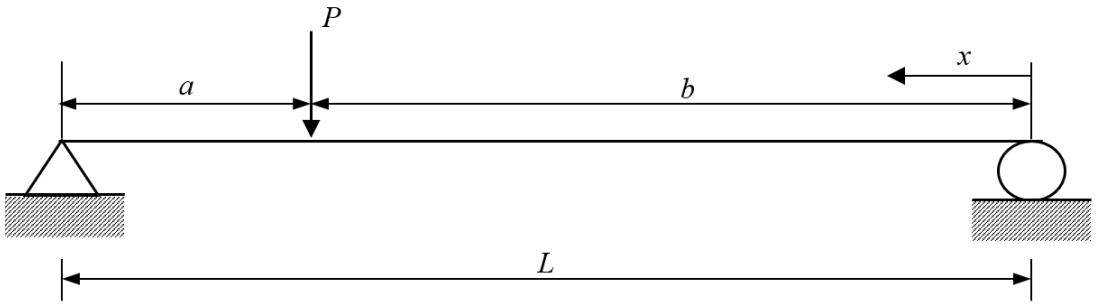

Figure 3.8: Free body diagram of the beam under concentrated load

Based on Euler's beam theory, the relation between the strain (S) and the deflection (y) of a simply supported beam at a distance x can be derived, as shown in Eq. (3.7), which further reduces to Eq. (3.8) for the current case, where the load acts at $L/4$ distance from the nearest support ($a = L/4$ and $b = 3L/4$).

$$S = \frac{d^2y}{dx^2} \times \frac{D}{2} \tag{3.7}$$

$$S = -\left(\frac{48}{23}\right)\frac{y_{L/2}D}{L^2} \tag{3.8}$$

where $\frac{D}{2}$ represents the depth of the neutral axis.

The relation between voltage (V) developed across the piezoelectric material due to the strain experienced by it is given by Eq. (2.3). It is assumed that the strain in the piezo transducer will be equal to the strain in the beam at the corresponding position on account of perfect bending. Therefore, the strains are calculated based on Eq. (3.8) and Eq. (2.3), and are depicted in Figure 3.9. As the vibrations are non-harmonic, the average acceleration is considered instead of the peak acceleration. It is expected that the strain calculated based on the open-circuit voltage of the CVS matches the strain calculated based on the acceleration of the beam. Also, the strain based on CVEH voltage is expected to be higher than the former ones due to the additional bending strain. Though the strain calculated based on experimental values of acceleration and open circuit voltages are in a similar range, the strain based on CVS voltage is a little lesser than the acceleration-based strain, which almost coincides with the strain in CVEH. The slight deviation from the expected results might be due to some eccentricity in the point of load application, losses while measuring the open circuit voltages or a minor calibration error in the oscilloscope.

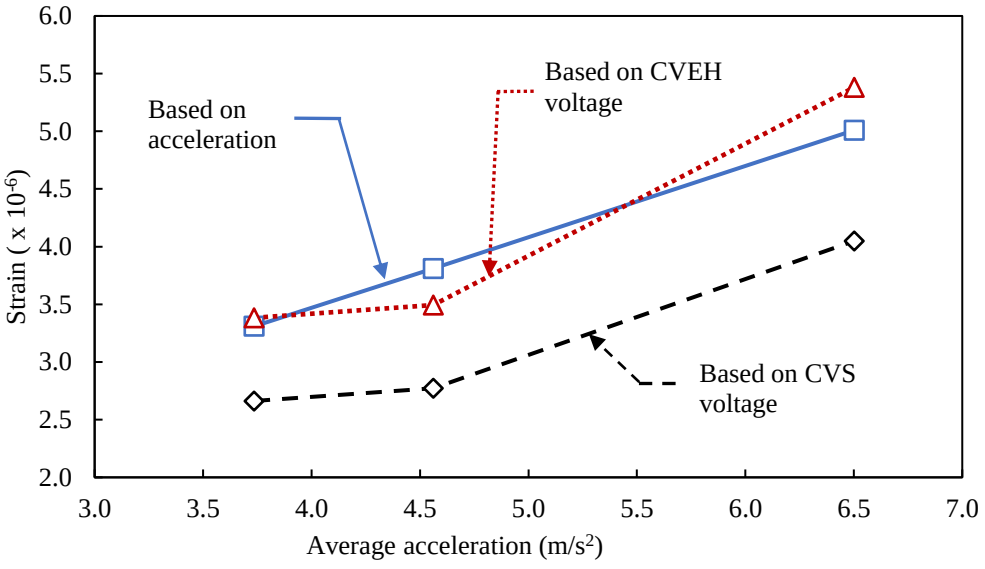

Figure 3.9: Comparison of the strain calculated based on the acceleration of the beam and direct piezoelectric effect of sensors

3.5 POTENTIAL OF POWER STORAGE

The energy generated from the piezo transducers due to the vibrations of the beam is stored in a 1000 μF capacitor. The experimental setup is similar to that of the power measurement setup, except that the power measurement circuit is replaced by a simple full bridge rectifier circuit (Figure 3.10).

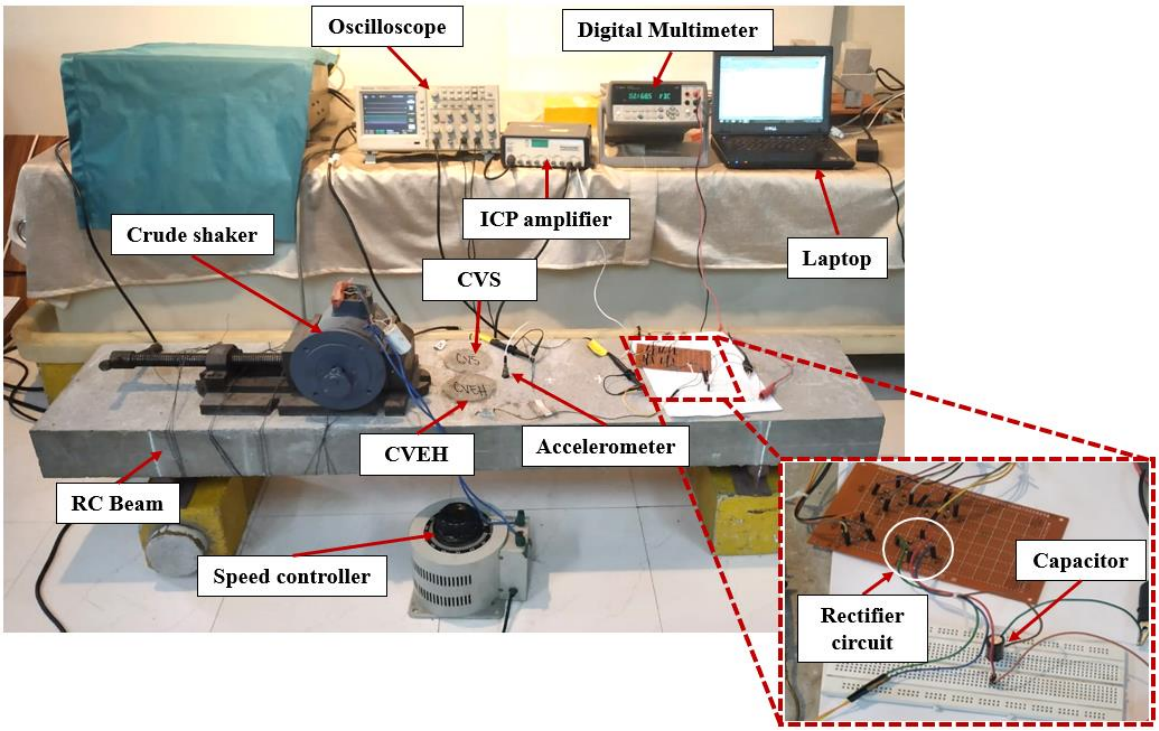

(a)

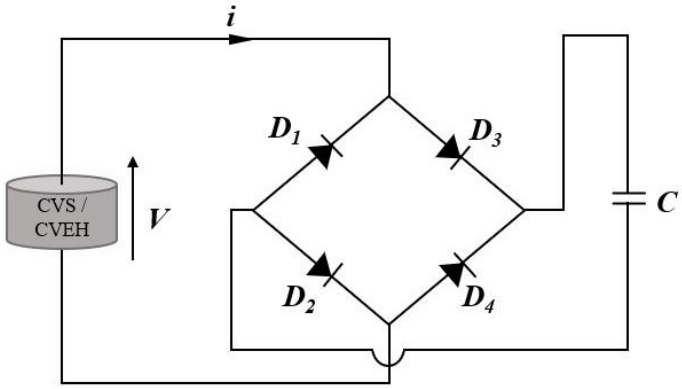

(b)

Figure 3.10: (a) Experimental setup for power storage in a capacitor

(b) Simple bridge rectifier circuit

The function of the rectifier circuit is to convert the output voltage generated by the piezo sensors in the alternating current (AC) mode to a stable power supply in the direct current (DC) mode so that it can be stored in a capacitor. In the rectifier circuit, four diodes named D_1 to D_4 are placed in "series pairs" such that in each half-cycle, only two diodes conduct the current, i.e., during the positive half cycle, diodes D_1 and D_4 will be in the ON position and conduct the current, while the diodes D_2 and D_3 will be reverse biased, and therefore kept in the OFF position. During the negative half-cycle, the former diodes will be reverse biased, while the latter ones will be forward biased (Balguvhar, 2020).

Two sets of experiments are conducted by vibrating the beam in two different accelerations, and the output voltage stored in the capacitor with respect to time is measured using an Agilent 34411A digital multimeter. The total energy stored in the capacitor is given by

$$E_T = \frac{1}{2} C V_c^2 \tag{3.9}$$

where C is the capacitance (1000 μF) and V_c is the output voltage of the rectifier circuit which is stored in the capacitor. The average power stored in the capacitor is related to the total charging time T_c by

$$P_{avg} = \frac{E_T}{T_c} \tag{3.10}$$

The average mid-point acceleration of the beam in the two experiments is 4.89 m/s^2 and 8.84 m/s^2. The reference voltage considered for the study is 1.6 V based on the charging curve of the capacitors, and the corresponding energy harvested in the capacitors is 1.28 mJ as per Eq (3.9). CVEH and CVS are charged in 236 seconds and 335 seconds for an average mid-point acceleration of 4.89 m/s^2 respectively, and their equivalent power storage is 5.42 μW and 3.82 μW. As the average acceleration is increased to 8.84 m/s^2, the charging time is lowered to 148 and 249 seconds respectively, and the power storage is increased to 8.65 μW and 5.14 μW. The charging curve of CVEH and CVS and their corresponding power storage are depicted in Figures 3.11, 3.12 and 3.13. CVEH has harvested an average of 1.55 times more power in each case, revealing its pre-eminence in the field of energy harvesting.

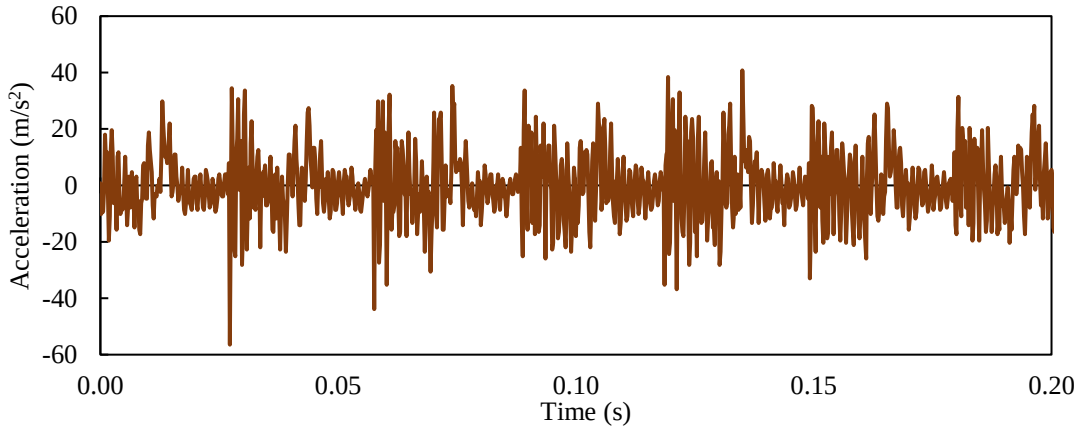

(a)

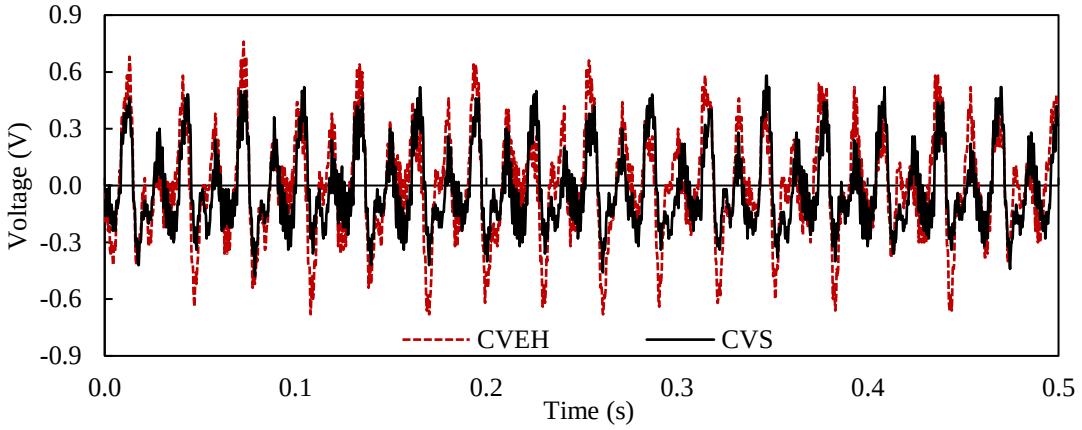

(b)

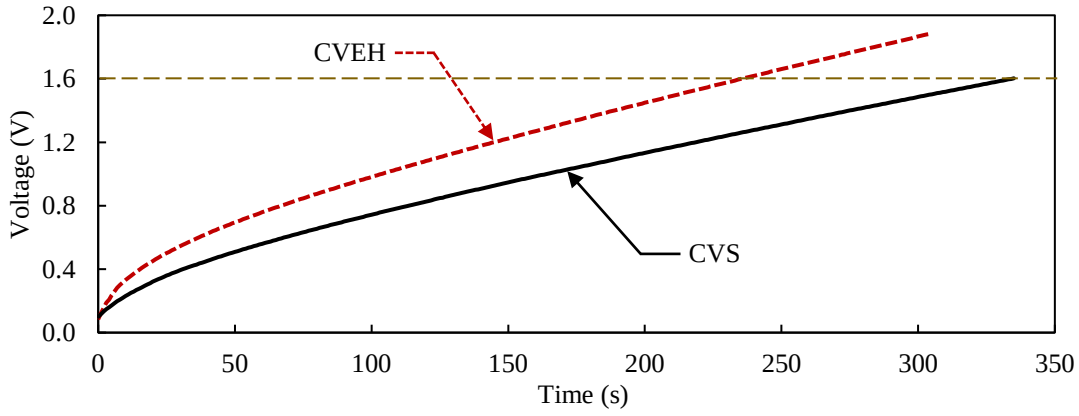

(c)

Figure 3.11: (a) Acceleration response of the beam for charging the capacitors: set 1

(b) Open circuit voltage developed across CVS and CVEH: set 1

(c) Charging curve of the capacitor: set 1

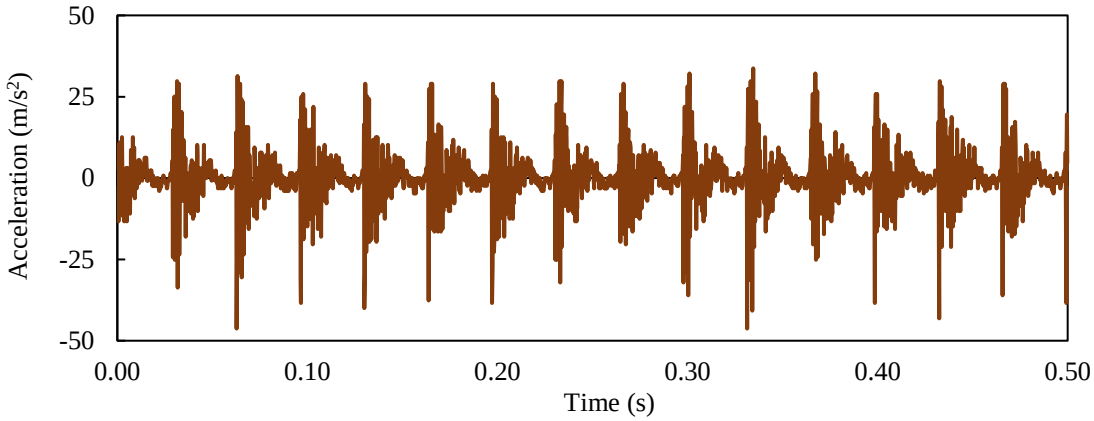

(a)

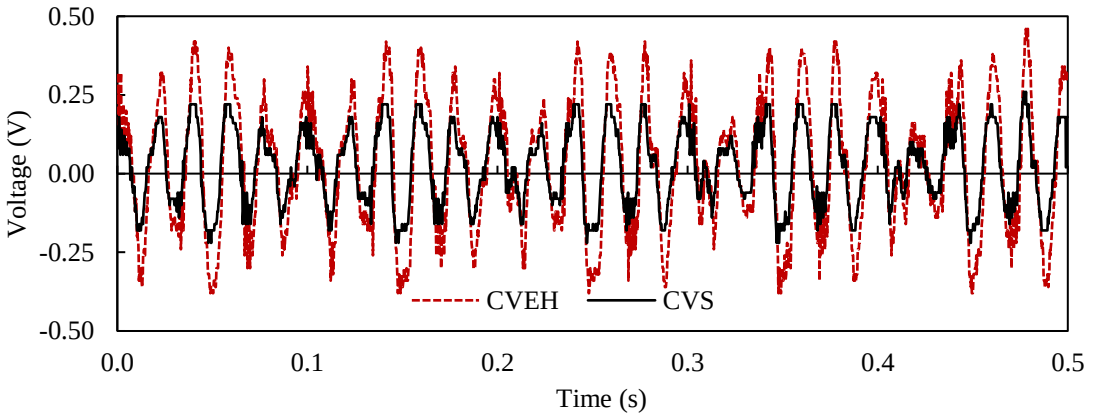

(b)

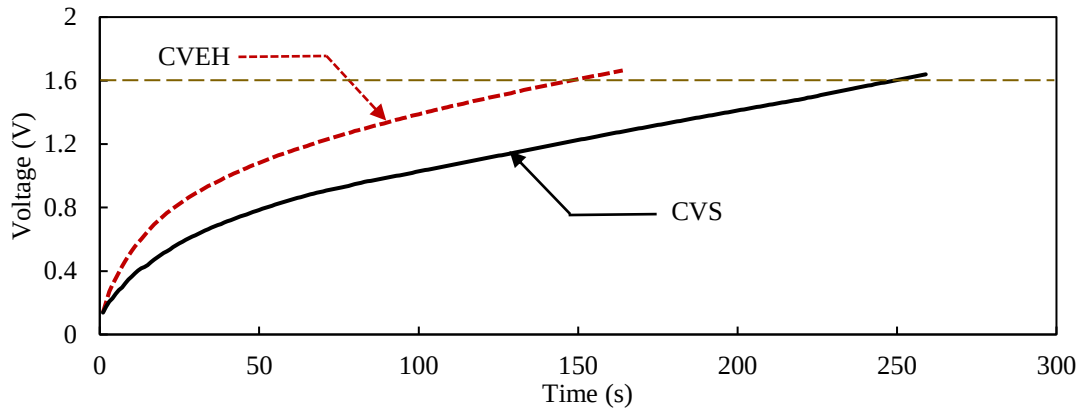

(c)

Figure 3.12: (a) Acceleration response of the beam for charging the capacitors: set 2

(b) Open circuit voltage developed across CVS and CVEH: set 2

(c) Charging curve of the capacitor: set 2

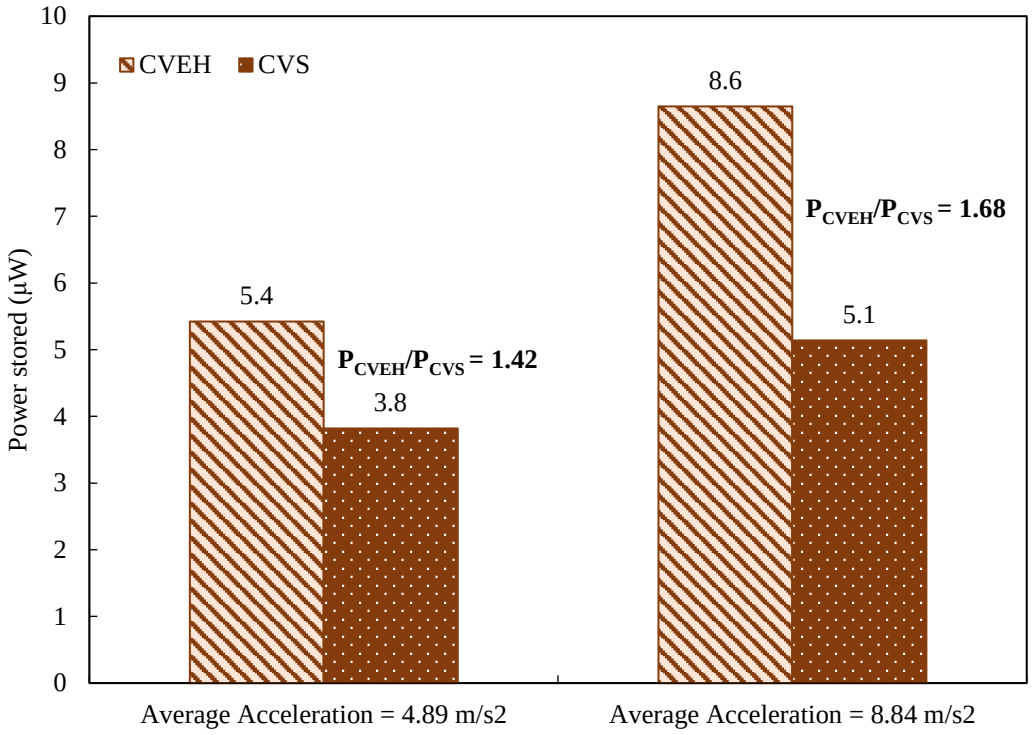

Figure 3.13: Histogram of average power stored in the capacitors

3.6 SUMMARY

This chapter has presented the findings of the experimental investigations carried out to analyse the efficiency of CVEH relative to CVS for energy harvesting. The poling direction of the curved piezo transducer (CVEH) considered in the study is perpendicular to its curvature. The open-circuit voltage generated by CVEH and CVS embedded at the mid-span of an RC beam is compared for various positions of harmonic excitations. The chapter also covers a comparison of the power generated by the piezo transducers subjected to periodic vibrations under impedance matching conditions. Finally, the amount of power that can be harvested by the transducers is analysed by storing the power generated by them in capacitors. The CVEH has performed substantially better in all the experiments, proving its supremacy in the field of energy harvesting. The next chapter analyses the suitability of CVEH for damage diagnosis.

CHAPTER 4

DAMAGE DETECTION POTENTIAL OF CVEH FOR STRUCTURAL HEALTH MONITORING

4.1 INTRODUCTION

Piezoelectric sensors have established their efficacy in the field of damage detection for the past few decades. They are suitable for global vibration techniques as well as for local electromechanical impedance (EMI) techniques. However, the potential of the curved configuration of piezo sensors for damage detection is not yet analysed. The damage detection ability of CVEH (curved configuration) and CVS (straight configuration) sensors embedded inside an RC beam using the EMI technique are compared in this chapter.

4.2 EXPERIMENTAL SETUP DETAILS

The experiment is conducted on the same beam installed with CVS and CVEH as mentioned in the previous chapter. The piezo sensors are connected to the Agilent E4980A LCR meter, which is further connected to the laptop for data acquisition. Throughout the experiment, a room temperature of 29 ^{o}C is maintained, which is ensured using a La Crosse Technology WS-9006U model digital thermometer. The experimental setup is depicted in Figure 4.1.

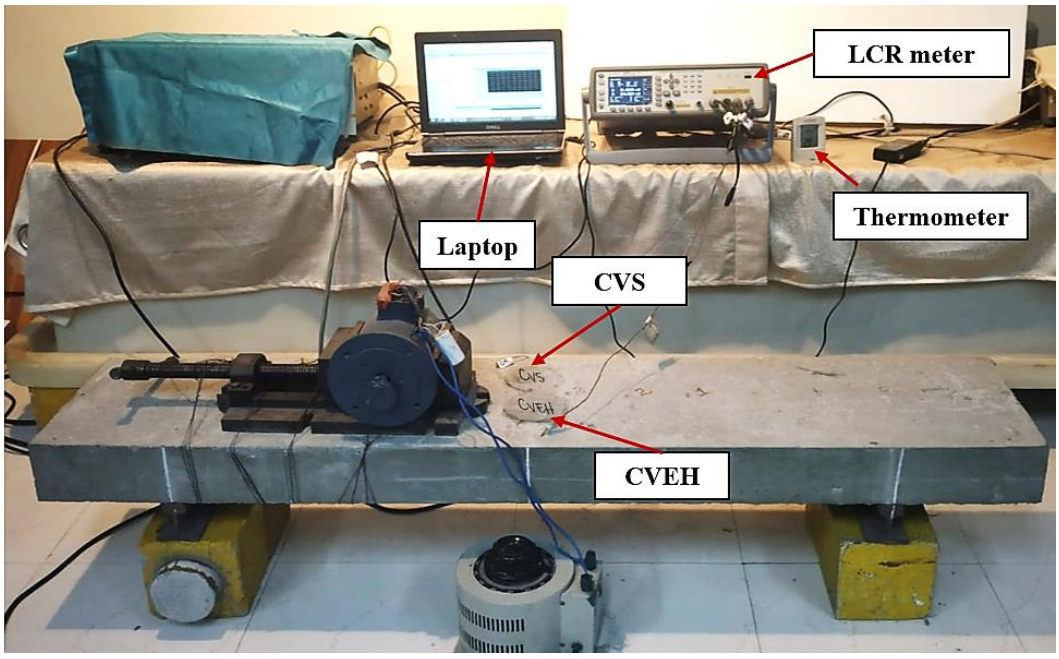

Figure 4.1: Experimental setup for damage detection in RC beam

The sensors are electrically excited by applying a harmonic electric potential across them in sweep mode with the LCR metre, and their corresponding admittance signatures (baseline signatures) are recorded. Damages are then induced in the structure by drilling three holes in the beam sequentially (equidistant from both CVS and CVEH), as illustrated in Figure 4.2. The associated admittance signatures are recorded after each damage is induced.

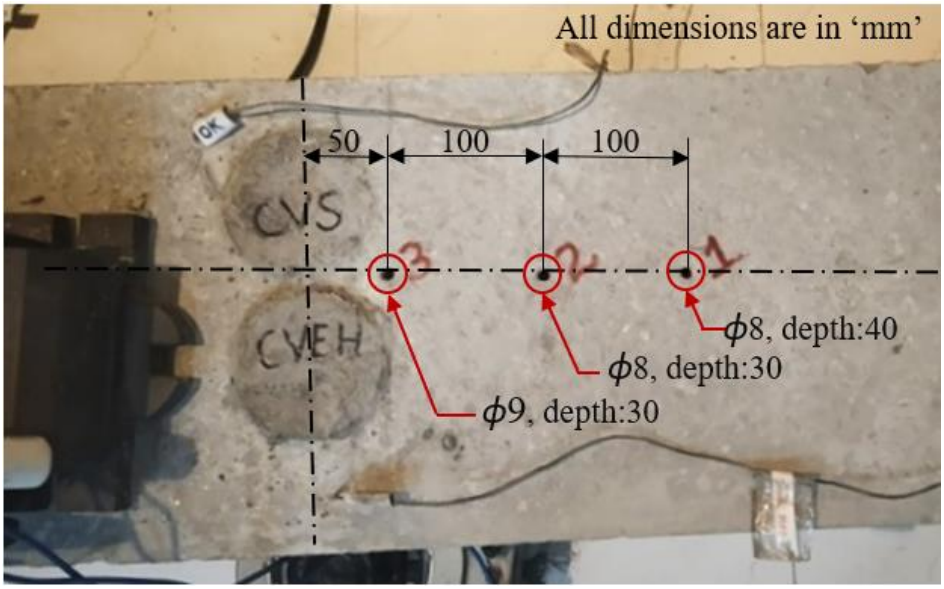

Figure 4.2: Damages induced in the RC beam

4.3 DAMAGE DETECTION POTENTIAL OF CVEH

For the inspection of damages in the RC beam, the admittance signatures are compared with the baseline signatures obtained during the healthy stage. In each stage (healthy stage and three damaged stages), the harmonic electric potential is applied across the piezo transducers in a coarser frequency range (1 kHz to 1000 kHz with a step interval of 1 kHz) as well as in a finer frequency range (100 kHz to 300 kHz with a step interval of 100 Hz). Two signatures are obtained in each case, and their correlation coefficient is calculated using Eq. (4.1). The correlation between the two signatures in each case shall be close to 1 if the sensors are working well. Identical signatures will not be generated if there is any failure or debonding of the MFC patch that leads to a decline in the value of the correlation coefficient. In this method, the Pearson correlation coefficient, a measure of the linear correlation between two samples of data, is used to check the correlation between two similar signatures.

The Pearson correlation coefficient is calculated as

$$CC = \frac{\sum_{i=1}^{n}(x_i - \bar{x})(y_i - \bar{y})}{\sqrt{\sum_{i=1}^{n}(x_i - \bar{x})^2}\sqrt{\sum_{i=1}^{n}(y_i - \bar{y})^2}} \tag{4.1}$$

where CC is the Pearson correlation coefficient, n is the sample size, x_i and y_i are the i^{th} values in the two signatures, and $\bar{x}$ and $\bar{y}$ represent the mean of the two signatures x and y respectively. In the experiment, a correlation coefficient greater than 0.99 is obtained in each case (refer Table 4.1), thereby ensuring the proper functioning of the sensors.

To quantify the variations in signatures from the baseline signature after inducing damages, the root mean square deviation (RMSD) value between the two is calculated using the Eq. (4.2) where n is the sample size, x_{di} and x_{hi} are the i^{th} values in the damaged and healthy signatures respectively.

$$RMSD(\%) = \sqrt{\frac{\sum_{i=1}^{n}(x_{di} - x_{hi})^2}{\sum_{i=1}^{n}x_{hi}^2}} \times 100 \tag{4.2}$$

From Figures 4.3 to 4.6, it is obvious that the deviation (leftward shift) of damaged signatures from healthy signatures is more significant in the CVEH than in the CVS. This leftward shift in the signatures represents the loss of stiffness in the structure due to the induced damage. Both conductance (real part of the admittance) and susceptance (imaginary part of the admittance) signatures corresponding to the wider range of frequencies ranging from 1 kHz to 1000 kHz are found to generate more reliable data for damage identification than the narrow range of frequencies from 100 kHz to 300 kHz. This is due to the significant peak observed in the former range. This eminent peak in the conductance signatures between 600 kHz and 800 kHz corresponds to the resonance frequency of the piezo transducer in the thickness mode. Therefore, it is always preferable to choose an excitation frequency range that includes such peaks. Figure 5.18 portrays the RMSD variation of the signatures in each case.

For 1 kHz to 1000 kHz excitation, the RMSD index of the conductance and susceptance signatures is significant in identifying the first and second damage. For CVEH and CVS, the RMSD index of conductance signature after second damage is 77% and 33% respectively. However, it has decreased to 34% and 20% respectively in the case of third damage. The shift of signatures has also changed the direction after the third damage. This is due to the limitation of the EMI technique. As the damage level escalates from incipient

to moderate, it becomes less distinguishable, though it is highly reliable for incipient damage cases (Kaur, 2015, Shanker et al., 2011). It is also notable that in all the three damaged stages, CVEH showed a higher RMSD index than the CVS. Similarly, the RMSD variation of susceptance signatures is also maximum for the second damage, with 91% and 37% respectively for CVEH and CVS, and decreased afterwards.

For 100 kHz to 300 kHz excitation, there is no substantial variation in the signatures, and therefore the RMSD values are less than 10% in each case. Minor variations in signatures may arise owing to external factors beyond our control. As a result, no valid conclusions can be drawn from these values. For this range of excitation, a performance comparison of CVEH and CVS for damage identification is also not possible as they do not follow a particular trend. Therefore, this frequency range is inappropriate for the current investigation.

Table 4.1: Correlation coefficient of the signatures

Signature 1	**Signature 2**	**1 kHz–1000 kHz**		**100 kHz–300 kHz**	
		CVEH	**CVS**	**CVEH**	**CVS**
Conductance Signatures					
Baseline 1	Baseline 2	0.9999	0.9999	1.0000	1.0000
1st damage 1	1st damage 2	0.9999	0.9999	1.0000	1.0000
2nd damage 1	2nd damage 2	0.9999	0.9999	1.0000	1.0000
3rd damage 1	3rd damage 2	0.9999	0.9999	1.0000	1.0000
Susceptance Signatures					
Baseline 1	Baseline 2	0.9999	0.9999	1.0000	1.0000
1st damage 1	1st damage 2	0.9999	0.9999	1.0000	1.0000
2nd damage 1	2nd damage 2	0.9999	0.9999	1.0000	1.0000
3rd damage 1	3rd damage 2	0.9999	0.9999	1.0000	1.0000

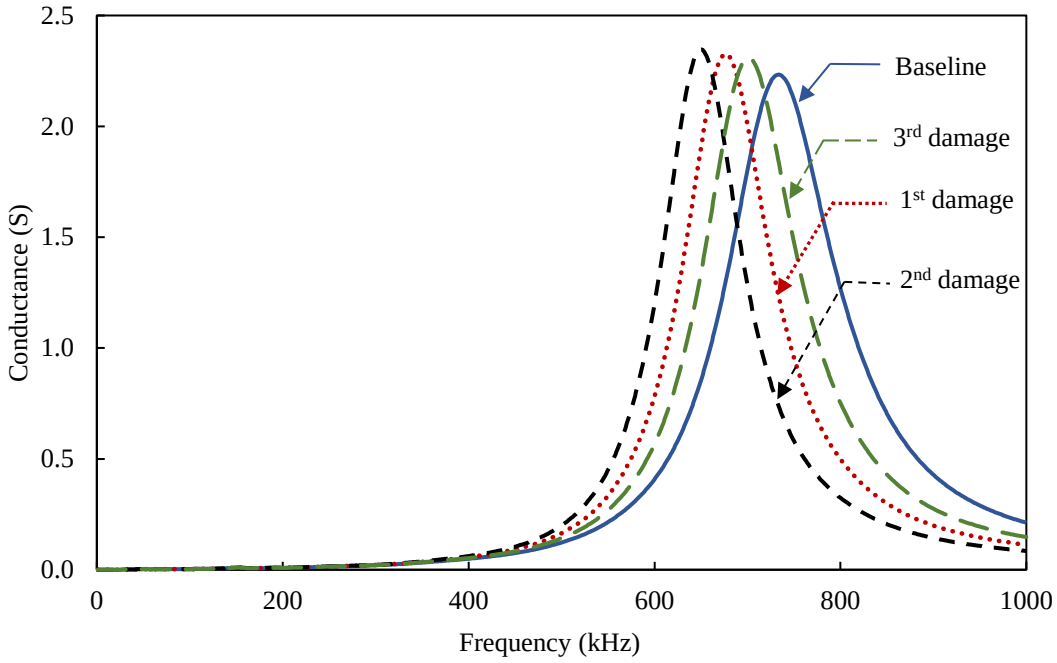

(a)

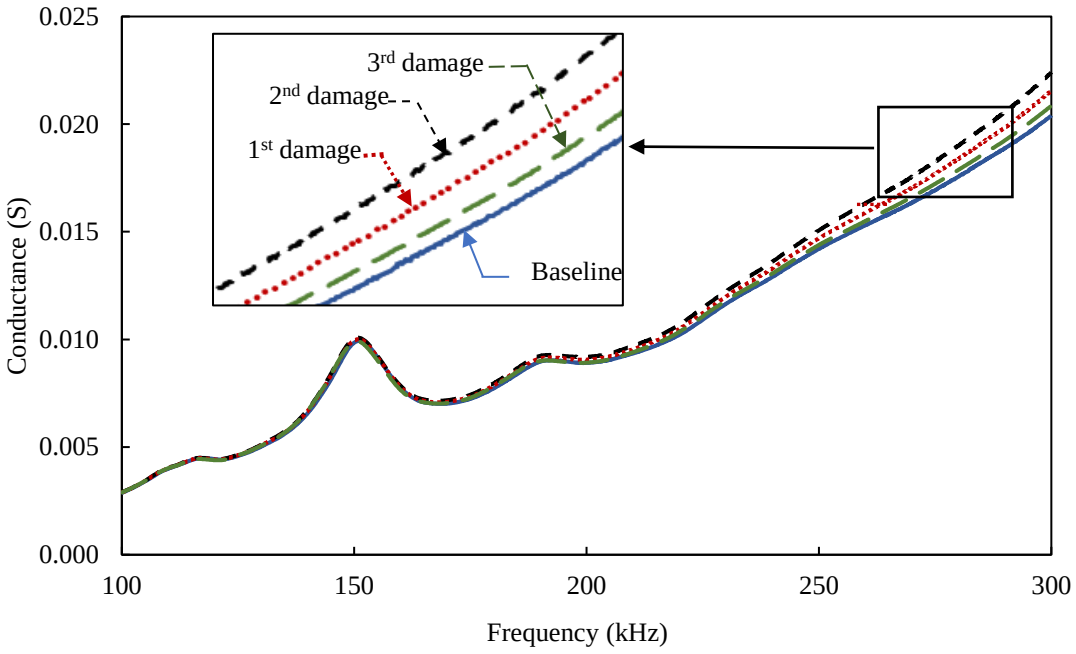

(b)

Figure 4.3: (a) Conductance signature of CVEH for a frequency range of 1 kHz to 1000 kHz

(b) Conductance signature of CVEH for a frequency range of 100 kHz to 300 kHz

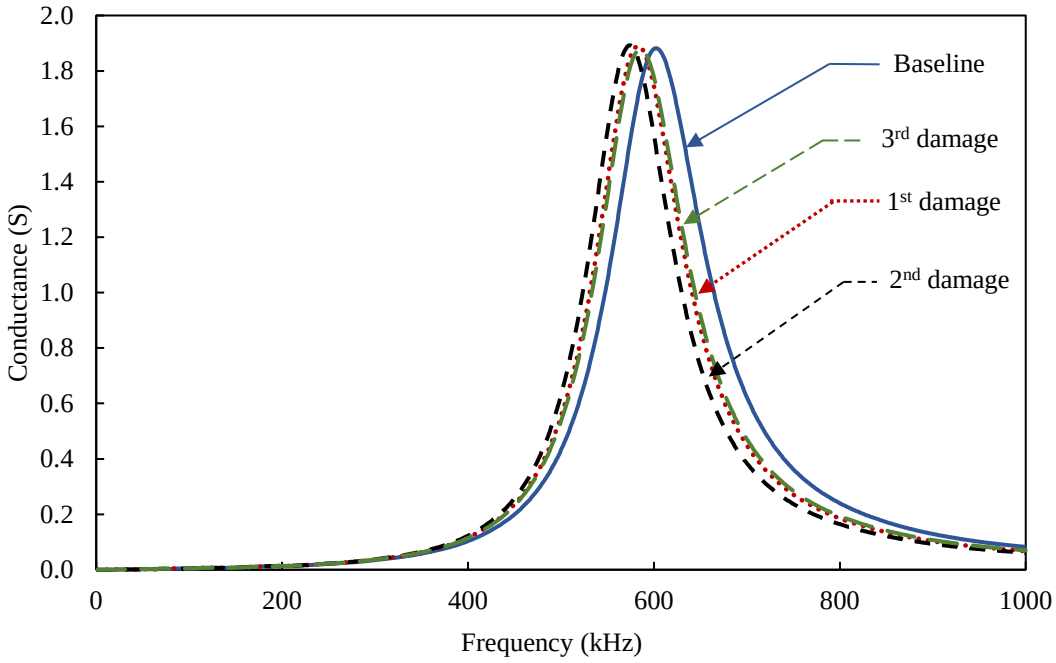

(a)

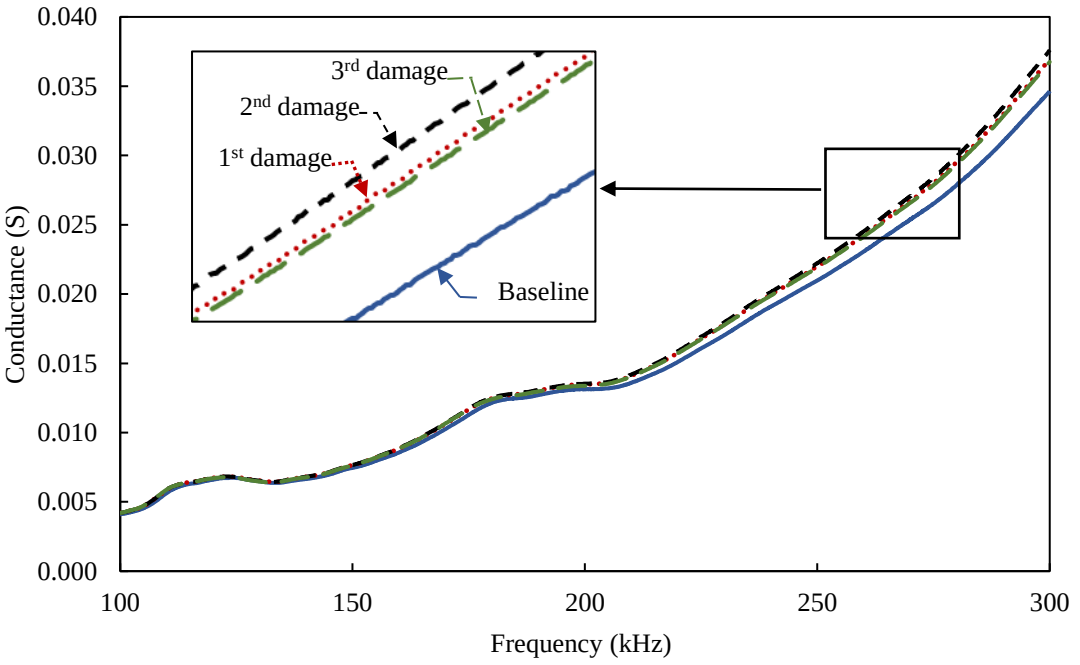

(b)

Figure 4.4: (a) Conductance signature of CVS for a frequency range of 1 kHz to 1000 kHz

(b) Conductance signature of CVS for a frequency range of 100 kHz to 300 kHz

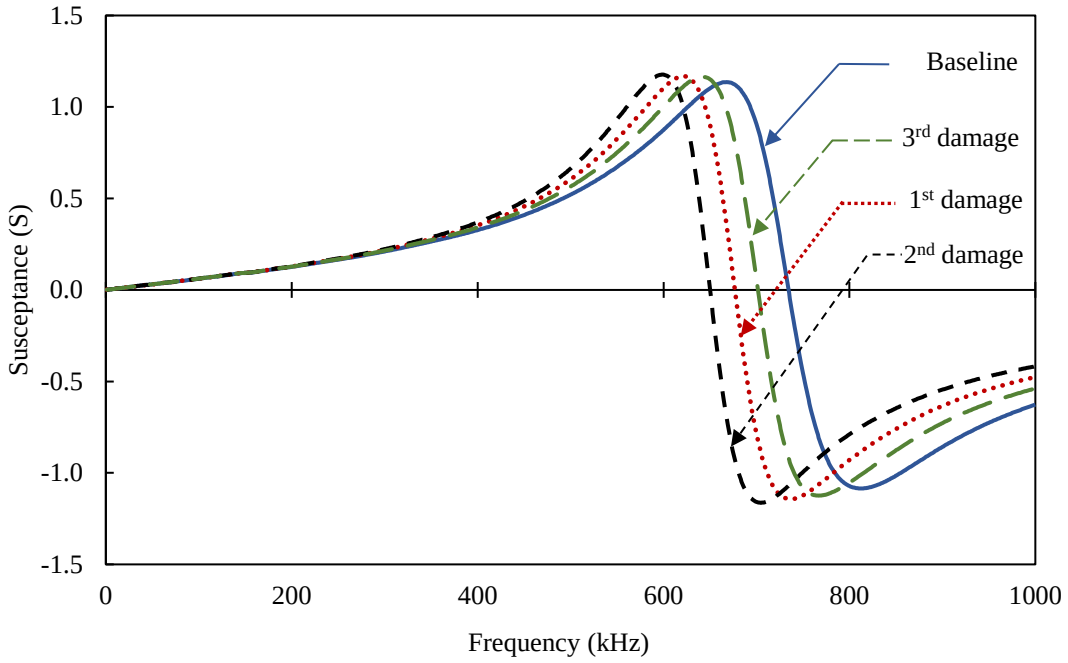

(a)

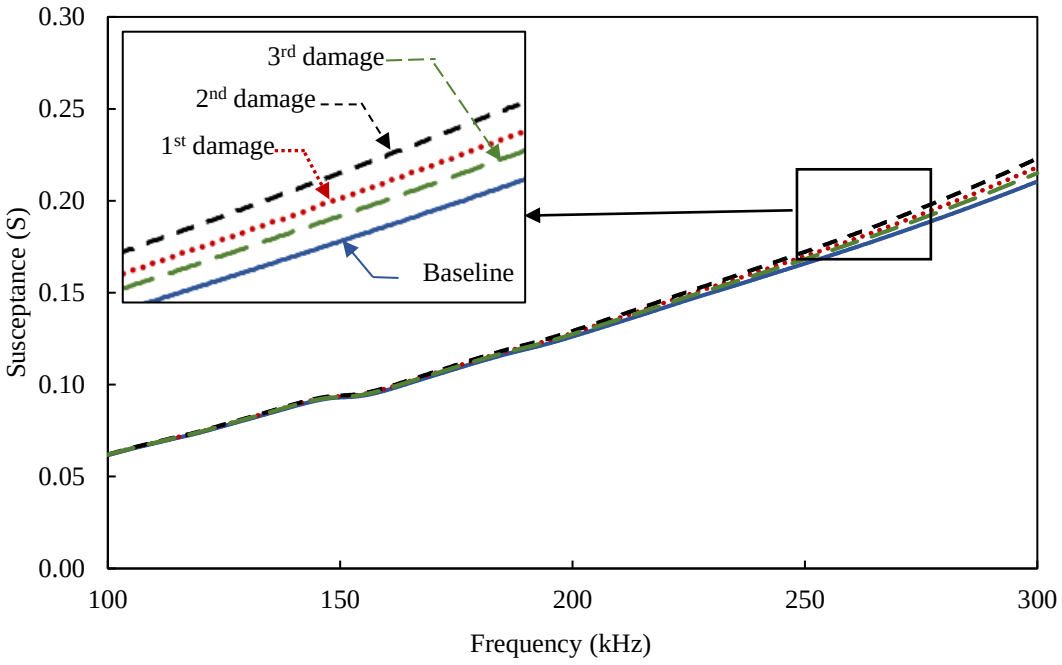

(b)

Figure 4.5: (a) Susceptance signature of CVEH for a frequency range of 1 kHz to 1000 kHz

(b) Susceptance signature of CVEH for a frequency range of 100 kHz to 300 kHz

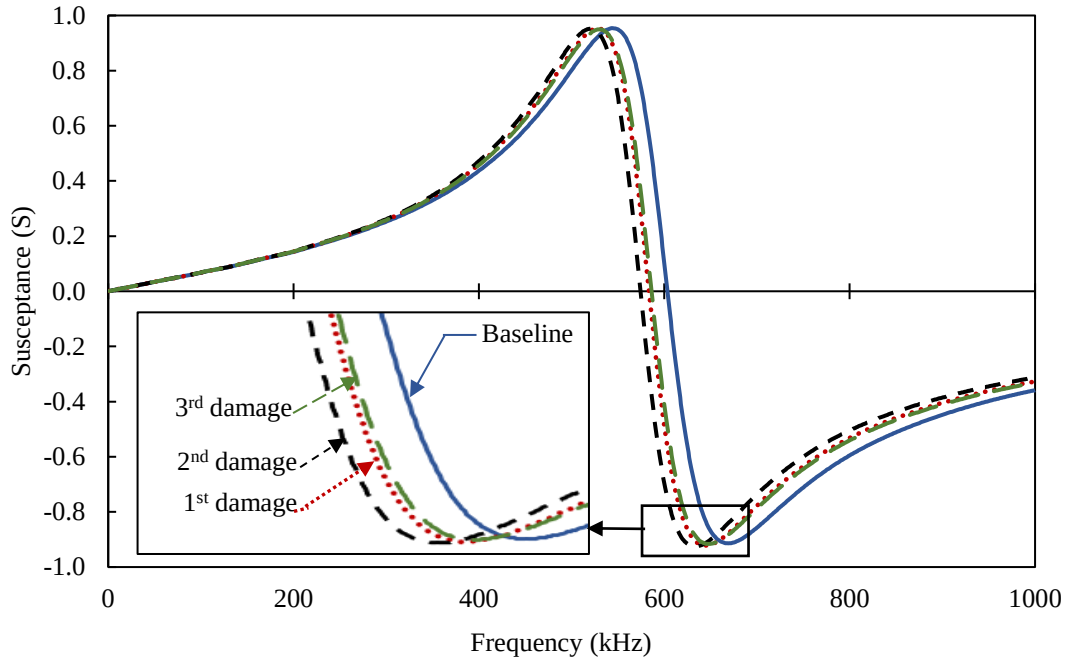

(a)

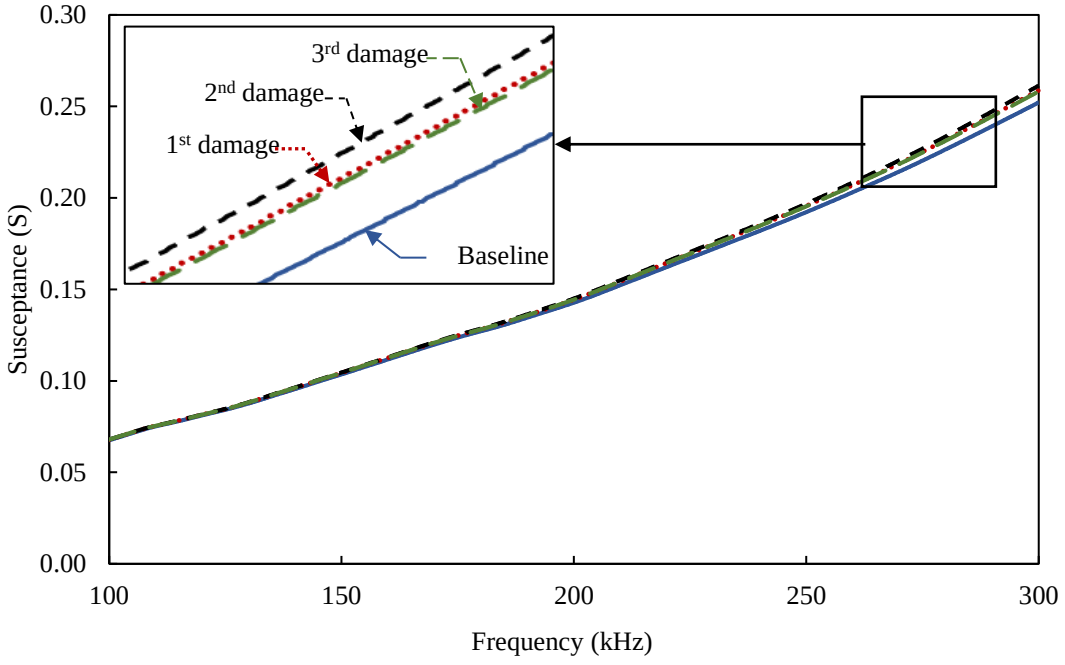

(b)

Figure 4.6: (a) Susceptance signature of CVS for a frequency range of 1 kHz to 1000 kHz

(b) Susceptance signature of CVS for a frequency range of 100 kHz to 300 kHz

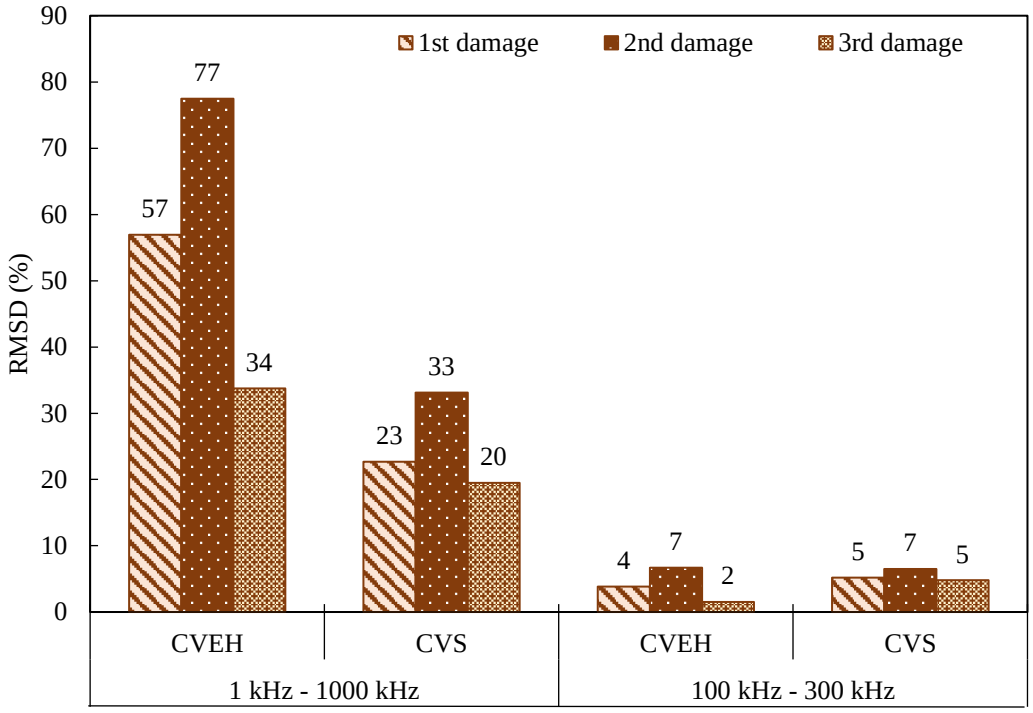

(a)

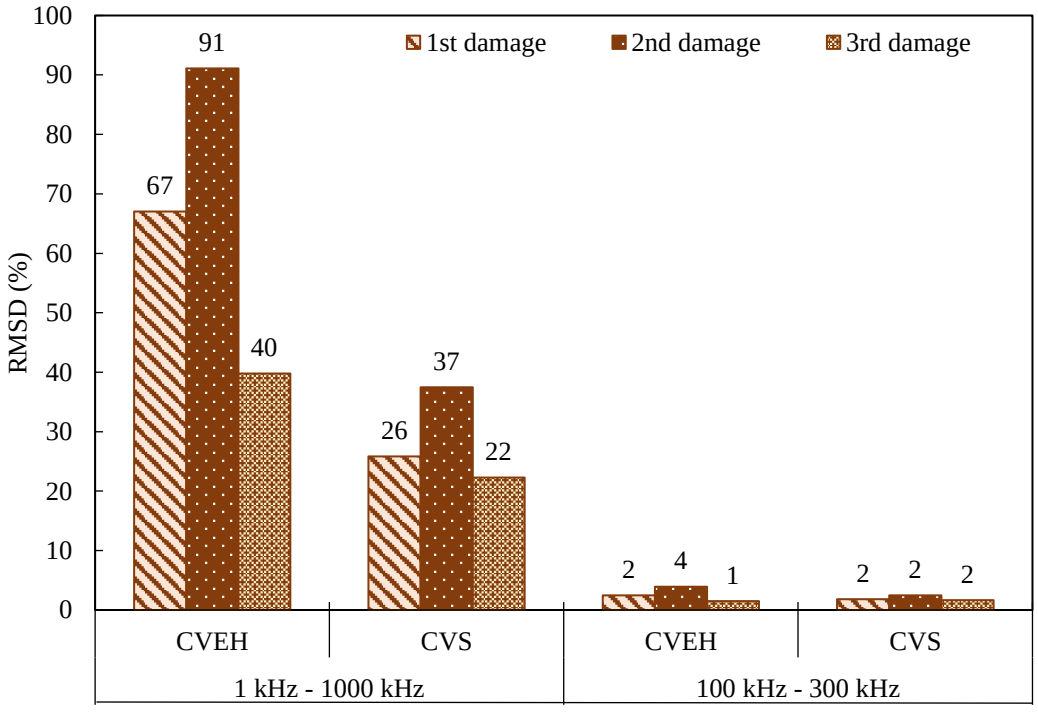

(b)

Figure 4.7: (a) RMSD index of conductance signatures

(b) RMSD index of susceptance signatures

4.4 EFFECT OF THE CURVATURE OF CVEH ON EMI SIGNATURES

In the previous section, it is observed that the curved configuration of the piezo transducer resulted in a higher RMSD index suggesting its suitability for damage detection. Also, the frequency range of 1 kHz to 1000 kHz provided better results, and therefore, the same frequency range is considered in this section as well. This section analyses the response of piezo transducers (MFC patches) when placed under two different curvatures while performing the EMI technique.

The MFC patch selected for the study is of the same model as mentioned in the previous section, i.e., the M5628-P2 model. The configurations considered for the study are (a) free MFC patch; (b) straight configuration of the MFC patch; (c) curved configuration with an angle of bend of 77 degrees; and (d) curved configuration with an angle of bend of 154 degrees. The MFC patches are kept in curved configurations by wrapping them on two concrete cylinders of diameters 100 mm and 50 mm using transparent tapes to make an angle of bend (θ) of 77 degrees and 154 degrees respectively. The experimental setup and configuration details are shown in Figures 4.8 and 4.9. The MFC transducers are electrically excited for a frequency range of 1 kHz to 1000 kHz with a step interval of 1 kHz using an Agilent E4980A LCR meter. The admittance signatures are captured for all the configurations and are depicted in Figure 4.10.

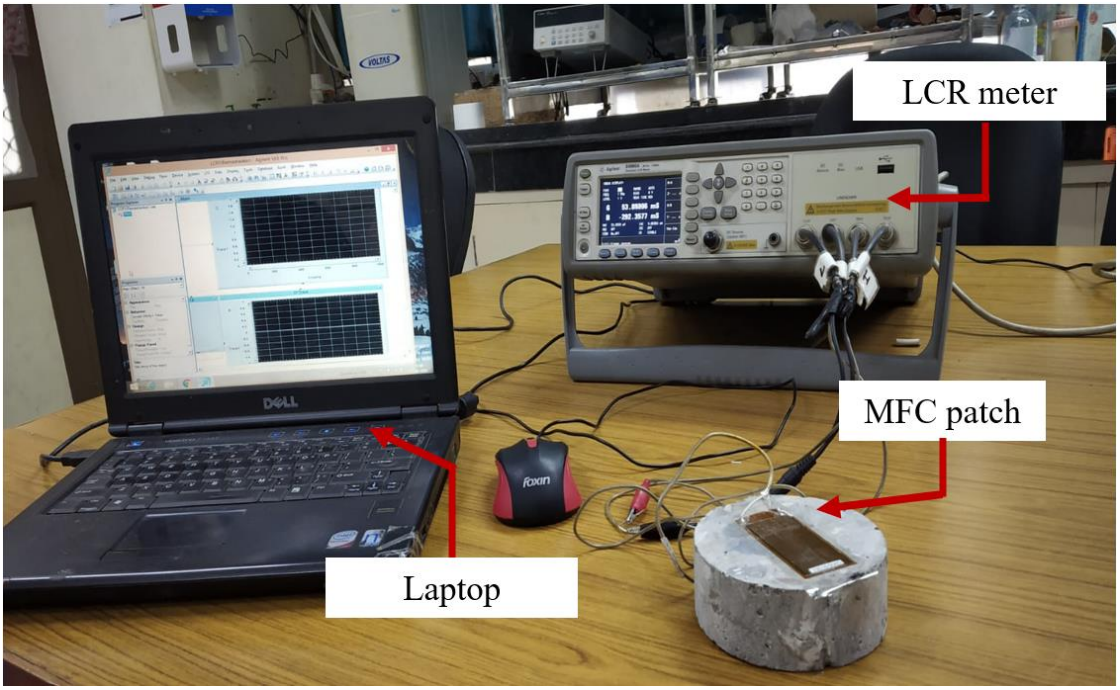

Figure 4.8: Experimental setup with MFC patch kept in straight configuration

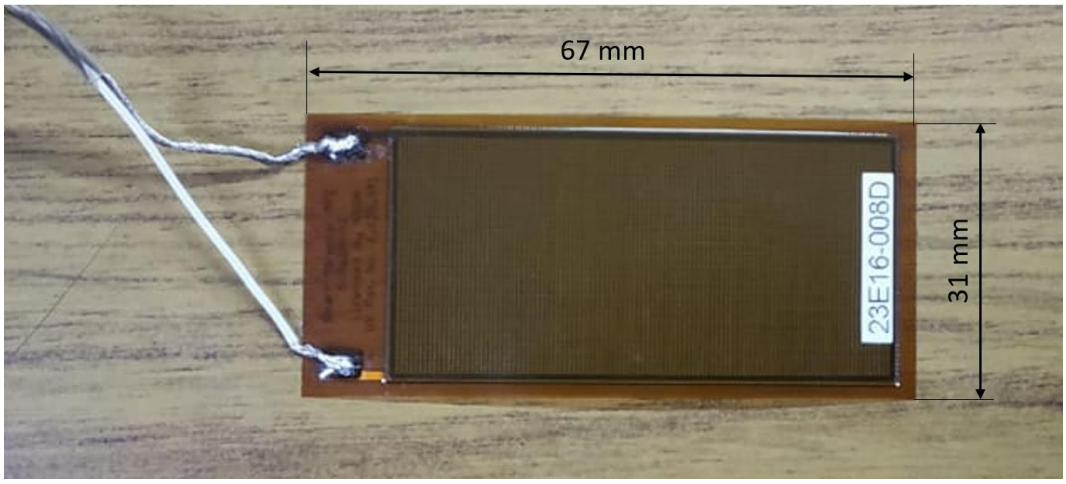

(a)

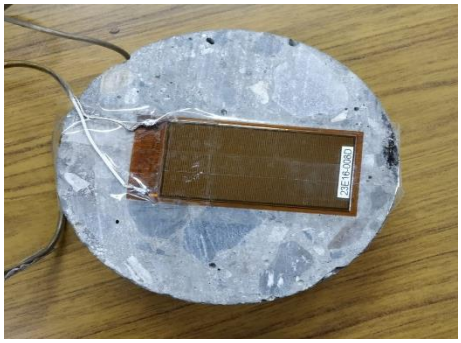

(b)

(c)

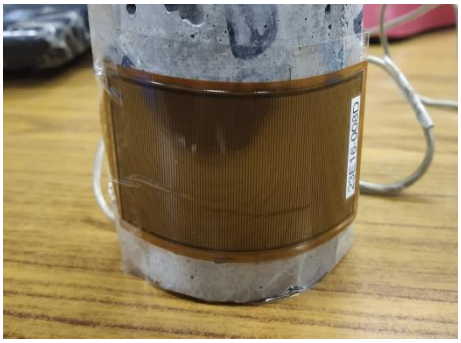

(d)

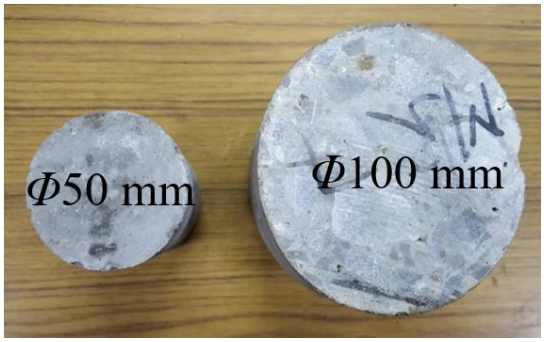

(e)

Figure 4.9: (a) Free MFC patch

(b) MFC patch placed in straight configuration

(c) MFC patch placed in curved configuration, θ = 77 deg

(d) MFC patch placed in curved configuration, θ = 154 deg

(e) Concrete cylinders used for making the desired curvatures

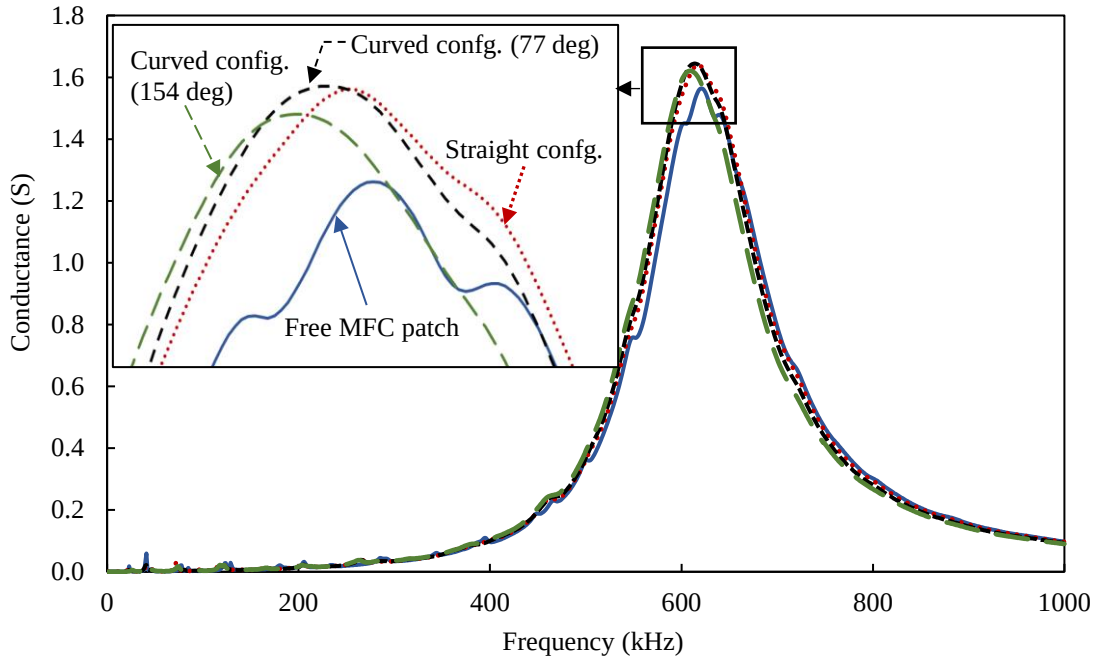

(a)

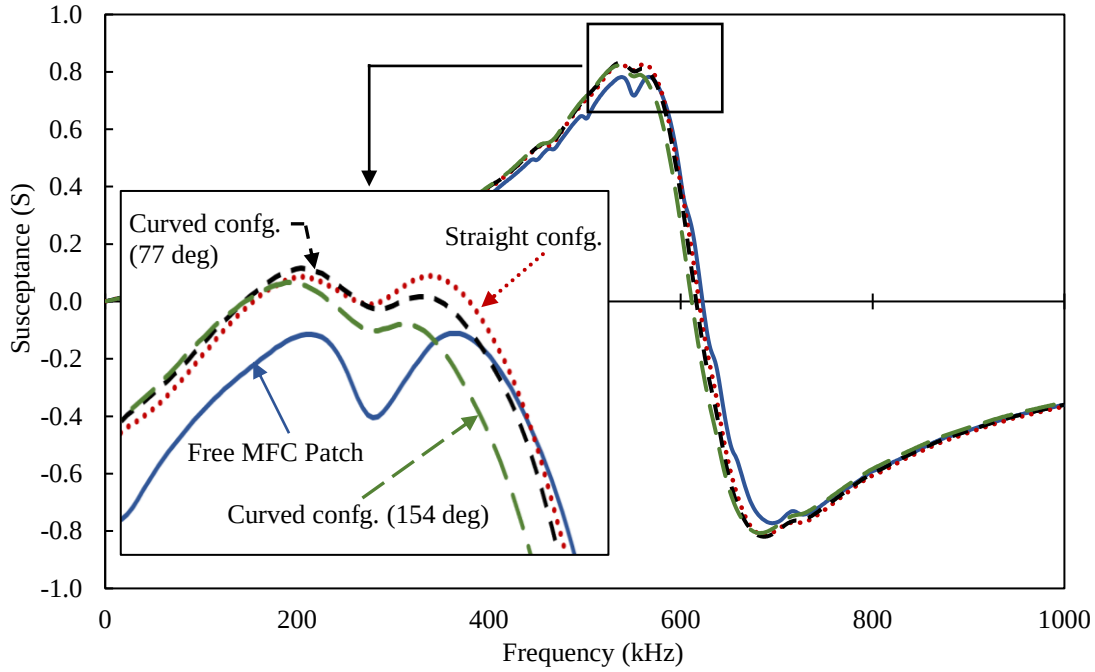

(b)

Figure 4.10: (a) Conductance signatures for various configurations of MFC patch
(b) Susceptance signatures for various configurations of MFC patch

From the figures, it is observed that the peak of the free MFC signature is of lesser magnitude than the other configurations. Also, the peak of the slightly curved arrangement (bend angle = 77 deg) is marginally greater than the straight one. The peak in the signature

has lessened as the bend angle has increased to 154 degrees. As the patch becomes more curved, the signatures begin to migrate to the left. Also, as we analyse the conductance signatures of CVS and CVEH (Figures 4.3(a) and 4.4(a)) mentioned in the previous section, a significant rise can be detected in the peak of CVEH's signature, which has a bend angle of about 60 degrees.

In short, slightly curved MFC patches generate higher magnitude peaks and highly curved transducers generate lower magnitude peaks than the straight configuration. So, the optimum bend angle for acquiring the maximum peak in the signatures might be below 77 degrees. However, the magnitude of the peak in the signatures is not the criteria to analyse the damage detection potential of the transducers, it is the shift in their signatures after damage or the RMSD values between the healthy and damaged signatures. Therefore, a 3-D FE analysis is recommended to arrive at the optimum curvature of the MFC patch or piezo transducer for structural health monitoring.

4.5 SUMMARY

The damage detection potential of CVEH has been examined in this chapter by using the EMI technique. The admittance signatures of the RC beam before and after inducing damages are compared for the damage diagnosis. The study considers two excitation ranges: (a) 1 kHz to 1000 kHz and (b) 100 kHz to 300 kHz. The former range of electrical excitations is proven to yield more reliable results in damage identification than the latter range, where no proper interpretations have been drawn. The response of the CVEH in terms of the shift in the signatures or RMSD index is substantially higher than the CVS. The chapter has also presented the effect of the curvature of CVEH in EMI signatures. The slightly curved CVEH is found to generate higher peaks in the admittance signatures. A thorough FE analysis is recommended since the peak in signatures is not the criteria for analysing the damage detection potential of CVEH. The results of the entire investigation proved for the first time that the CVEH is also suitable for SHM in addition to energy harvesting. The forthcoming chapter covers the numerical and analytical analysis of CVEH relative to CVS for energy harvesting.

CHAPTER 5

NUMERICAL AND ANALYTICAL INVESTIGATIONS OF CVEH FOR ENERGY HARVESTING

5.1 INTRODUCTION

The experimental investigations have been performed in chapter 3 to analyse the energy harvesting potential of CVEH relative to CVS. The effect of various parameters such as curvature, thickness, the position of placement, etc. of CVEH for energy harvesting is not analysed in the previous chapters as the whole experiments are conducted using a particular CVEH. Therefore, this chapter numerically analyses the effect of such parameters of CVEH for energy harvesting by the method of finite element (FE) analysis using 3D elements. The commercially available FE modelling software, COMSOL Multiphysics version 4.4, MEMS module, is used for the numerical investigation. As a preliminary study toward the formulation of a closed-form solution of the voltage generated by the curved piezo transducers, analytical modelling is also performed towards the end of the chapter, and the effect of the curvature and thickness of the transducer is analysed.

5.2 DETAILS OF 3-D FE MODELLING

Three-dimensional models of the RC beam with CVS/CVEH embedded at its mid-span are developed in the COMSOL 4.4 FE software. The dimensions of the beam considered for the study are 3000 mm × 300 mm × 500 mm. The length, breadth, and depth of the beam are taken along the global X, Y, and Z directions respectively. The beam is simply supported, with supports being considered at 100 mm from both ends of the beam. The grade of the concrete is M30. The major physical properties of the beam and the piezo transducer are listed in Table 5.1. Concrete is considered as linearly elastic and isotropic material. The reinforcement bars are ignored in the model.

CVS and CVEH are considered as concrete cylinders of the same grade as that of the beam/element in which it has to be installed, with dimensions of 100 mm diameter and 30 mm height. The piezo transducers are embedded in the concrete cylinders in straight and curved configurations for CVS and CVEH respectively. These are embedded in such a way that the centroid of the cylinder and the transducer coincides. The piezo transducer considered for the study is the same M5628-P2 model MFC patch utilised for the

experimental investigations in the previous chapter. Though the actual thickness of the MFC transducer is 300 μm, it is taken as 1 mm in the model due to the difficulty in meshing the minute dimensions in the COMSOL 4.4 version for higher curvatures of the piezo transducer. As it is a comparative study between the CVS and CVEH models, the change in thickness will not affect the relative voltage generated in both cases. The piezoelectric properties of the MFC patch considered for the study are listed in Table 5.2. The CVS or CVEH, whichever the case may be, are placed inside the beam so that the top surface of the CVS/CVEH coincides with that of the beam, and is placed centrally with respect to the plan dimension of the beam, as shown in Figure 5.1.

Table 5.1: Properties of the RC beam and piezo (MFC) patch

Sl No	Parameter	RC Beam	Piezo patch
1	Length (L)	3000 mm	56 mm
2	Breadth (B)	300 mm	28 mm
3	Depth (D)	500 mm	1 mm
4	Density (ρ)	2500 kg/m^3	5440 kg/m^3
5	Young's Modulus (Y)	27.3×10^9 Pa	
6	Poisson's ratio (μ_r)	0.3	0.3
7	Mass (m)	375 kg/m	0.15 kg/m

The 'Piezoelectric Devices Interface' listed under the category of 'Structural Mechanics' has been utilised for the FE modelling of the MFC transducer. The interface has the ability to simulate both the direct as well as the converse piezoelectric effects by the method of piezoelectric coupling using stress or strain charge formulations. The strain charge form is considered for the current study. Makkonen et al., (2001) provides the detailed procedure for the finite element formulations and coupled field analysis of the piezoelectric materials. Free tetrahedral elements are used for the FE analysis. As the piezo transducer considered for the study is a d_{31} variant, the poling direction of the transducer is normal to its surface. However, in the COMSOL 4.4 software, the poling direction is taken along the global Z direction. For CVS, this poling direction is in agreement with the actual poling direction, whereas for CVEH, each point has a different polling direction due to its curvature. Therefore, the best way to model the curved patch is to consider it as a

combination of numerous linear elements with the poling direction taken normal to each element by the method of coordinate transformation. For the current study, the curved piezo transducer is modelled as a combination of 5 linear elements, as shown in Figure 5.2. Also, the 3-D models of the CVS and CVEH are depicted in Figure 5.3.

As the piezo transducer is supposed to act as an electric circuit, ground condition or electric potential equal to zero condition is applied to the top surface of the MFC patch. The bottom surface of the same is considered as terminal 1 with a terminal charge equal to zero coulombs. A dynamic load of 1 kN is applied at a point at a one-fourth distance from the left end of the beam. The frequency of the load considered for the study ranges from 70 Hz to 100 Hz with an interval of 5 Hz. A frequency-domain analysis is performed in COMSOL 4.4 for various curvatures of CVEH, and the voltage generated is determined.

Table 5.2: Piezoelectric properties considered for the study (Kaur, 2015 and Smart Materials, 2021)

Sl. No.	Parameters	Symbols	Values	Unit
1	Compliance matrix	$[S^E]$	$\begin{matrix} 15 & -4.5 & -5.7 & 0 & 0 & 0 \\ 0 & 19 & -5.7 & 0 & 0 & 0 \\ 0 & 0 & 19 & 0 & 0 & 0 \\ 0 & 0 & 0 & 39 & 0 & 0 \\ 0 & 0 & 0 & 0 & 39 & 0 \\ 0 & 0 & 0 & 0 & 0 & 49.4 \end{matrix}$	$(\times 10^{-12})$ Pa^{-1}
2	Coupling matrix or piezoelectric strain coefficients	$[d^E]$	$\begin{matrix} 0 & 0 & 0 & 0 & 0 & 0 \\ 0 & 0 & 0 & 0 & 0 & 0 \\ 2.1 & 2.1 & 0 & 0 & 0 & 0 \end{matrix}$	$(\times 10^{-10})$ C/N
3	Relative permittivity	ξ_r	$\begin{matrix} 1977.4 & 0 & 0 \\ 0 & 1977.4 & 0 \\ 0 & 0 & 2395.5 \end{matrix}$	-
4	Dielectric loss factor	δ_{ES}	0.02	-
5	Compliance Matrix loss factor	η_{CE}	0.02	

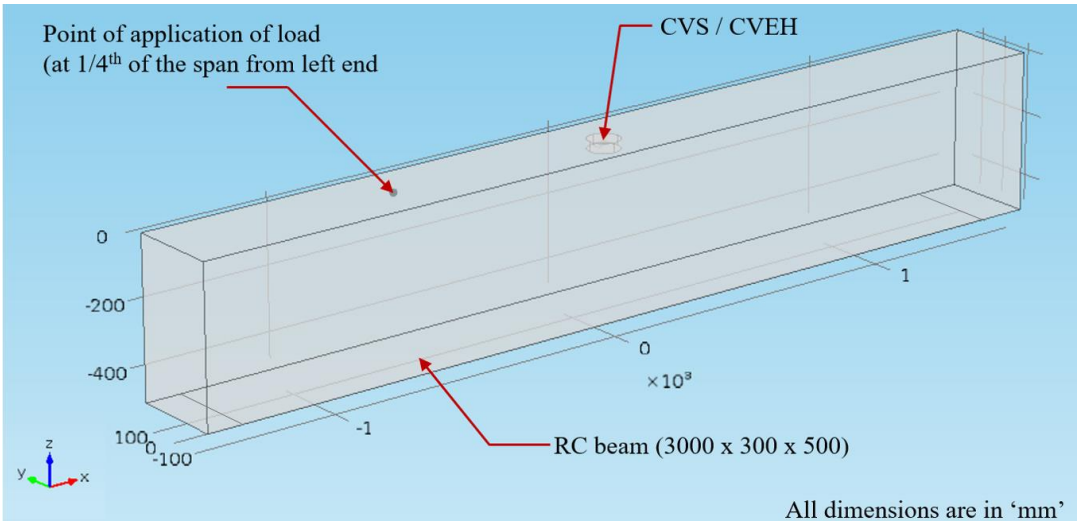

Figure 5.1: Isometric view of the RC beam with CVS/CVEH embedded inside

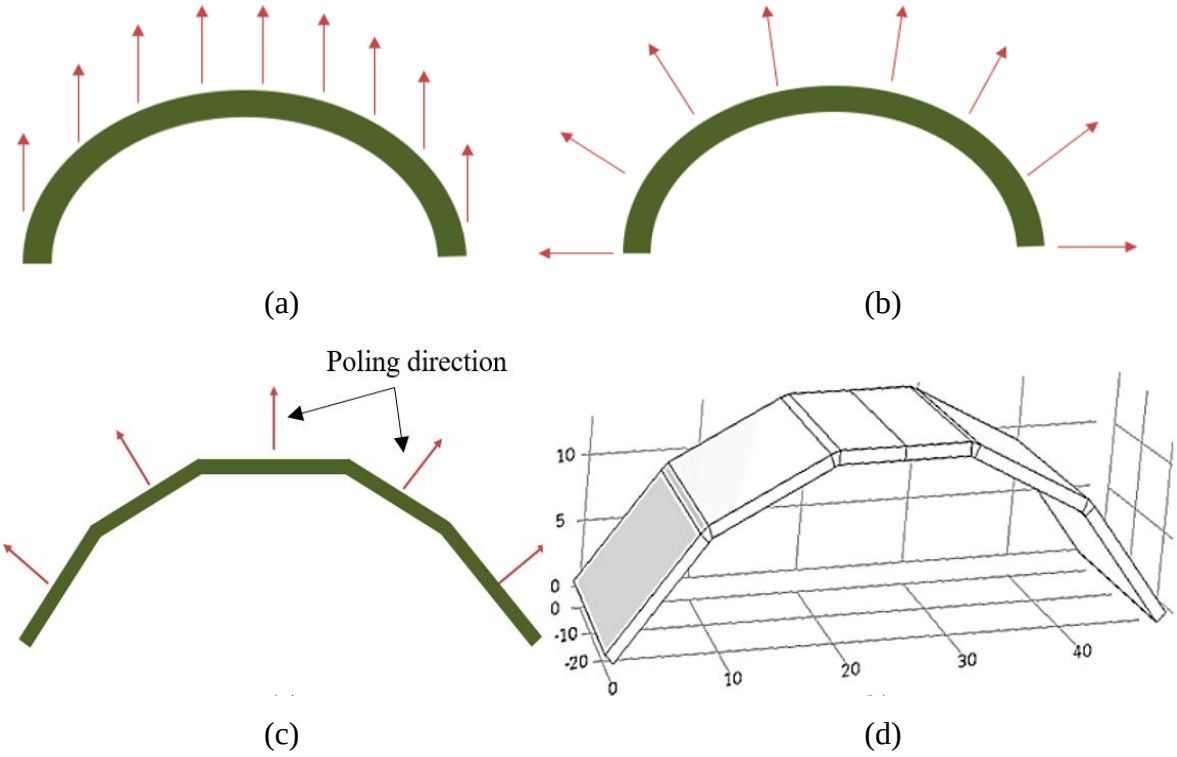

Figure 5.2: (f) Direction of polarisation considered in COMSOL 4.4 FE software

(g) Actual direction of polarisation

(h) Line model of curved piezo transducer considered for the study

(i) 3-D model of the piezo transducer developed in COMSOL 4.4

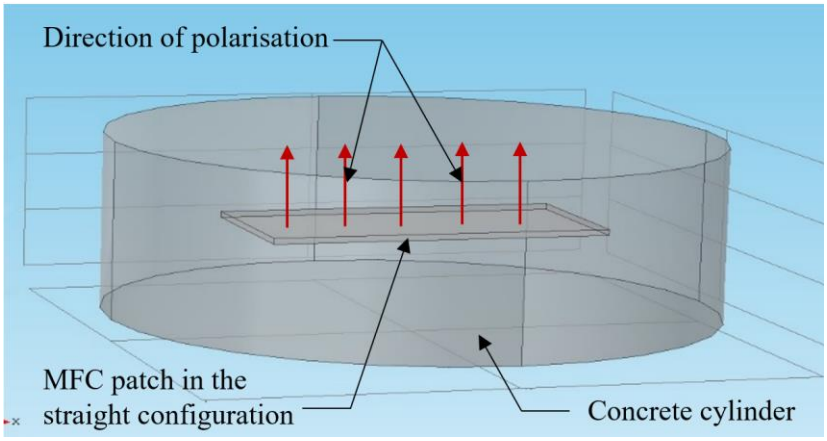

(a)

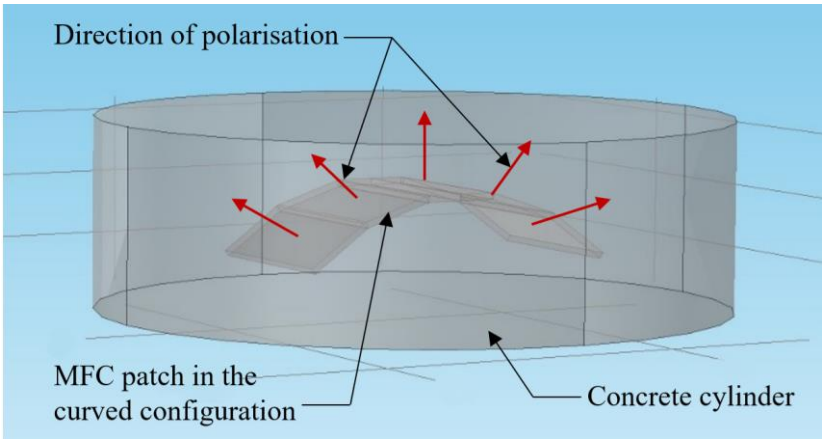

(b)

Figure 5.3: (a) CVS model in COMSOL 4.4 FE software
(b) CVEH model in COMSOL 4.4 FE software

5.3 MODEL VALIDATION

The natural frequency of the simply supported beam is determined analytically as 83 Hz as per the Eq. (5.1), where f_n is the natural frequency of the beam in Hz, E is the modulus of elasticity in N/m^2, I is the moment of inertia in m^4, m is mass per unit length in kg/m and L is the effective length of the beam in meters.

$$f_n = \frac{\pi}{2}\sqrt{\frac{EI}{mL^4}} \tag{5.1}$$

When the external load frequency matches the natural frequency of the beam, the beam experiences maximum vibration, and therefore, the voltage developed across the transducer

reaches its maximum value. According to the frequency analysis conducted on the 3-D FE model, the peak value of voltage for both CVS and CVEH is acquired at 85 Hz, as shown in Figure 5.4, which closely matches the natural frequency of the beam calculated analytically (83 Hz). This validates the designed model to a certain extent.

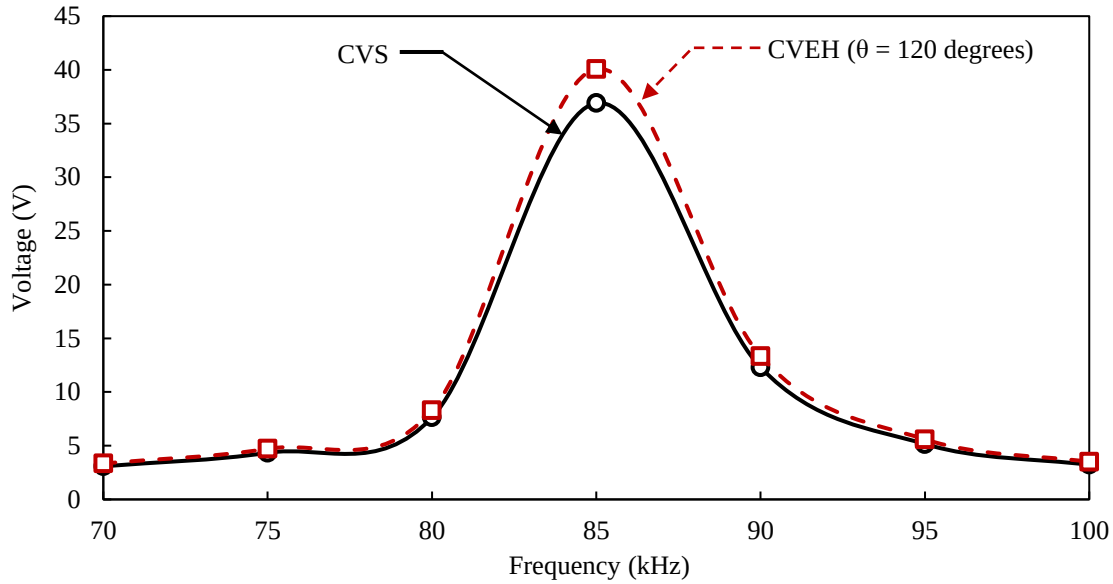

Figure 5.4: Voltage vs frequency plot for CVS and CVEH (angle of bend =120^{o})

5.4 EXPERIMENTAL VALIDATION OF THE FE ANALYSIS

The experimental validation is conducted on the same RC beam of grade M30 and dimensions 1500 × 300 × 100 mm mentioned in chapters 3 and 4. The beam is placed in a simply supported condition with an effective span of 1300 mm. The angle of bend of the CVEH installed in the beam at the mid-span is approximately 60 degrees. The major properties of the beam and the piezo transducer are given in Table 5.3.

The CVEH is connected to the TDS 2004B oscilloscope to capture the response signals, and the impact load is applied using a hammer at a one-fourth distance from the left end of the beam, as shown in Figure 5.5. The time-domain response is converted to the frequency domain using the Fast Fourier Transform (FFT). A 3-D model of the experimental beam with CVEH (angle of bend = 60 degrees) embedded at its mid-span is developed in COMSOL 4.4, as shown in Figure 5.6. The response of CVEH as per the FE analysis is compared with the experimental results, and is plotted in Figure 5.7.

As per the analytical analysis based on Eq. (5.1), the natural frequency of the beam model is 88.8 Hz and the peak voltages are expected to occur at this frequency. The FE analysis and experimental analysis suggest the natural frequency of the beam as 90 Hz and

89.6 Hz respectively, which is in close agreement with the analytical value, and thereby validates the FE analysis.

Table 5.3: Properties of the experimental RC beam and the piezo transducer

Sl No	Parameter	RC Beam	Piezo transducer
1	Length (L)	1500 mm	56 mm
2	Breadth (B)	300 mm	28 mm
3	Depth (D)	100 mm	0.3 mm
4	Density (ρ)	2500 kg/m^3	5440 kg/m^3
5	Young's Modulus (Y)	27.3*10^9 Pa	
6	Poisson's ratio (μ_r)	0.3	0.3
7	Mass (m)	75 kg/m	0.045 kg/m

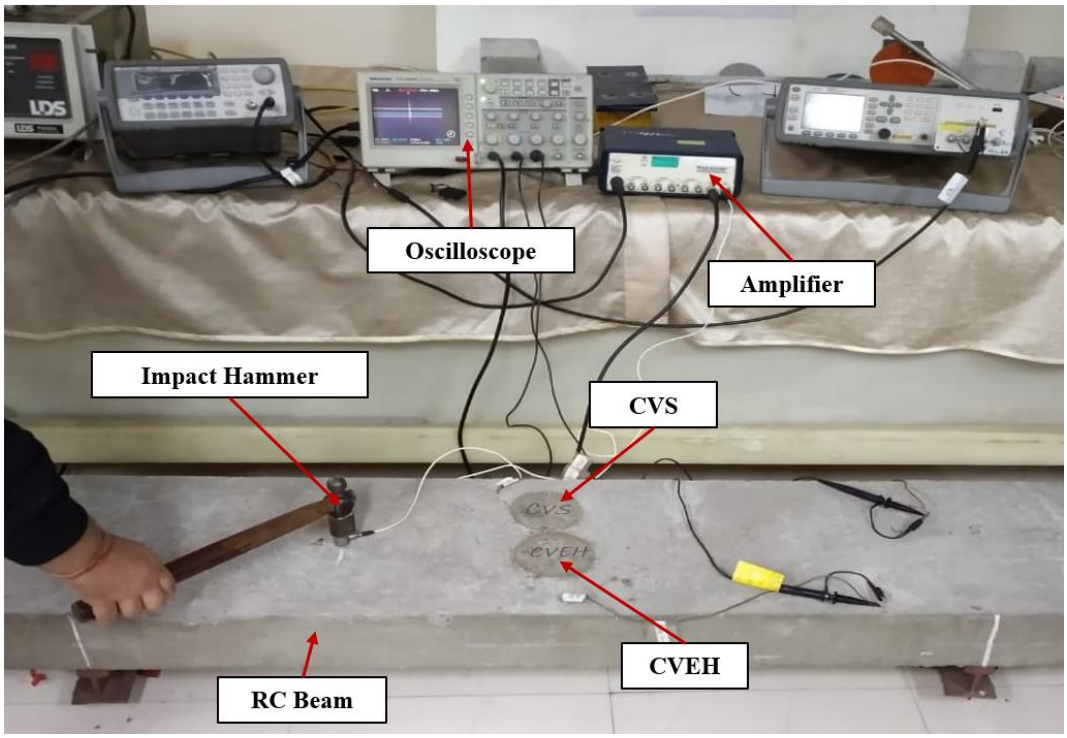

Figure 5.5: Experimental setup

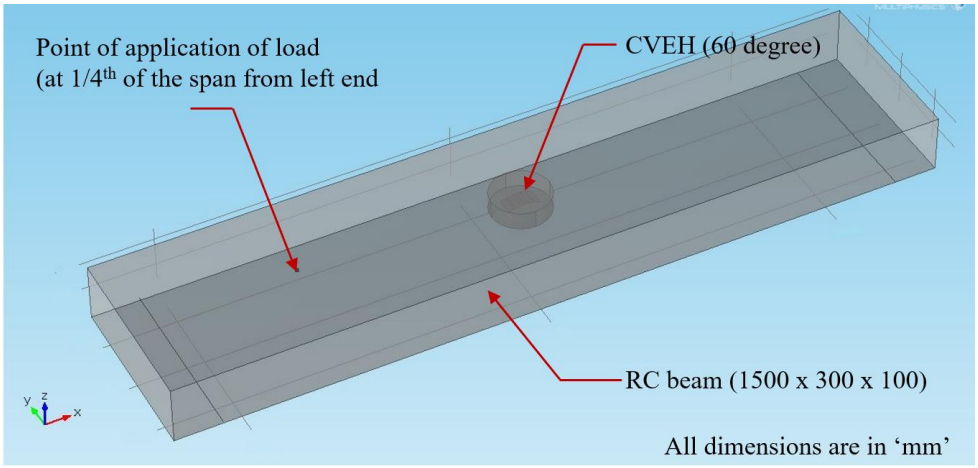

Figure 5.6: COMSOL model of the experimental beam

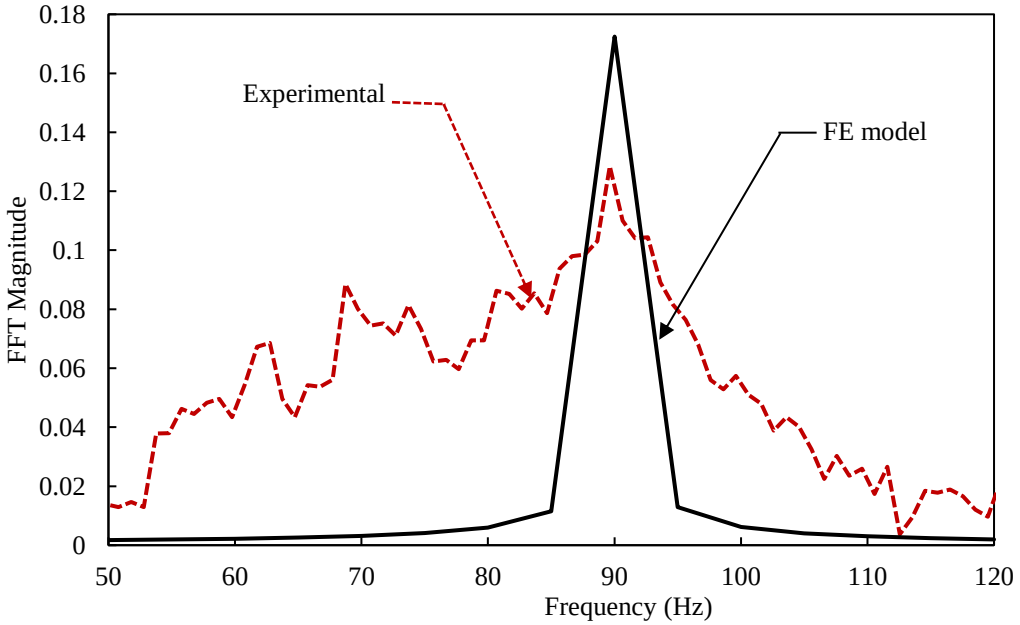

Figure 5.7: Results of the experimental and 3-D analysis

5.5 EFFECT OF THE CURVATURE OF PIEZO TRANSDUCER

Various configurations of CVEH embedded inside the RC beam are developed in COMSOL 4.4, as per section 5.1, to analyse the relative piezoelectric energy harvesting capacity of each system. A sweep analysis is conducted for frequencies ranging from 70 Hz to 100 Hz with a step interval of 5 Hz, and the results are plotted in Figure 5.8 (a). The peak voltage is obtained when excited at its natural frequency for all the curvatures or angles of bend, and it matches with the theoretical natural frequency of 83 Hz based on Eq. (5.1). The peak voltage developed across the piezo transducer is least for the straight configuration. Though the peak voltage rises with the curvature of CVEH, a deviation is

observed in the 170 degrees curved model. Therefore, further study is conducted to analyse the variation of peak voltage for a wide range of curvatures of CVEH by exciting the structure at its natural frequency. The results of the analysis are depicted in Figure 5.8 (b).

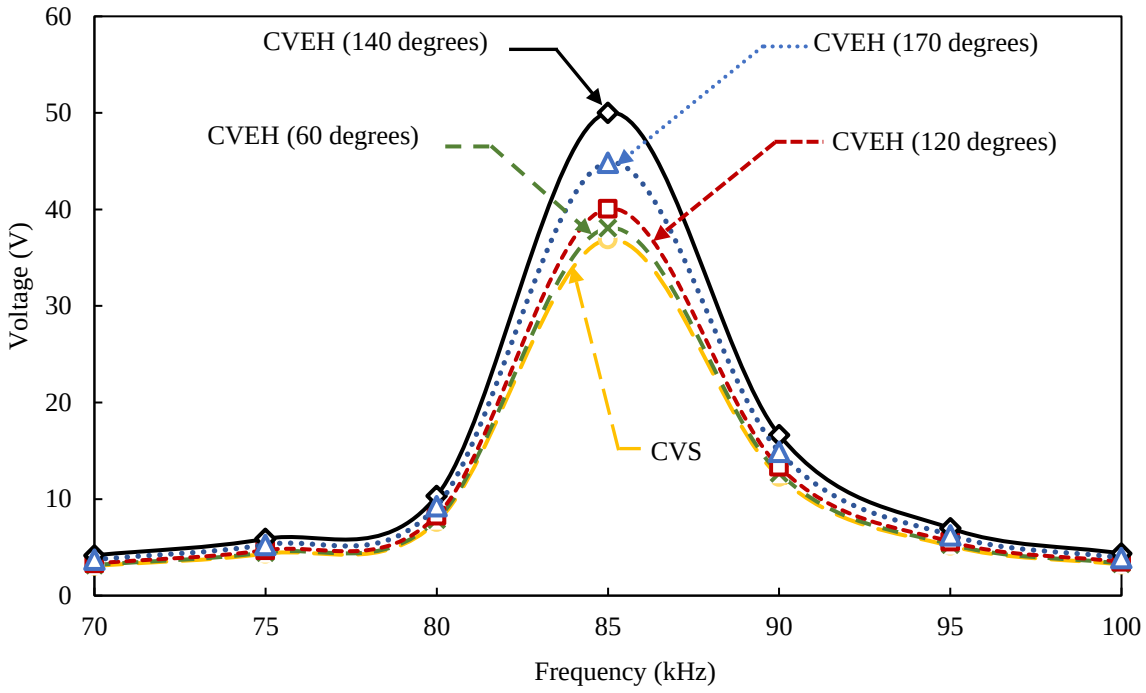

(a)

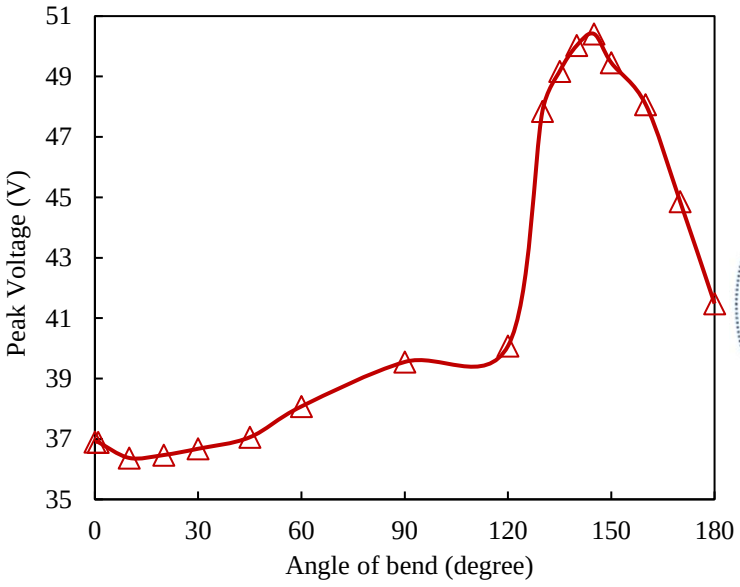

(b)

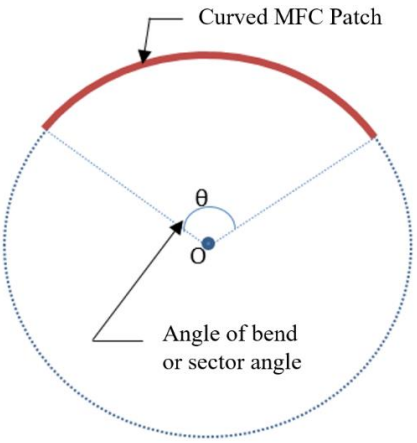

(c)

Figure 5.8: (a) Voltage vs frequency plot for CVS and various curvatures of CVEH
(b) Variation of peak voltage with respect to the angle of bend
(c) 1-D model of the curved MFC patch depicting the angle of bend

From the figures, it is observed that for very small sector angles, i.e., up to 30 degrees, voltage shows a decreasing trend with the curvature. However, after 30 degrees, the curved configuration generates a higher voltage than the straight configuration. For angles of bend between 30 degrees and 120 degrees, the increase in voltage with respect to the angle of bend is at a slow rate whereas it has a significant effect beyond 120 degrees. Therefore, a sector angle or angle of bend between 120 degrees to 180 degrees can be considered the optimum range of curvature for piezoelectric energy harvesting with maximum peak voltage at 145 degrees curved configuration.

5.6 EFFECT OF MODEL REFINEMENT

The studies mentioned in the previous section are conducted on 5-element CVEH models, and a 145-degrees (the optimum angle of bend) curved configuration generated 1.4 times higher voltage than the straight configuration. An increase in the number of linear elements in the curved transducer model can give a better representation of the actual configuration of the transducer. Hence, an 11-element model and a 15-element model are also generated, as shown in Figure 5.9 (a) and (b) respectively for 145 degrees bend. Sweep analysis is performed on these models, and the results are plotted in Figure 5.10. It is observed that the peak voltage is increasing with the increase in the number of elements considered in the model. A higher peak is observed in the 15-element model, which is 1.63 times that of the CVS model. However, convergence can be observed in the results of 11 and 15-element models, pointing out that a 15-element model is a good representation of the actual system.

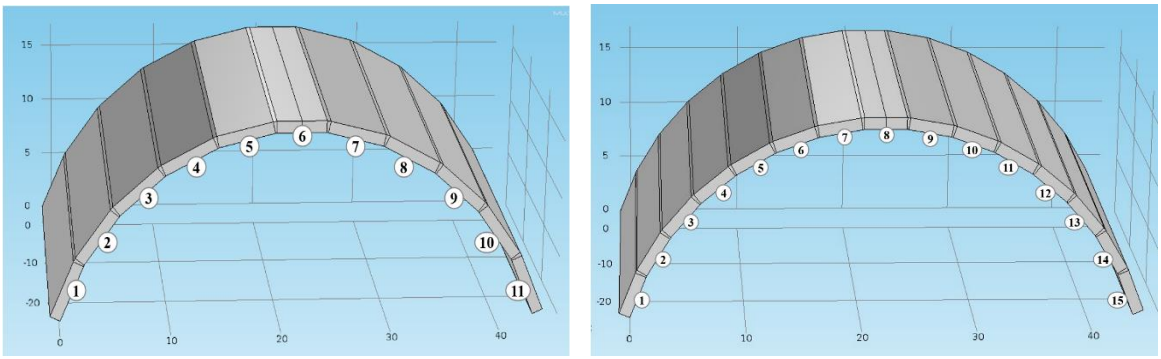

(a) (b)

Figure 5.9: (a) 11-element model of CVEH (θ =145 degree) developed in COMSOL 4.4
(b) 15-element model of CVEH (θ =145 degree) developed in COMSOL 4.4

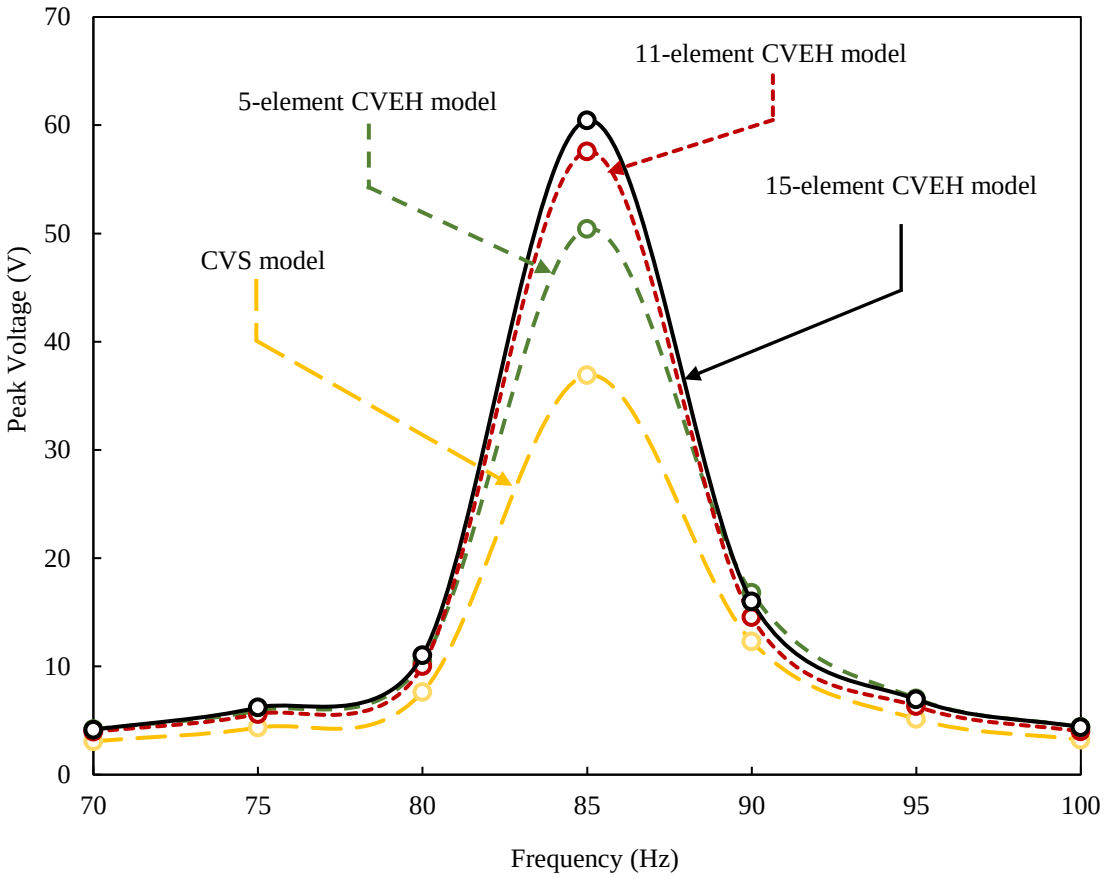

Figure 5.10: Voltage comparison of CVS, 5-element, 11-element and 15-element models of the CVEH (θ =145 degree)

5.7 EFFECT OF THE THICKNESS OF PIEZO TRANSDUCER

To analyse the effect of thickness of the piezo transducer in voltage generation, FE models mentioned in the previous section are redesigned for various values of thickness of the transducer, and are analysed for an excitation frequency of 85 Hz. The thickness range of the piezo transducer considered for the study is 0.6 mm to 1.5 mm. A sweep analysis is also conducted for more clarity regarding the effect of thickness in voltage generation, and the results are presented in Figures 5.11 (a) and (b). The findings of the analysis portray that the thickness of the piezo transducer has a favourable effect on boosting the voltage generated. This is analogous to the trend of embedded CVS in RC beams, as mentioned by Kaur and Bhalla, (2016).

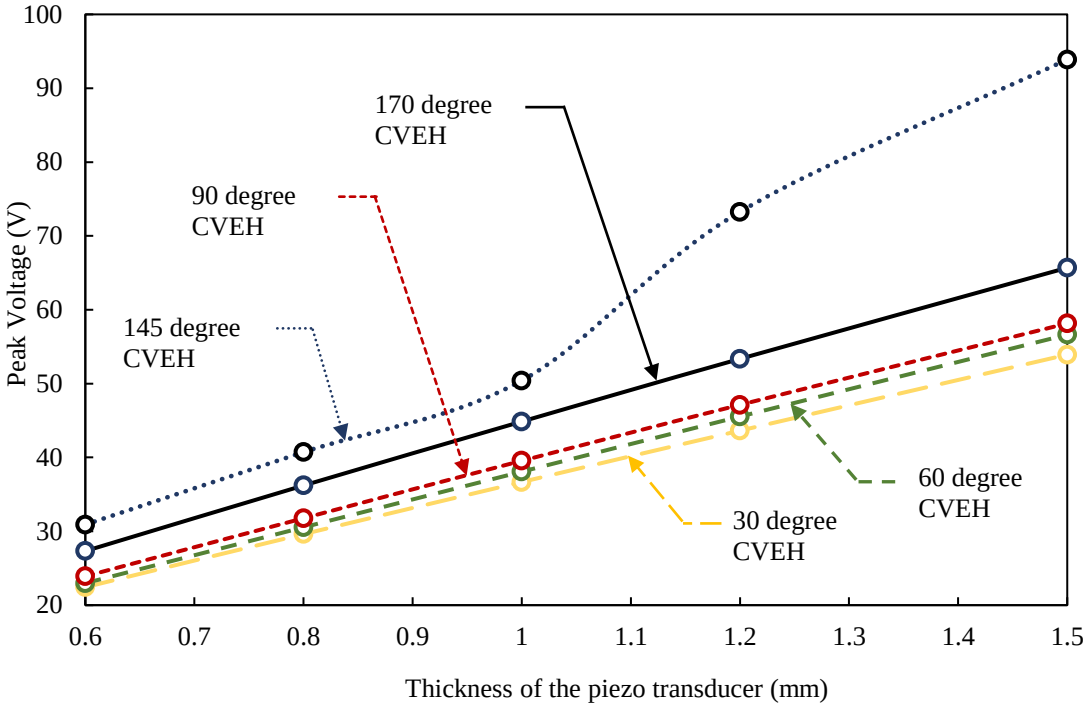

(a)

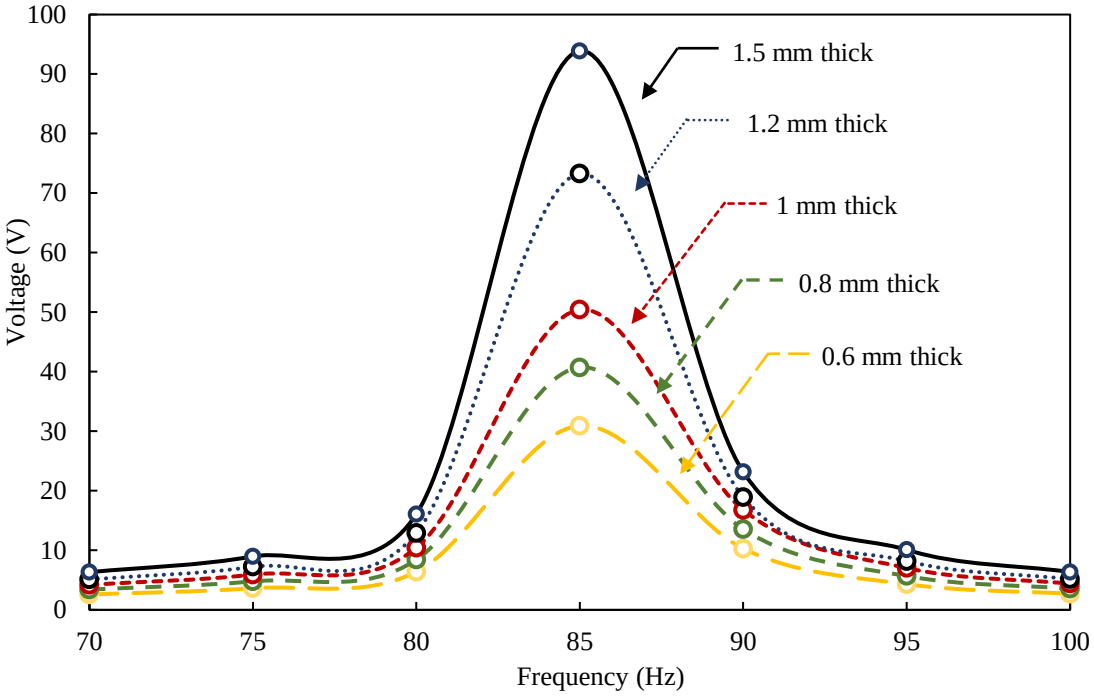

(b)

Figure 5.11: (a) Voltage vs thickness of the piezo transducer for various curvatures of CVEH

(b) Voltage vs frequency plot for various thicknesses of the piezo transducer (θ =145 degree)

5.8 EFFECT OF THE LOCATION OF CVEH

It is necessary to find the position at which CVEH has to be placed along the depth of the beam to obtain maximum voltage. A sweep analysis is therefore conducted by varying the position of CVEH along the depth of the beam for the same load at a frequency of 85Hz. The results of the analysis are plotted in Figure 5.12.

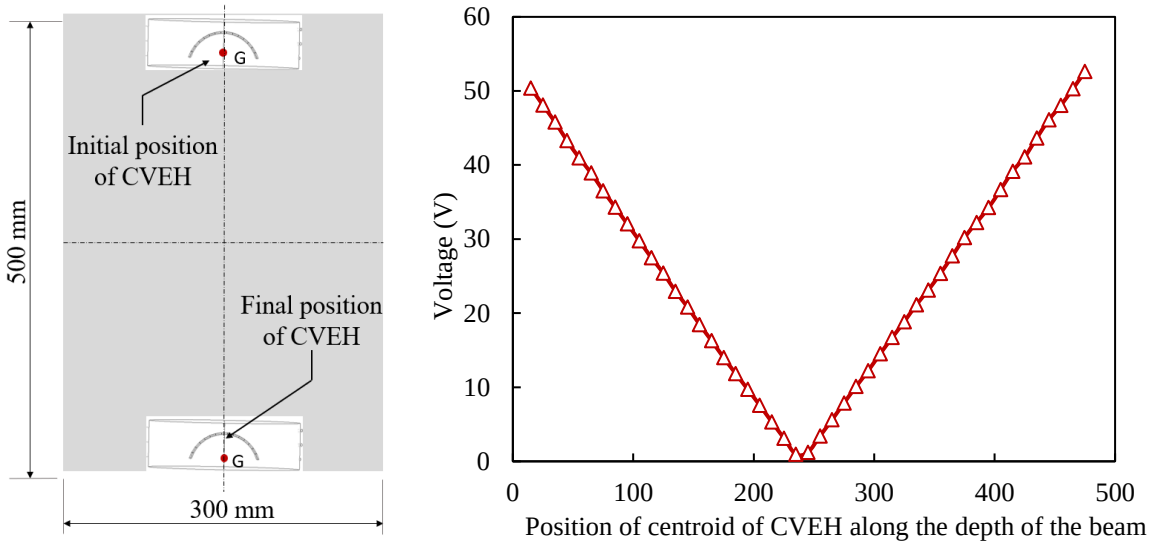

(a) (b)

Figure 5.12: (a) Cross-section of the RC beam showing the initial and final position of CVEH *(Figure not to scale)*

(b) Variation of voltage generated for various positions of CVEH along the depth of the beam

From the figures, it is observed that the maximum voltage is generated when CVEH is placed towards the top or bottom of the beam whereas almost no voltage is generated when CVEH is at the mid-depth of the beam. This is because the strain developed in a beam under bending action is maximum at the extreme fibres, and reduces linearly to zero towards the centre of the beam cross-section. Also, as per the direct effect of piezoelectricity, the mechanical stress or strain (S) applied across the piezoelectric material is directly proportional to the terminal voltage (V) developed across them, as depicted by Eq. (2.3). Therefore, the same effect of linear reduction can be seen in the voltage generated across the piezo transducer towards the mid-depth of the beam. Hence, it is suggested to embed the CVEH either towards the top or bottom surface of the beam, where the strain development is maximum.

The FE analysis and the associated parametric studies conducted so far provide an insight into the practical deployment of CVEH in RC structures for energy harvesting. The

experimental investigations to analyse the efficacy of CVEH for energy harvesting and SHM are already covered in the previous chapters. However, the analytical modelling of CVEH embedded inside RC beams for energy harvesting and SHM has not been conducted so far, and no closed-form solution of the voltage generated by the curved piezo transducers has been derived. Therefore, the study is further extended to the analytical modelling of curved piezo transducers for energy harvesting.

5.9 ANALYTICAL MODELLING OF CURVED PIEZO TRANSDUCERS FOR ENERGY HARVESTING

A simply supported RC beam (3000 mm × 300 mm × 500 mm) of grade M30, with an MFC transducer embedded at its mid-span, is chosen as the model. A MATLAB code is formulated utilising the concepts of the direct stiffness approach. The beam with a piezo transducer embedded inside is considered as a 2-D skeletal structure in the analysis. The identical parameters of the beam and piezo transducer that are addressed in the numerical analysis (Table 5.1) are considered in the analytical modelling.

The direct stiffness approach is a matrix method for determining the member forces and displacements in structures by making use of the stiffness relations of the members. It is the most popular implementation of the FE method. In this method, the entire system is modelled as a set of idealised elements interconnected at the nodes, as shown in Figure 5.13. Each element is considered as a structure, and the stiffness matrix of each element is formulated. In this analysis, the entire structure is divided into 32 nodes and elements, each element is considered as a 1-D element. The stiffness matrix in the local coordinates $[K]_L$ for a beam element is as follows:

$$[K]_L = \begin{bmatrix} \frac{EA}{L} & 0 & 0 & -\frac{EA}{L} & 0 & 0 \\ 0 & \frac{12EI}{L^3} & \frac{6EI}{L^2} & 0 & -\frac{12EI}{L^3} & \frac{6EI}{L^2} \\ 0 & \frac{6EI}{L^2} & \frac{4EI}{L} & 0 & -\frac{6EI}{L^2} & \frac{2EI}{L} \\ -\frac{EA}{L} & 0 & 0 & \frac{EA}{L} & 0 & 0 \\ 0 & -\frac{12EI}{L^3} & -\frac{6EI}{L^2} & 0 & \frac{12EI}{L^3} & -\frac{6EI}{L^2} \\ 0 & \frac{6EI}{L^2} & \frac{2EI}{L} & 0 & -\frac{6EI}{L^2} & \frac{4EI}{L} \end{bmatrix} \quad (5.2)$$

As the MFC patch is having a curved configuration, the transformation matrix [*T*] is used for the coordinate transformation from local to global coordinates. The global stiffness matrix $[K]_G$ for each element is thus calculated as

$$[K]_G = [T]^T [K]_L [T] \tag{5.3}$$

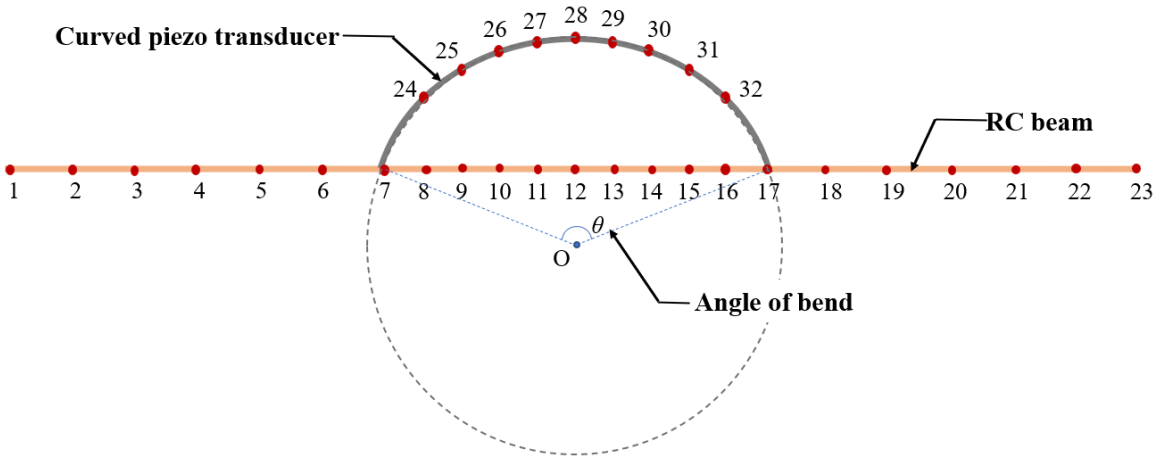

Figure 5.13: 2-D skeletal model of the RC beam with curved piezo transducer (*Figure not to scale*)

The total stiffness matrix [*K*] of the entire structure is then formulated by superimposing the global stiffness matrices of the elements at the designated locations so that an element of [*K*] equals the sum of the corresponding elements of global member stiffness matrices of corresponding degrees of freedom of the members connected to that joint. The total stiffness matrix is generated using the code number approach. According to this approach, every degree of freedom of the members in global coordinates corresponds to a specific degree of freedom of the entire structure. These details are determined and stored in the association matrix. Therefore, based on the association matrix, the total stiffness matrix can be generated accurately. The mass matrix is developed considering that the masses are lumped at each node.

Dynamic analysis based on Galerkin finite discretization is performed to determine the displacements at every node. The dynamic equation of motion considered for the analysis is given by Eq. (5.4), which is further reduced to Eq. (5.5), where the damping matrix [*C*] is formulated based on Eq. (5.6) (Tanwar,2021).

$$[M][\overline{\ddot{u}}]+[C][\overline{\dot{u}}]+[K][\overline{u}]=[\overline{F}] \tag{5.4}$$

$$\begin{bmatrix} -\omega^2[M]+[K] & -\omega[C] \\ \omega[C] & -\omega^2[M]+[K] \end{bmatrix}\begin{bmatrix} u_1 \\ u_2 \end{bmatrix}=\begin{bmatrix} F_1 \\ F_2 \end{bmatrix} \tag{5.5}$$

$$[C]=\frac{\eta}{\omega}[K] \tag{5.6}$$

In the above equations, ω is the natural frequency of the system (in rad/s), [M] is the mass matrix, [K] is the stiffness matrix, and [C] is the damping matrix. $[\overline{u}]$ and $[\overline{F}]$ are the complex displacement and force vectors respectively. u_1, u_2 and F_1, F_2 represent the real and imaginary parts of the displacement and force vectors. η is the mechanical loss factor. The global displacements can be obtained by solving the above equations. The internal forces on each element are then determined as

$$\{f\}=[K]_L[T]\{D\} \tag{5.7}$$

where {f} is the internal force vector, and {D} is the global displacement vector.

As per the direct piezoelectric effect, Tanwar (2021) formulated the following equations to determine the charge produced Q and the capacitance C of the curved piezo transducer.

$$Q=\sum d_{31} f_i \frac{dl}{h} \tag{5.8}$$

$$C=\frac{\pi\varepsilon_0 l}{\ln\left\{\frac{R+h}{R}\right\}}\times\frac{\theta}{360} \tag{5.9}$$

where d_{31} is the piezoelectric strain coefficient of the piezo transducer, f_i is the internal force on the i^{th} element of the curved piezo transducer, and dl and h are respectively the length and thickness of the elements. ε_0 is the electric permittivity. l, R, and θ are respectively the length, radius of curvature and angle of bend of the curved piezo transducer. The voltage V generated by the piezo transducer is then calculated using the following expression.

$$V=\frac{Q}{C} \tag{5.10}$$

5.10 RESULTS FROM THE ANALYTICAL MODELLING

The effect of the curvature of the piezo transducer in voltage generation is analysed by varying the angle of bend from 0 to 360 degrees with a step interval of 2 degrees. The results of the analysis are plotted in Figure 5.14. It is observed that the curvature has a significant effect on the voltage generated by the transducer. The optimum angle of the bend as per the analytically modelling is found to be 196 degrees, while the numerical modelling (refer section 5.5) suggests the optimum angle of the bend as 145 degrees. The 3-D effects of the structure are ignored in the analytical model as it considers each element of the model as a 1-D element. This might be the major reason for the slight deviation in the results of the 3-D numerical model and the 1-D analytical model.

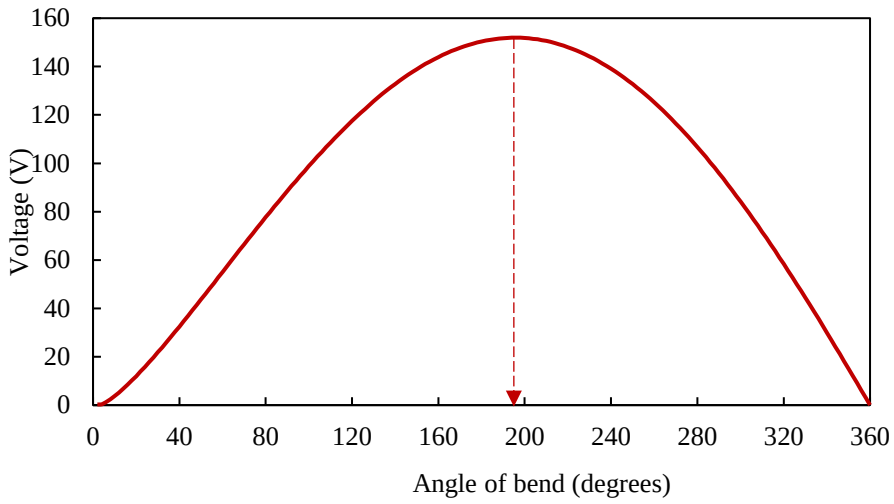

Figure 5.14: Variation of voltage with respect to the angle of bend as per the analytical model

The effect of the thickness of the piezo transducer in voltage generation is also analysed. A thickness range of 1 μm to 1 mm is considered in the analysis, and the results are plotted in Figure 5.15. As per the analysis, the thickness of the transducer has negligible effects on the voltage generated, which contravenes the findings of the 3-D model (refer section 5.7), which has proven that the thickness has a positive impact on voltage generation. This is because the variation of the strain experienced by the piezo transducer across its thickness is ignored in the analytical model since it considers each element as 1-D element. The developed analytical model is, therefore, suitable only for preliminary investigations, and is not as realistic as the 3-D FE models. Hence, it is recommended to further extend the study to 3-D analytical models.

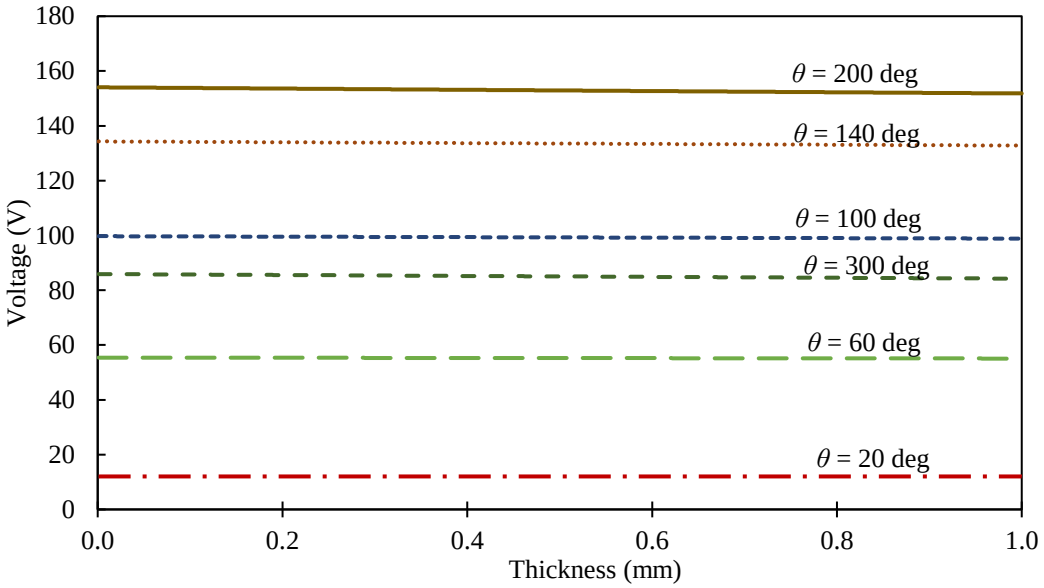

Figure 5.15: Variation of voltage with respect to the thickness of the curved piezo transducer

5.11 SUMMARY

This chapter has presented the findings of the numerical investigations carried out to analyse the efficiency of CVEH for energy harvesting. A 3-D model of the RC beam with CVEH embedded at the midspan is modelled in COMSOL Multiphysics version 4.4 FE software. The model is validated experimentally by conducting an impact hammer test. The effect of various parameters of CVEH such as curvature, thickness and the position of placement is analysed in this chapter. The curved piezo transducer is modelled as a combination of linear elements and hence the effect of model refinement is also assessed. As a first step toward the analytical analysis of curved piezo transducers, an analytical model is formulated in MATLAB using the concepts of the direct stiffness approach. The beam with the curved piezo transducer at the midspan is modelled as a 2-D skeletal structure. Since the 3-D effects of the structure are ignored in the analytical model, some anomalies have been observed between the results of the 3-D numerical model and the analytical model. Therefore, it is recommended to extend the studies to 3-D analytical models. The next chapter summarises the conclusions of the investigative research and the future recommendations.

CHAPTER 6

CONCLUSIONS AND FUTURE RECOMMENDATIONS

6.1 INTRODUCTION

This chapter summarises the key findings of the investigative research undertaken for this project. The primary aim of the research was to analyse the potential of the curved configuration of thin piezo transducers in the fields of energy harvesting and SHM. Experimental investigations have been conducted to compare the terminal voltage, power and energy generated by the CVEH (curved configuration of the piezo transducer) over CVS (straight configuration of the piezo transducer). Their potential for power storage in capacitors has also been analysed experimentally. The suitability of CVEH in SHM has been assessed experimentally by investigating its damage detection potential using the EMI technique. Numerical investigations based on 3-D models and finite element analysis for several geometric configurations have also been conducted to analyse the influence of various parameters affecting the output potential such as curvature, thickness, the position of placement, etc. of the curved piezo transducer in the field of energy harvesting. The study has also been extended to the formulation of analytical models based on the direct stiffness approach and associated parametric studies.

6.2 CONCLUSIONS

A summary of the major conclusions of the research are as follows:

i. Various experimental studies have been conducted to analyse the efficacy of embedded piezo transducers in the curved configuration (CVEH) relative to the straight configuration (CVS) for energy harvesting in RC structures. The RC beam embedded with the piezo transducers at the mid-span has been harmonically vibrated at various frequencies, and the open-circuit voltage generated across them is measured. CVEH has performed substantially better than CVS in most cases. It has generated approximately 1.6 times and 1.3 times higher voltage than CVS for various harmonic excitations at an $L/3$ and $L/2$ distance from the nearest support, respectively. The slight drop in voltage ratio while exciting at $L/2$ distance might be due to the 3-D stress effects generated by the shaker's weight, which in this case is right above the sensors. When the shaker is positioned closer to the support (at an $L/6$ distance from the support),

the voltage ratio has dropped to roughly 0.9. Even though this unexpected behaviour of CVEH is not fully explainable, it is possibly due to some support effects and the generation of certain complex stress situations. However, the results of the first two excitation positions prove the superiority of CVEH in energy harvesting. It is also notable that a better signal-to-noise ratio is obtained for embedded piezo sensors in comparison to the surface-mounted accelerometer.

ii. The relative power generated across the piezo transducers under the impedance matching conditions has been analysed for various periodic excitations at one-fourth distance of the RC beam and found that the CVEH can generate an average of 10 times higher power than the CVS. Based on the mid-point acceleration of the beam and the terminal voltage generated by the transducers, the strain developed across the piezo sensors has been theoretically estimated. The strains calculated based on both approaches are found to be in a similar range, proving the validity of the experiments. Further studies have been conducted to investigate the potential of power storage in 1000 μF capacitors.

iii. For harvesting 1.28 mJ of energy, CVEH has taken 236 and 148 seconds for an average mid-point acceleration of 4.9 m/s^2 and 8.8 m/s^2 with equivalent power storage of 5.42 μW and 8.65 μW respectively. For harvesting the same amount of energy, the CVS has taken more time (335 and 249 seconds) with equivalent power storage of 3.8 μW and 5.1 μW. Considering the two cases, CVEH has harvested an average of 55% higher power than CVS for periodic excitations at one-fourth of the span. In comparison to the generated power, there is a decrease in the harvested power. This is because, unlike power harvesting tests, power generation experiments are carried out under impedance matching conditions, allowing for maximum power generation. Furthermore, circuit losses have an impact on the power harvested.

iv. The damage detection potential of CVEH and CVS has been examined using the EMI technique by comparing the baseline admittance signature of the RC beam with those after inducing damage to it. Correlation values greater than 99% are obtained for the repetition of signatures of both transducers in each stage, pointing to the fidelity of CVS and CVEH. A higher deviation or shift in the signatures is obtained in the response of CVEH than in CVS. The RMSD index has also shown higher values in the case of CVEH, suggesting its

propriety in SHM. When comparing the signatures in the range of 1 kHz to 1000 kHz and 100 kHz to 300 kHz, significant deviation or higher RMSD values have been obtained in the former range. A significant peak corresponding to the resonance frequency in the thickness mode of the piezo transducer has been observed in the former range, and therefore, higher deviations are obtained near the peak, leading to higher RMSD values. However, the latter range of frequencies is quite narrow to include such peaks, and therefore the results are found to be less reliable. Hence, it has been recommended to wisely choose the frequency ranges for excitation. The RMSD index of the signatures corresponding to first and second damage has represented significant values, however, it has decreased in the case of third damage. The shift in the signature of the third damage has been found to be in the reverse direction to that of the former two. This is because the EMI technique is more impeccable in detecting incipient damage, and is uncertain for moderate to severe damage. However, the results of the experimental investigation have proved for the first time the suitability of CVEH for SHM in addition to energy harvesting.

v. Numerical investigations have been conducted to analyse the impact of various parameters of CVEH for energy harvesting based on 3-D FE models. The 3D model is validated experimentally by frequency matching. The FE analysis has proved the significant influence of the curvature of piezo transducers on voltage generation. The optimum range for the angle of bend has been observed to be 120-180 degrees, with the peak voltage being attained at 145 degrees. The increase in voltage with respect to the curvature is found to be at a slow rate for angles of bend less than 120 degrees.

vi. As per the FE analysis, the peak voltage generated by CVEH for an angle of bend of 145 degrees is found to be 1.4 times higher than the CVS, where CVEH is modelled as a combination of 5 linear elements. As part of the model refinement, CVEH has been remodelled as a combination of 11-linear elements and 15-linear elements. Convergence has been witnessed in the voltage generated by the transducers with a higher number of elements in the model. The 15-element model of the curved piezo transducer has generated a 1.63 times higher peak voltage than the CVS for a bend angle of 145 degrees.

vii. The effect of the thickness of the piezo transducer on terminal voltage has also been analysed based on the 3-D model. A thickness range of 0.6 mm to 1.5 mm

has been considered for the study and found that the thickness has a positive impact on boosting the voltage generated for all the curvatures of CVEH. The results of the analysis follow a similar trend as observed by Kaur and Bhalla, (2016) for the embedded CVS in RC beams.

viii. Also, as per the FE analysis, it is advised to place the CVEH towards the top or bottom of the beam cross-section where the beam experiences maximum strain. The CVEH experiences almost zero voltage when placed at the neutral axis, where the bending strain is zero.

ix. As a preliminary study of the analytical investigations on CVEH for energy harvesting, an analytical model has been formulated in MATLAB based on the direct stiffness approach. The RC beam with a curved piezo transducer at the mid-span is modelled as a 2-D skeletal structure with 32 nodes. The optimum angle of bend of the piezo transducer for maximum voltage generation is found to be 196 degrees. The deviation in the results from that of the numerical investigation (145 degrees) might be due to the ignorance of the 3-D effects in the analytical model. The thickness of the transducer is found to have barely any effect on the voltage generated across them. This is because the strain variation across the thickness of the transducer has been neglected in the analytical model. Therefore, it is recommended to extend the study to 3-D analytical models.

6.3 RECOMMENDATIONS FOR FUTURE WORK

The current research has focused mainly on the energy harvesting potential of curved piezo transducers. Various experiments and numerical investigations have been conducted to analyse its efficacy in this field. The suitability of curved piezo transducers for SHM has also been assessed for the first time through this research. The following suggestions are recommended to extend the research in these realms.

i. In this research, the energy generated by the curved piezo transducer due to the periodic vibrations of the RC beam has been stored in capacitors. This energy storage can be further extended into batteries, which would be more useful in real-life situations.

ii. The CVEH is fabricated by manually bending the straight MFC transducer into a curved configuration. Instead, an inbuilt curved piezo transducer can provide more perfection in the curvature and might yield better results.

iii. The adhesive layer between the piezo transducer and the concrete has been ignored in the 3-D model. These adhesive layers can cause some shear lag effects. Therefore, a more detailed study can be conducted to explore the same.

iv. Further parametric studies such as the effect of size of the piezo transducer, bond layer, etc. can also be investigated.

v. More experiments can be conducted to analyse the efficacy of CVEH for SHM by assessing the response of CVEH towards various kinds of damage.

vi. 3-D numerical analysis can also be conducted to optimise the parameters of the curved piezo transducer for structural health monitoring.

vii. So far, the curvature in a single direction has been analysed both experimentally and numerically by FE methods for energy harvesting. The potential of double curvature or spherically curved piezo transducers can be explored for both SHM and energy harvesting in the near future.

It is believed that the outcomes of this research will encourage future researchers to extend the studies in these realms and will also open the door to the deployment of curved piezo transducers in real-world structures for energy harvesting and structural health monitoring.

REFERENCES

1. Balguvhar, S. (2020), "Piezoelectric energy harvesting through low-frequency non-sinusoidal vibrations of civil structures", *PhD Thesis*, Department of Civil Engineering, Indian Institute of Technology (IIT) Delhi, India.
2. Baptista, F.G., Budoya, D.E., Almeida, V.A. and Ulson, J.A.C. (2014), "An experimental study on the effect of temperature on piezoelectric sensors for impedance-based structural health monitoring", *Sensors*, Vol. 14, pp. 1208-1227.
3. Beeby, S.P., Cao, Z. and Almussallam, A. (2013), "Kinetic, thermoelectric and solar energy harvesting technologies for smart textiles", *Multidisciplinary Know-How for Smart-Textiles Developers. Woodhead Publishing*, pp. 306-328.
4. Bhalla, S. (2004), "A mechanical impedance approach for structural identification, health monitoring and non-destructive evaluation using piezo-impedance transducers," *PhD Thesis*, Nanyang Technological University, Singapore.
5. Bhalla, S. and Gupta, A. (2007), "A novel vibration sensor for concrete structures" *Invention disclosure* (FT/IPR/CE/SB/2007/0570), *Foundation for Innovation and Technology Transfer* (*FITT*), IIT Delhi, Patent application no. 1011/DEL/2011.
6. Bhalla, S. and Soh, C.K. (2004a), "Structural health monitoring by piezo-impedance transducers modelling," *Journal of Aerospace Engineering*, ASCE, Vol. 17, No. 4, pp. 154-165.
7. Bhalla, S. and Soh, C.K. (2004b), "Impedance based modelling for adhesively bonded piezo- transducers," *Journal of Intelligent Material Systems and Structures*, Vol. 15, No. 12, pp. 955-972.
8. Bhalla, S., Moharana, S., Talakokula, V. and Kaur, N. (2017), "Piezoelectric materials: applications in SHM, energy harvesting and biomechanics", p. 352, Chichester, *UK:: Wiley*.
9. Calio, R., Rongala, U.B., Camboni, D., Milazzo, M., Stefanini, C., Petris, G. and Oddo, C.M. (2014), "Piezoelectric energy harvesting solutions", *Sensors*, Vol. 14, No. 3, pp. 4755-4790.
10. Covaci, C. and Gontean, A. (2020), "Piezoelectric energy harvesting solutions: A review", *Sensors*, Vol. 20, Vol. 12, pp. 3512-3549.

11. Giurgiutiu, V. and Zagrai, A. N. (2002), "Embedded self-sensing piezoelectric active sensors for on-line structural identification", *ASME Journal of Vibration and Acoustics*, Vol. 124, No. 1, pp. 116-125.
12. Giurgiutiu, V. and Zagrai, A. N. (2005), "Damage detection in thin plates and aerospace structures with the electro-mechanical impedance method", *Structural Health Monitoring*, Vol. 4, No. 2, pp. 99-118.
13. Howells, C.A. (2009), "Piezoelectric energy harvesting", *Energy Conversion and Management*, Vol. 50, No. 7, pp. 1847-1850.
14. Kathpalia, B., Tan, D., Stern, I., Valdes, F., Kim, S. and Erturk, A. (2017), "Modeling and characterization of a curved piezoelectric energy harvester for smart paver tiles", *Procedia Computer Science*, Vol. 109, pp. 1060-1066.
15. Kaur, N. (2015), "Integrated structural health monitoring and energy harvesting potential of adhesively bonded thin piezo patches operating in *d*31 mode", *PhD Thesis*, Department of Civil Engineering, Indian Institute of Technology (IIT) Delhi, India.
16. Kaur, N. and Bhalla, S. (2014), "Feasibility of energy harvesting from thin piezo sensor patches via axial strain actuation mode", *Journal of Civil Structural Health Monitoring*, Vol. 4, No. 1, pp. 1-15.
17. Kaur, N. and Bhalla, S. (2015), "Combined energy harvesting and structural health monitoring potential of embedded piezo-concrete vibration sensors", *Journal of Energy Engineering*, Vol. 141, No. 4, pp. D4014001-18.
18. Kaur, N. and Bhalla, S. (2016a), "Concrete vibration energy harvester". Patent application no: 201611014500 A, Indian Patent Office.
19. Kaur, N. and Bhalla, S. (2016b), "Numerical investigations on energy harvesting potential of thin PZT patches adhesively bonded on RC structures", *Sensors and Actuators A: Physical*, Vol. 241, pp. 44-59.
20. Liang, C., Sun, F.P. and Rogers, C.A. (1994), "Coupled electro-mechanical analysis of adaptive material systems-determination of the actuator power consumption and system energy transfer," *Journal of Intelligent Material Systems and Structures*, Vol. 8, No. 4, pp. 335-343.
21. Lin, T.H., Lu, Y.C. and Hung, S.L. (2014), "Locating damage using integrated global-local approach with wireless sensing system and single-chip impedance measurement device", *The Scientific World Journal*, pp. 1-13.

22. Makkonen, T., Holappa, A., Ella, J. and Salomea, M.M. (2001), "Finite element simulations of thin-film composite BAW resonators", *IEEE transactions on ultrasonics, ferroelectrics, and frequency control*, Vol. 48, No. 5, pp. 1241-1258.
23. Mittal, P. (2017), "Fabrication and evaluation of concrete vibration energy harvester (CVEH) using piezoelectric ceramic ring". *M.Tech Thesis*, Department of Civil Engineering, Indian Institute of Technology (IIT) Delhi, India.
24. Park, S.H., Yi, J.H., Yun, C.B. and Roh, Y.R. (2004), "Impedance-based damage detection for civil infrastructures", *KSCE Journal of Civil Engineering*, Vol. 8, No. 4, pp. 425-433.
25. PI Ceramic (2021), *Product Information Catalogue*, Lindenstrasse, Germany, https://www.piceramic.com/en/products (Date of access: 24 Dec, 2021)
26. Rosiek, M., Martowicz, A., Uhl, T., Stępiński, T. and Łukomski, T. (2010), "Electromechanical impedance method for damage detection in mechanical structures", *Proceedings of 11th IMEKO TC*, Vol. 10, pp.18-20.
27. Shanker, R., Bhalla, S., Gupta, A. and Praveen Kumar, M. (2011), "Dual use of PZT patches as sensors in global dynamic and local electromechanical impedance techniques for structural health monitoring", *Journal of Intelligent Material Systems and Structures*, Vol. 22, No. 16, pp. 1841-1856.
28. Singamsetty, S., Kaur, N. and Bhalla, S. (2014), "Energy harvesting from structural vibrations using piezo transducers: A parametric study", *3rd International Conference on Sustainable Innovative Techniques in Architecture, Civil and Environmental Engineering (SITACEE - 2014)* organized by "Krishi Sanskriti", April 26th -27th, Jawaharlal Nehru University, New Delhi, India, pp. 331-334.
29. Singh, N. (2017), "Fabrication and evaluation of concrete vibration energy harvester (CVEH)", *M.Tech Thesis*, Department of Civil Engineering, Indian Institute of Technology (IIT) Delhi, India.
30. Smart Materials (2021), https://www.smart-material.com/MFC-product-mainV2.html. (Date of access: 29 November, 2021)
31. Starner, T. (1996), "Human-powered wearable computing", *IBM Systems Journal*, Vol. 35, No. 3.4, pp. 618-628.
32. Sun, F.P., Chaudhry, Z.A., Rogers, C.A., Majmundar, M. and Liang, C. (1995), "Automated real-time structure health monitoring via signature pattern recognition", In *Smart structures and materials 1995: smart structures and integrated systems*, Vol. 2443, pp. 236-247, International Society for Optics and Photonics.

33. Tanwar, S. (2019), “Modelling of straight/curved piezo-bond-structural system for investigations in structural health monitoring and energy harvesting”, *M.Tech Thesis*, Department of Civil Engineering, Indian Institute of Technology (IIT) Delhi, India.
34. Zhao, J. and You, Z. (2014), “A shoe-embedded piezoelectric energy harvester for wearable sensors”, *Sensors,* Vol. 14, No. 7, pp. 12497-12510.

APPENDIX A

RESPONSE OF CVEH AND CVS EMBEDDED INSIDE AN RC BEAM SUBJECTED TO DYNAMIC EXCITATIONS

A.1 POSITION OF EXCITATION: AT *L*/2 DISTANCE FROM THE SUPPORT

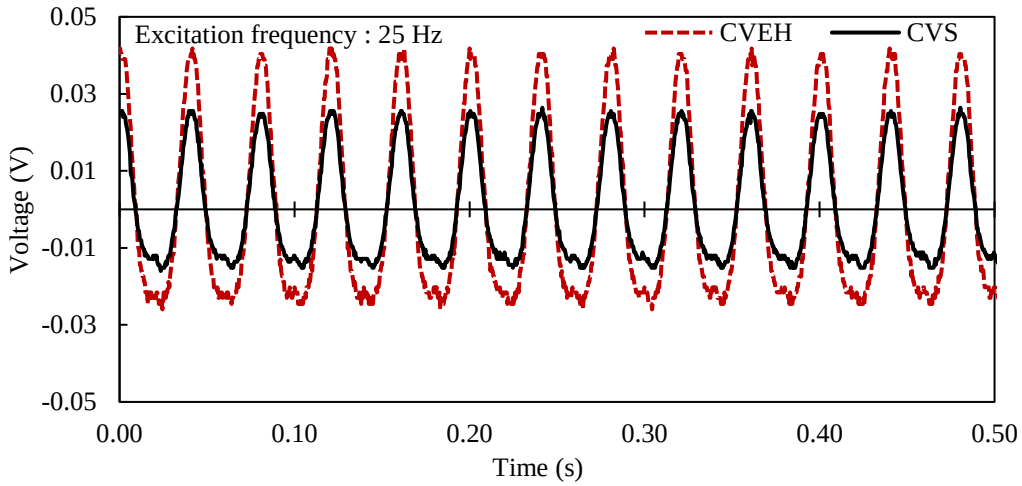

(a)

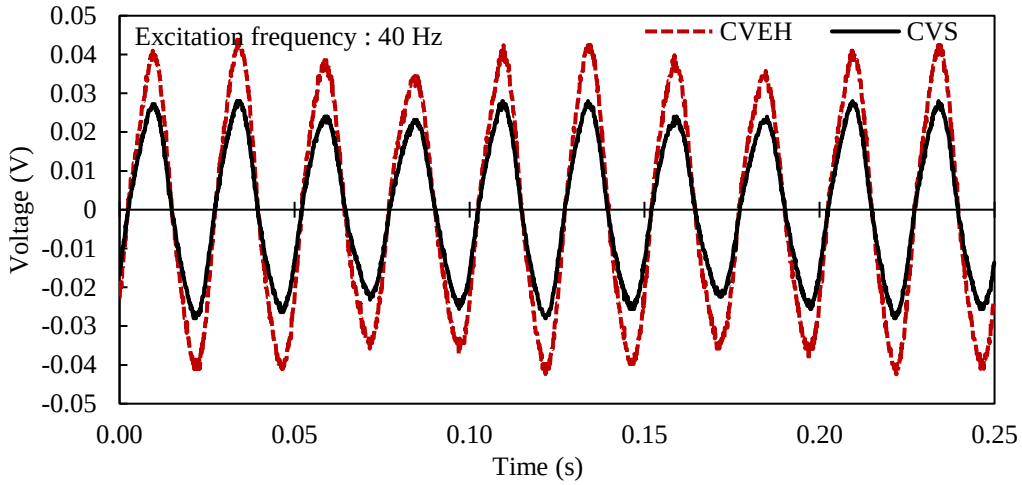

(b)

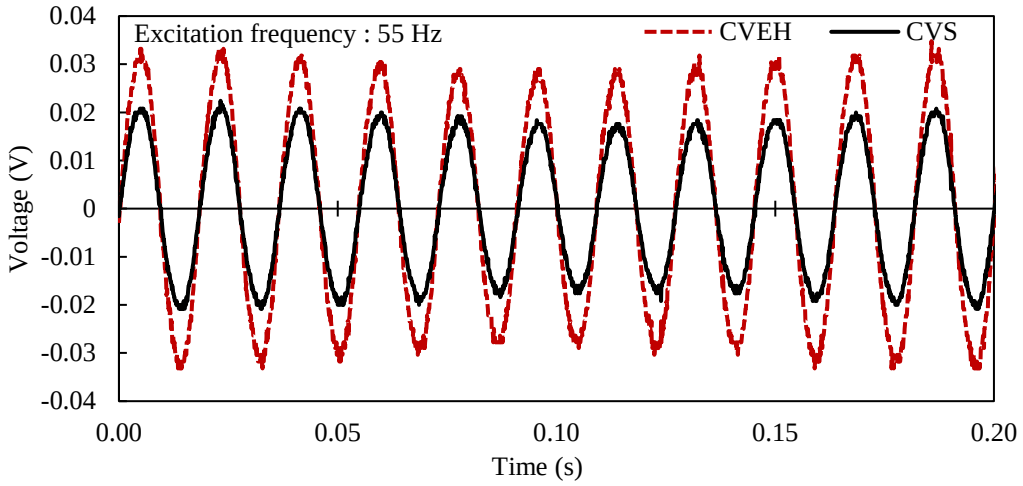

(c)

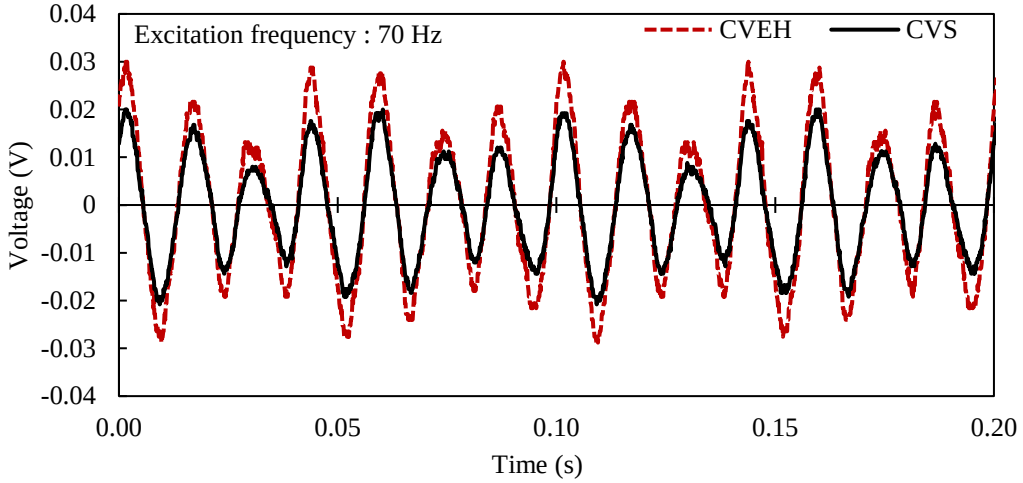

(d)

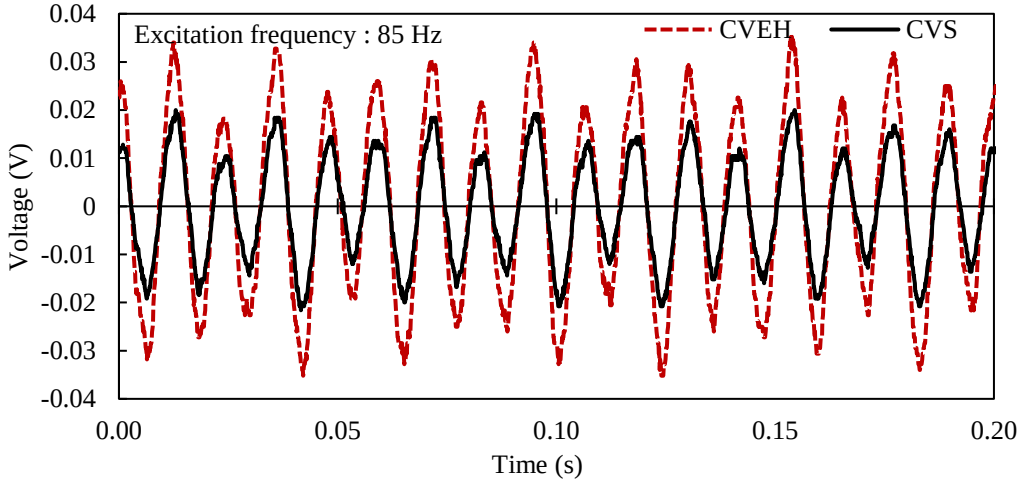

(e)

Figure A.1: Response of CVEH and CVS when the shaker is placed at $L/2$ distance from the support for the following frequencies of excitation: (a) 25 Hz; (b) 40 Hz; (c) 55 Hz; (d) 70 Hz; (e) 85 Hz

A.2 POSITION OF EXCITATION: AT *L*/3 DISTANCE FROM THE SUPPORT

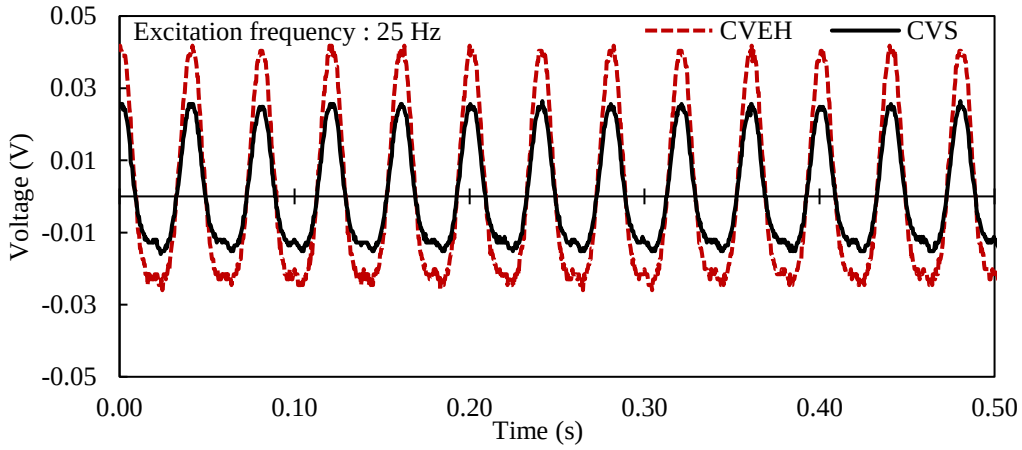

(a)

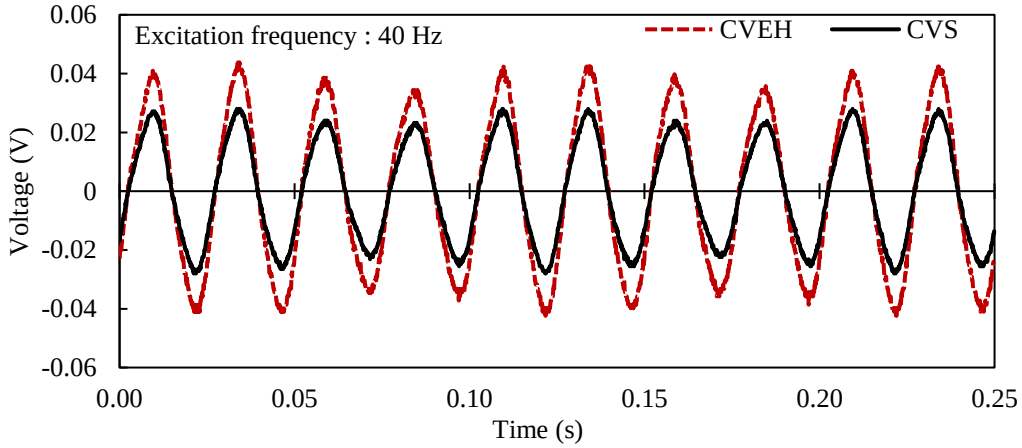

(b)

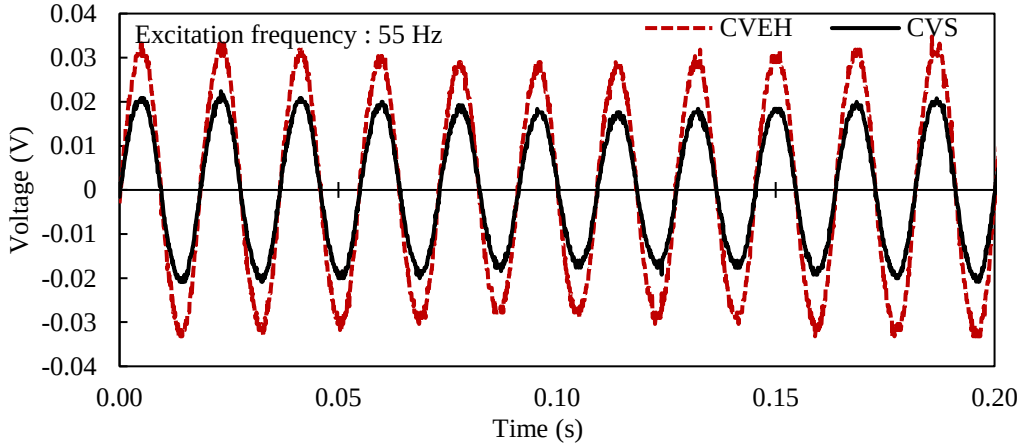

(c)

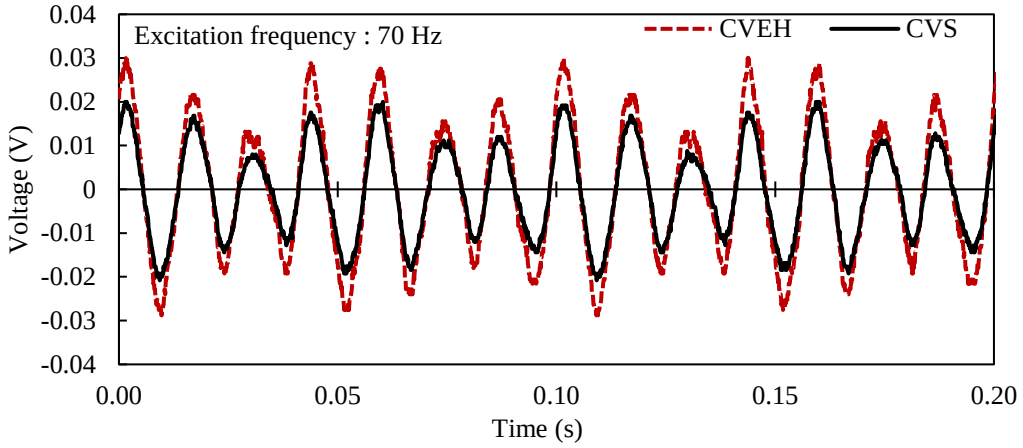

(d)

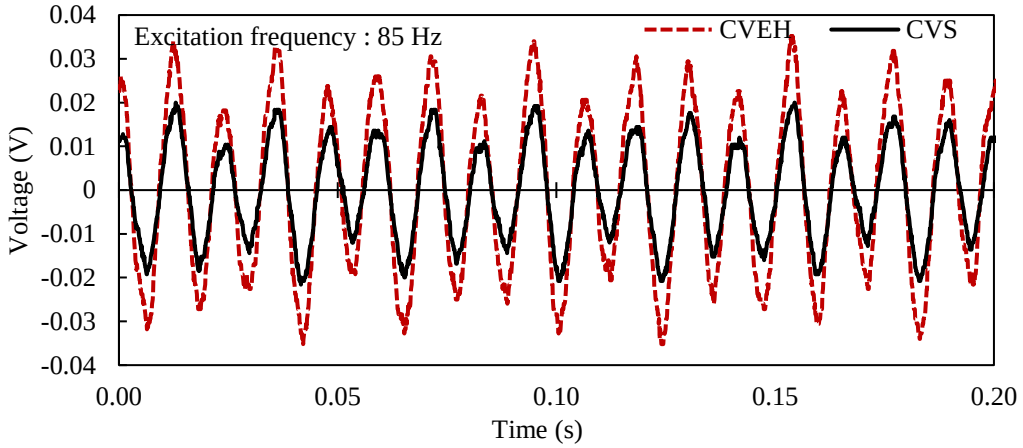

(e)

Figure A.2: Response of CVEH and CVS when the shaker is placed at $L/3$ distance from the support for the following frequencies of excitation: (a) 25 Hz; (b) 40 Hz; (c) 55 Hz; (d) 70 Hz; (e) 85 Hz

A.3 POSITION OF EXCITATION: AT *L*/3 DISTANCE FROM THE SUPPORT

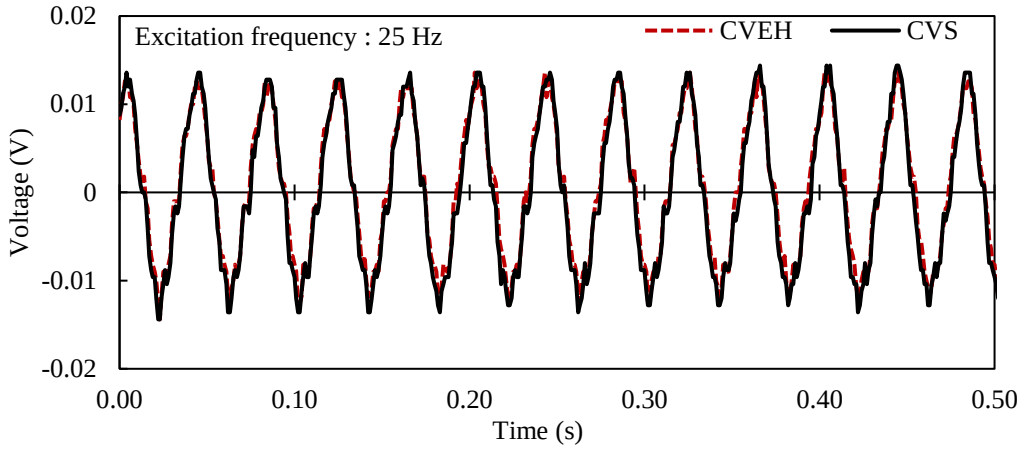

(a)

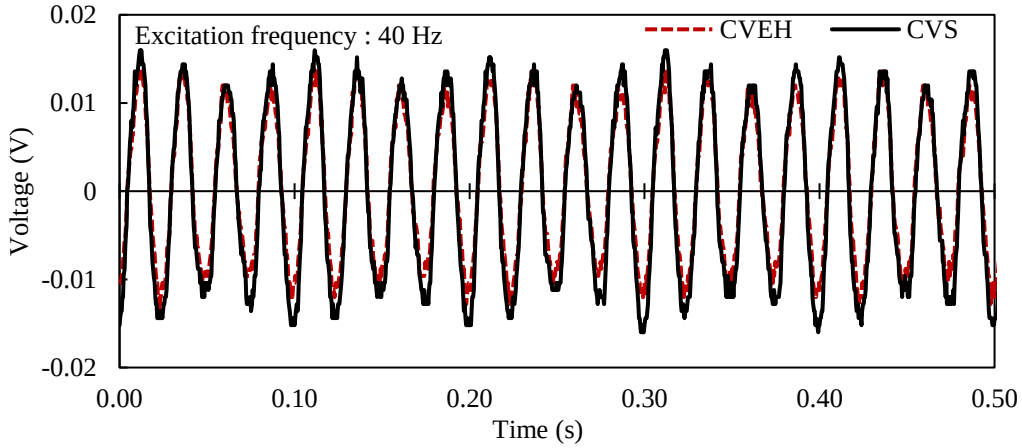

(b)

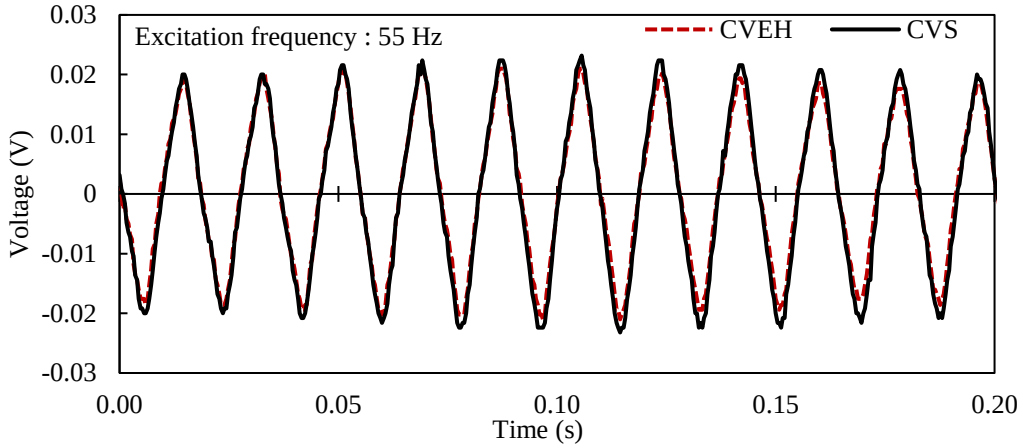

(c)

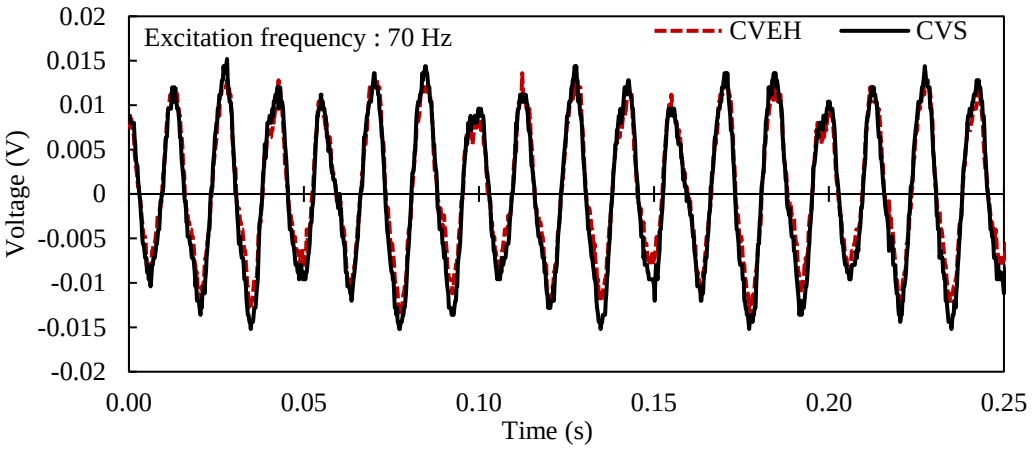

(d)

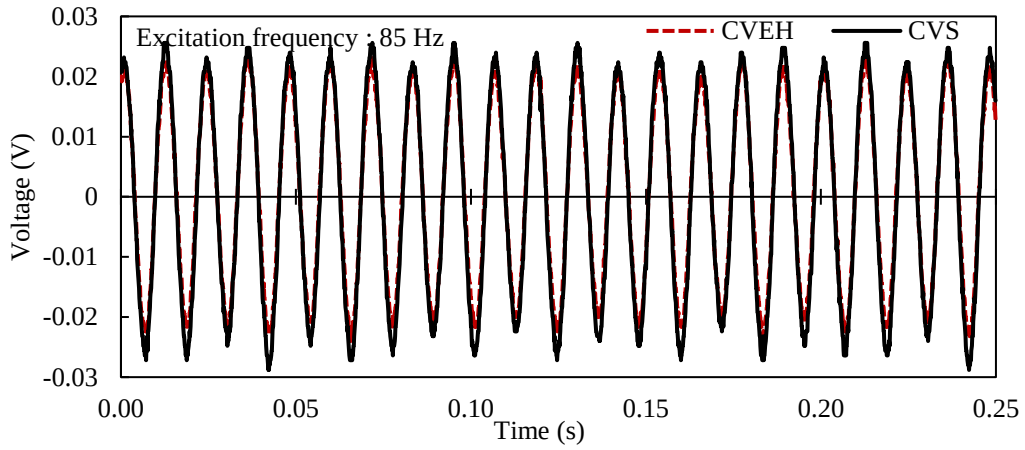

(e)

Figure A.3: Response of CVEH and CVS when the shaker is placed at $L/6$ distance from the support for the following frequencies of excitation: (a) 25 Hz; (b) 40 Hz; (c) 55 Hz; (d) 70 Hz; (e) 85 Hz

APPENDIX B

MATLAB CODE TO ANALYSE THE INFLUENCE OF THE CURVATURE OF THE PIEZO TRANSDUCER IN VOLTAGE GENERATION BY 1-D ANALYTICAL MODELLING

```
clc
close all
clear all

%Properties of the beam
Lb=3; % length of the beam in m
Bb=0.3; % breadth of the beam in m
Hb=.5; % depth of the beam in m
Ab=Bb*Hb; % c/s area
Ib=(Bb*Hb^3)/12; % Moment of inertia of the beam
Eb=27.3e9; % Young's Modulus of the beam
dstyb=2500; % density of the beam

%Properties of piezo patch
 L =0.056; % length of piezo patch in m
hp =1e-3; % thickness of the piezo patch in m
Bp = 0.028; % breadth of the piezo patch in m
Ap =hp*Bp; % area of the piezo patch
Ip =Bp*(hp^3)/12; % Moment of inertia of piezo patch
Ep =30.336*10^9; % Young's Modulus of the piezo patch
dstyp=5440; % density of the piezo patch
theta=1:1:180;

stp=180; % no of steps
for z=1:stp
   R=(L*180)/(2*theta(z)*3.14);

% Transformation Matrix
   % for members 1 to 22
   R1=[1 0 0;
     0 1 0;
     0 0 1]; % Joint Transformation Matrix
   O = zeros(3,3);
   T1 = [R1 O;
       O R1]; % Member Transformation Matrix

   % for members 23 to 31(piezo patch)
     x = theta(z)/5*[5,4,3,2,1,-1,-2,-3,-4,-5].*pi()/180;
   T3(:,:,10) = zeros(6,6);
```

```
   for i=1:10
      R3 =[cos(x(i)) sin(x(i)) 0;
         -sin(x(i)) cos(x(i)) 0;
          0 0 1];
       T3(:,:,i) = [R3 O;
                  O R3];
   end

% Stiffness Matrix, considring 3 dof at each node i.e., x,y and theta
% Local stiffness matrix for members 1 to 6 and 17 to 22
L1=(Lb-L)/12; % Length of members 1 to 6 and 17 to 22
a1 = Ab*Eb/L1;
b1 = 12*Eb*Ib/L1^3;
c1 = 6*Eb*Ib/L1^2;
d1 = 4*Eb*Ib/L1;
e1 = 2*Eb*Ib/L1;

K1 =[a1 0 0 -a1 0 0;
     0 b1 c1 0 -b1 c1;
     0 c1 d1 0 -c1 e1;
    -a1 0 0 a1 0 0;
     0 -b1 -c1 0 b1 -c1;
     0 c1 e1 0 -c1 d1];
 KG1= transpose(T1)*K1*T1;

%Local stiffness matrix for members for 7 to 16
L2=L/10; % approximate length of each member from 7 to 16
a2 = Ab*Eb/L2;
b2 = 12*Eb*Ib/L2^3;
c2 = 6*Eb*Ib/L2^2;
d2 = 4*Eb*Ib/L2;
e2 = 2*Eb*Ib/L2;

K2 =[a2 0 0 -a2 0 0;
     0 b2 c2 0 -b2 c2;
     0 c2 d2 0 -c2 e2;
    -a2 0 0 a2 0 0;
     0 -b2 -c2 0 b2 -c2;
     0 c2 e2 0 -c2 d2];
 KG2= transpose(T1)*K2*T1;

% Local stiffness matrix for members for 23 to 32
L3=R*theta(z)/5*pi()/180;
a3 = Ap*Ep/L3;
b3 = 12*Ep*Ip/L3^3;
c3 = 6*Ep*Ip/L3^2;
d3 = 4*Ep*Ip/L3;
e3 = 2*Ep*Ip/L3;
```

```
K3 =[a3 0 0 -a3 0 0;
    0 b3 c3 0 -b3 c3;
    0 c3 d3 0 -c3 e3;
   -a3 0 0 a3 0 0;
    0 -b3 -c3 0 b3 -c3;
    0 c3 e3 0 -c3 d3];

 %Combined Global stiffness matrix of piezo patch and middle portion (23 to 32) of the beam
 KG3(:,:,10) = zeros(6,6);
 for i=1:10
   KG3(:,:,i)= transpose(T3(:,:,i))*K3*T3(:,:,i)+KG2;
 end

 KTS = zeros(69);
 for i=1:6
    for j=1:6
       for k =0:4
          KTS(i+3*k,j+3*k)=KTS(i+3*k,j+3*k)+KG1(i,j); % for members 2 to 6
       end
       for k =0:9
          KTS(i+3*k+15,j+3*k+15)=KTS(i+3*k+15,j+3*k+15)+KG3(i,j,k+1); % for combined
members 7 to 16 and 21 to 30
       end
       for k = 0:5
          KTS(i+3*k+45,j+3*k+45)=KTS(i+3*k+45,j+3*k+45)+KG1(i,j); % for members 17 to 21
       end
    end
 end
 %For member 1
 for i=1:3
    for j=1:3
       KTS(i+66,j+66)=KTS(i+66,j+66)+KG1(i,j);
       KTS(i,j)=KTS(i,j)+KG1(i+3,j+3);
    end
 end

 % Mass Matrix
 M1=dstyb*Ab*L1; % lumped mass at nodes 2 to 6 and 18 to 22
 M2=dstyb*Ab*(L1+L2)/2 + dstyp*Ap*L2/2; % lumped mass at node 7 and 17
 M3=dstyb*Ab*L2+dstyp*Ap*L3; % lumped mass at nodes 8 to 16

 M=zeros(69,69);
 M(68,68)=M1/2; % lumped mass at node 1
 M(65,65)=M1/2; % lumped mass at node 23
 for i=0:4
    M(2+3*i,2+3*i)=M1; % lumped mass at nodes 2 to 6
    M(50+3*i,50+3*i)=M1; % lumped mass at nodes 18 to 22
```

```
end
 M(17,17)=M2; % lumped mass at node 7
M(47,47)=M2; % lumped mass at node 17
for i=0:8
   M(20+i*3,20+i*3)=M3; % lumped mass at nodes 8 to 16
end

% Damping Matrix
w=2*3.14*85;
beta=.02/w; % damping coefficient
C = beta*KTS; % damping matrix

% Dynamic Analysis
w=2*3.14*85;
A=zeros(138,138);
 A = [ -w*w*M+KTS -w*C;
    w*C -w*w*M+KTS];
 F1 = zeros(69,1);
 F1(8,1)=-100;
 F1(65,1)=.25*F1(8,1);
 F1(65,1)=.75*F1(8,1);
 F2 = zeros(69,1);
 U1 = zeros(69,1);
 U2 = zeros(69,1);
 F = [ F1;F2];
 U = [ U1;U2];
 U = A\F;% U =inverse(A)*F
 D = zeros(69,1);
 for i=1:69
    U1(i,1) = U(i,1);
    U2(i,1) = U(i+69,1);
    D(i,1) = sqrt(U1(i,1)^2-U2(i,1)^2); % Global displacement
 end

 %local displacements of the piezo patch
 Dp(:,:,10)=zeros(6,1); % Global displacement of piezo patch
 d(:,:,10)=zeros(6,1); % local displacement of piezo patch
 f(:,:,10)=zeros(6,1); % member forces
 d31=-2.1e-10; % Piezoelectric strain coefficient (?_31)

 sumaf=0;
 elp=2.12e-8; % electric permitivity in Farad/m
 for i=1:10 % for each member
    for j=1:3
      Dp(j,1,i)= D(j+12+(i-1)*3,1);
      Dp(j+3,1,i)= D(j+15+(i-1)*3,1);
    end
    d(:,1,i)=T3(:,:,i)*Dp(:,1,i);
```

```
    f(:,1,i)=K3*d(:,1,i);
    %Q(z)= Q(z)+ d31*f(1,1,i)*L3/hp;
    sumaf=sumaf+f(1,1,i);
  end
  Q(z)= d31*sumaf*L3/hp;
  Cpt(z)= elp*R/abs(log(R+hp))*theta(z)*pi()/180; % Capacitance
  V(z)= abs(Q(z)/Cpt(z));
end
figure(1)
plot(2*theta,V)
xlabel('Angle of bend(degrees)');
ylabel('Voltage(V)');
title('Voltage vs Curvature');
```

APPENDIX C

MATLAB CODE TO ANALYSE THE INFLUENCE OF THE THICKNESS OF THE CURVED PIEZO TRANSDUCER IN VOLTAGE GENERATION BY 1-D ANALYTICAL MODELLING

```
clc
close all
clear all

%Properties of the beam
Lb=3; % length of the beam in m
Bb=0.3; % breadth of the beam in m
Hb=.5; % depth of the beam in m
Ab=Bb*Hb; % C/s area
Ib=(Bb*Hb^3)/12; % Moment of inertia of the beam
Eb=27.3e9; % Young's Modulus of the beam
dstyb=2500; % density of the beam

%Properties of piezo Patch
L =0.056; % length of piezo patch in m
hp =1e-6:1e-6:1e-3; % thickness of the piezo patch in m
Bp = 0.028; % breadth of the piezo patch in m
%Ap =hp*Bp; % area of the piezo patch
%Ip =Bp*(hp^3)/12; % Moment of inertia of piezo patch
Ep =30.336e9; % Young's Modulus of the piezo patch
dstyp=5440; % density of the piezo patch
theta=180;
stp=(1e-3-1e-6)/(1e-6) + 1;

for z=1:stp
   Ap=hp(z)*Bp;
   Ip =Bp*(hp(z)^3)/12;
   R=(L*180)/(2*theta*3.14);

% Transformation Matrix
   % for members 1 to 22
   R1=[1 0 0;
     0 1 0;
     0 0 1]; % Joint Transformation Matrix
   O = zeros(3,3);
   T1 = [R1 O;
       O R1]; % Member Transformation Matrix
```

```
   % for members 23 to 31(piezo patch)
     x = theta/5*[5,4,3,2,1,-1,-2,-3,-4,-5].*pi()/180;

   T3(:,:,10) = zeros(6,6);
   for i=1:10
      R3 =[cos(x(i)) sin(x(i)) 0;
         -sin(x(i)) cos(x(i)) 0;
          0 0 1];
       T3(:,:,i) = [R3 O;
                  O R3];
   end

% Stiffness Matrix, considring 3 dof at each node i.e., x,y and theta
% Local stiffness matrix for members 1 to 6 and 17 to 22
L1=(Lb-L)/12; % Length of members 1 to 6 and 17 to 22
a1 = Ab*Eb/L1;
b1 = 12*Eb*Ib/L1^3;
c1 = 6*Eb*Ib/L1^2;
d1 = 4*Eb*Ib/L1;
e1 = 2*Eb*Ib/L1;

K1 =[a1 0 0 -a1 0 0;
     0 b1 c1 0 -b1 c1;
     0 c1 d1 0 -c1 e1;
    -a1 0 0 a1 0 0;
     0 -b1 -c1 0 b1 -c1;
     0 c1 e1 0 -c1 d1];
 KG1= transpose(T1)*K1*T1;

%Local stiffness matrix for members for 7 to 16
L2=L/10; % approximate length of each member from 7 to 16
a2 = Ab*Eb/L2;
b2 = 12*Eb*Ib/L2^3;
c2 = 6*Eb*Ib/L2^2;
d2 = 4*Eb*Ib/L2;
e2 = 2*Eb*Ib/L2;

K2 =[a2 0 0 -a2 0 0;
     0 b2 c2 0 -b2 c2;
     0 c2 d2 0 -c2 e2;
    -a2 0 0 a2 0 0;
     0 -b2 -c2 0 b2 -c2;
     0 c2 e2 0 -c2 d2];
 KG2= transpose(T1)*K2*T1;

% Local stiffness matrix for members for 23 to 32
L3=R*theta/5*pi()/180;
a3 = Ap*Ep/L3;
```

```
b3 = 12*Ep*Ip/L3^3;
c3 = 6*Ep*Ip/L3^2;
d3 = 4*Ep*Ip/L3;
e3 = 2*Ep*Ip/L3;

K3 =[a3 0 0 -a3 0 0;
    0 b3 c3 0 -b3 c3;
    0 c3 d3 0 -c3 e3;
   -a3 0 0 a3 0 0;
    0 -b3 -c3 0 b3 -c3;
    0 c3 e3 0 -c3 d3];

 %Combined Global stiffenes matrix of piezo patch and middle portion (23 to 32) of the beam
 KG3(:,:,10) = zeros(6,6);
 for i=1:10
   KG3(:,:,i)= transpose(T3(:,:,i))*K3*T3(:,:,i)+KG2;
 end

 KTS = zeros(69);
 for i=1:6
    for j=1:6
       for k =0:4
          KTS(i+3*k,j+3*k)=KTS(i+3*k,j+3*k)+KG1(i,j); % for members 2 to 6
       end
       for k =0:9
          KTS(i+3*k+15,j+3*k+15)=KTS(i+3*k+15,j+3*k+15)+KG3(i,j,k+1); % for combined
members 7 to 16 and 21 to 30
       end
       for k = 0:5
          KTS(i+3*k+45,j+3*k+45)=KTS(i+3*k+45,j+3*k+45)+KG1(i,j); % for members 17 to 21
       end
    end
 end
 %For member 1
 for i=1:3
    for j=1:3
       KTS(i+66,j+66)=KTS(i+66,j+66)+KG1(i,j);
       KTS(i,j)=KTS(i,j)+KG1(i+3,j+3);
    end
 end

 % Mass Matrix
 M1=dstyb*Ab*L1; % lumped mass at nodes 2 to 6 and 18 to 22
 M2=dstyb*Ab*(L1+L2)/2 + dstyp*Ap*L2/2; % lumped mass at node 7 and 17
 M3=dstyb*Ab*L2+dstyp*Ap*L3; % lumped mass at nodes 8 to 16

 M=zeros(69,69);
 M(68,68)=M1/2; % lumped mass at node 1
```

```
M(65,65)=M1/2; % lumped mass at node 23
for i=0:4
   M(2+3*i,2+3*i)=M1; % lumped mass at nodes 2 to 6
   M(50+3*i,50+3*i)=M1; % lumped mass at nodes 18 to 22
end
 M(17,17)=M2; % lumped mass at node 7
M(47,47)=M2; % lumped mass at node 17
for i=0:8
   M(20+i*3,20+i*3) = M3; % lumped mass at nodes 8 to 16
end

% Damping Matrix
w=2*3.14*85;
beta=.02/w; % damping coefficient
C = beta*KTS; % damping matrix

% Dynamic Analysis
w=2*3.14*85;
A=zeros(138,138);
 A = [ -w*w*M+KTS -w*C;
    w*C -w*w*M+KTS];
 F1 = zeros(69,1);
 F1(8,1)=-100;
 F1(65,1)=.25*F1(8,1);
 F1(65,1)=.75*F1(8,1);
 F2 = zeros(69,1);
 U1 = zeros(69,1);
 U2 = zeros(69,1);
 F = [ F1;F2];
 U = [ U1;U2];
 U = A\F;% U =inverse(A)*F
 D = zeros(69,1);
 for i=1:69
    U1(i,1) = U(i,1);
    U2(i,1) = U(i+69,1);
    D(i,1) = sqrt(U1(i,1)^2-U2(i,1)^2); % Global displacement
 end

 %local displacements of the piezo patch
Dp(:,:,10)=zeros(6,1); % Global displacement of piezo patch
d(:,:,10)=zeros(6,1); % local displacement of piezo patch
f(:,:,10)=zeros(6,1); % member forces
d31=-2.1e-10; % Piezoelectric strain coefficient (?_31)

 sumaf=0;
elp=2.12e-8; % electric permitivity in Farad/m
for i=1:10 % for each member
   for j=1:3
```

```
      Dp(j,1,i)= D(j+12+(i-1)*3,1);
      Dp(j+3,1,i)= D(j+15+(i-1)*3,1);
    end
    d(:,1,i)=T3(:,:,i)*Dp(:,1,i);
    f(:,1,i)=K3*d(:,1,i);
    %Q(z)= Q(z)+ d31*f(1,1,i)*L3/hp;
    sumaf=sumaf+f(1,1,i);
  end
  Q(z)= d31*sumaf*L3/hp(z);
  Cpt(z)= elp*R/abs(log(R+hp(z)))*theta*pi()/180; % Capacitance
  V(z)= abs(Q(z)/Cpt(z));
end
figure(1)
plot(hp,V)
xlabel('Thickness of piezo patch');
ylabel('Voltage(V)');
title('Voltage vs Thickness');
```

APPENDIX D

JOURNAL PAPER READY FOR SUBMISSION TO SENSORS AND ACTUATORS A: PHYSICAL

EFFICACY OF CURVED EMBEDDED CONFIGURATION OF PIEZO TRANSDUCERS FOR STRUCTURAL HEALTH MONITORING AND ENERGY HARVESTING FROM RC STRUCTURES

Aleena V K[1], Suresh Bhalla[2] and Naveet Kaur[3]

ABSTRACT

Piezoelectric materials have secured a significant position in the field of structural health monitoring (SHM) and energy harvesting over the past two decades. These materials are available in several forms and configurations but their efficacy in these fields for most of the configurations is still unexplored. This article investigates both experimentally and numerically the potency of the curved configuration over the straight configuration of the piezo transducers embedded in reinforced concrete (RC) structures for energy harvesting and SHM. The study includes the analysis of (1) open-circuit voltage generated across the piezo transducers, (2) the power developed by the method of impedance matching and (3) the capability of power storage into capacitors for both the configurations. The article also experimentally scrutinizes the damage detection capability of the curved piezo transducers by the method of electro-mechanical impedance (EMI) technique. Curved piezo transducers exhibit better performance in comparison to straight configuration for both structural health monitoring and energy harvesting. A finite element (FE) analysis is also conducted by developing a 3-D model of the real life-sized RC beam embedded with straight and curved configurations of the piezo sensors to evaluate the various parameters including the angle of bend, thickness, number of elements and position of placement of the curved transducers for energy harvesting. The FE simulations revealed an optimum angle of bend of the piezoelectric transducer as 120 to 180 degrees and a positive impact of the increase in thickness of the transducers for voltage generation. The outcomes of the investigation are very pivotal for the implementation of curved piezo transducers in real-life RC structures for energy harvesting and structural health monitoring.

Keywords: Curved configuration, piezoelectric energy harvesting, structural health monitoring, EMI technique.

[1] M.Tech. Research Student, Department of Civil Engineering, Indian Institute of Technology (IIT) Delhi, New Delhi - 110 016, (India). E-Mail: vkaleena@gmail.com
[2] Professor (Corresponding Author), Department of Civil Engineering, Indian Institute of Technology (IIT) Delhi, New Delhi - 110 016, (India). Email: sbhalla@civil.iitd.ac.in, Phone: (91)-11-2659-1040
[3] Scientist(Corresponding Author), CSIR-Central Road Research Institute, New Delhi – 110025, (India). E-Mail: naveet.kaur1985@gmail.com, Phone: +91-8130-332121

1. INTRODUCTION

Structural health monitoring (SHM) is an advancing engineering field that integrates leading sensor technologies with brilliant scientific codes to assess structures' state of "health", thereby improving their durability and performance most safely. It is always incorporated with the installation of several sensors and other electronic gadgets that demand power throughout their life cycle. Piezoelectric materials, which are considered as smart-materials, apart from their efficacy as sensors for SHM, can function as energy harvesters utilising the mechanical vibrations of the structures as their energy input. The ambient energy is harvested in real-time, thereby reducing the requirement for numerous batteries as the energy needs to be stored only temporarily. It also allows the devices to acquire a lifetime that is theoretically infinite, restrained only by the life span of their constituent units. Kaur and Bhalla, (2015) proposed that the same piezoelectric ceramics such as Lead Zirconate Titanate (PZT) patches in the form of concrete vibration sensor (CVS) can be utilised for SHM as well as energy harvesting of concrete structures. Nowadays, piezoceramics are available in various forms such as macro fibre composites (MFC), DuraAct, quick packs, etc as well as in various configurations such as disks, plates, rings, tubes, spheres, and so on. However, the potential of these configurations in the field of SHM and energy harvesting needs to be explored.

The energy harvesting potential of piezoelectric materials is based on the direct piezoelectric effect, the phenomenon of developing electric potential or voltage across the sides of a piezoelectric crystal when subjected to mechanical stress whereas the sensor properties are based on its converse effect which states that under the presence of an electric field, the crystals will get stressed mechanically. Structural data recorded by these piezo materials can be employed to monitor and detect damages in these structures. The surface-bonded or embedded PZT patches can be utilised for global dynamic techniques as they can provide the curvature mode shapes directly (Shanker et al., 2011). These patches have also proved their potency in localised damage detection by the method of electro-mechanical impedance (EMI) technique. The technique has been gaining wide popularity in the field of structural damage detection due to its non-destructive testing characteristics, easy implementation, and cost-effective nature of piezoelectric (PZT) transducers installed on the structure and reduction in manual inspection methods. The concept of the EMI technique was invented by Liang et al., (1994). Installation and operation particulars of the EMI technique for structural damage detection are well explained by Baptista et al., (2014) and Bhalla and Soh (2004 a). Once the PZT sensors are installed in the host structure, it is excited electrically by applying a harmonic electric potential across the PZT patch by an impedance analyser or by an LCR meter (L stands for inductance, C for capacitance, and R for resistance) at high frequencies in sweep mode. As a result, an interaction occurs between the PZT sensor's electrical impedance and the host structure's mechanical impedance. The PZT transducers which simultaneously act as sensors and actuators generate the electrical impedance signature in the same frequency range as that of the excitation signal. These signatures are then compared with the baseline signature (the signature acquired during the healthy stage of the structure) for any anomalies or damages. Previous studies have proved that the EMI technique is extremely delicate in detecting incipient damages.

Several studies have been conducted to analyse the energy harvesting potential of piezoelectric materials for the past two decades. Starner (1996) proposed that 67 W of energy can be produced from human motion by installing a piezoelectric device inside the shoe. Zhao et al., (2014) designed a piezo sandwiched thin structure

specifically for installation in shoes as an energy harvester and claimed that the harvester generated average output power of 1 mW at a frequency of approximately 1 Hz during a normal walk. Sodano et al. (2005) proved the capability of storing the energy generated by a piezoelectric plate subjected to vibrations in a Nickel-metal hydride battery. Singamsetty et al., (2014) experimentally analysed the output power generated from a PZT patch bonded to a parasitic steel structure, which is further attached to an RC beam. A maximum power output of 2.2 μW was obtained when excited at the fundamental frequency of the beam. Kaur and Bhalla (2014) researched the energy harvesting potential of surface-bonded thin piezo transducers in steel structures and concluded that a power of 1.417 μW was generated against a peak displacement of 0.289 mm in d_{31} mode. Kaur and Bhalla (2015, 2016) evaluated the energy harvesting potential of a concrete vibration sensor (CVS) which is a ready-to-cast sensor for RC structures primarily developed as an SHM device by Bhalla and Gupta (2007) [Patent application no. 1011/DEL/2011 (2007)]. The CVS can be embedded into the reinforced concrete (RC) structure while concreting and can withstand extreme conditions in contrast to the surface-bonded PZT patches (SBPS). Though SBPS generated higher voltage, CVS was found to be more beneficial in terms of various piezo parameters like the higher thickness of the piezo patch. The researchers have also investigated the potential of the CVS for SHM by interlinking global dynamic and local EMI techniques and experimentally proved that the power required to run the sensors can be harvested during the idle time from the structural vibrations.

Concrete vibration energy harvester (CVEH) is also ready to cast sensor similar to CVS but the PZT patch is placed in a curved configuration unlike the straight one in CVS, developed in SSDL, IIT Delhi with a patent filed by Kaur and Bhalla, (2016) [Patent application no. IN201611014500A]. Due to the curved configuration, the additional bending stress/strain developed across the PZT patch results in higher voltage generation. However, all piezo patches cannot be used for developing CVEH as the piezoceramics are brittle in nature. Singh (2017) was successful in fabricating a CVEH using an MFC patch and experimentally proved that the CVEH has a far higher voltage generation capacity than CVS. The piezo element used for the fabrication of CVEH should be selected in such a way that it has only a d_{31} effect. The d_{33} effect can reduce the efficiency of CVEH. Mittal (2017) performed a comparative study between the energy harvesting potential of piezoelectric ceramic rings (PCR) and straight PZT patches and experimentally demonstrated that the PCR can generate a voltage output that is 5.5 times higher than the latter one. For PCR, the poling direction was taken normal to the plane of the ring. A semi-circular-shaped piezo ring was able to generate a higher voltage than a PCR of the same arc length but a lesser angle than 180 degrees. The current study focuses on analysing the curved embedded configuration of Piezo transducers (CVEH) with radial poling direction in the field of SHM and energy harvesting for RC structures.

2. EXPERIMENTATION: MATERIALS, FABRICATION AND SETUP

Piezoceramics have secured a significant position in the field of SHM and energy harvesting due to their high stiffness, strength and coupling factors. However, these materials are brittle which restricts their suitability for curved surfaces. Therefore, a very flexible and high-performance smart material known as Macro-Fiber Composite (MFC) developed by the National Aeronautics and Space Administration (NASA) was selected for the fabrication of CVEH. MFC was prepared by sandwiching piezo ceramic rods between interdigitated electrodes, layers of adhesives, and polyimide film that enables sensing, actuation, and in-plane poling in a

durable, sealed, and ready-to-use manner. The MFC patch selected for the study was a d_{31} variant designated as M5628-P2 with a thickness of 300 μm as shown in Figure 1(a).

To compare the performance of straight and curved configurations of MFC patches, CVS and CVEH were prepared by individually encapsulating M5628-P2 MFC patches in a 1:3 cement mortar cylinder of 100 mm diameter and 30 mm height in the above-mentioned configurations respectively (Figure 1). A protective layer of epoxy was applied to MFC patches to avoid degradation during casting. The CVS and CVEH were demoulded and cured for 7 days. The sensors were then installed in an RC beam (M30 grade) of dimensions 1500 x 300 x 100 mm at the mid-span of the beam in such a way that the top surface of the sensors and the beam coincides. The properties of the RC beam and the piezo transducer are given in Table 1. The sensors were tied to the compression reinforcement at the top surface while casting the beam. It was ensured that the electrical connections are safe and secure during the curing process and are untouched by water. The RC beam embedded with CVS and CVEH sensors was placed in simply supported condition with an effective span of 1100 mm.

3. TEST PROCEDURE AND OBSERVATIONS

3.1 Open circuit voltage measurement

To measure the open-circuit voltage generated across the sensors, the RC beam was excited harmonically using an LDS V406 series portable shaker placed at the mid-span of the beam, i.e., directly above the piezo transducers. Electrical signals are generated using an Agilent 33210A function generator, which was amplified by an LDS PA500L power amplifier and transmitted to the portable shaker. The electrical signals were converted to mechanical force by the shaker. The CVS and CVEH sensors were connected to the first two channels of the TDS 2004B oscilloscope to measure the open-circuit voltage generated across the sensors. A PCB 352C34 accelerometer with a sensitivity of 100 mV per *g* was placed on the beam, closer to the shaker, and was connected to the PCB 482C Series ICP amplifier which was further connected to the third channel of the oscilloscope (Figure 2). The beam was initially subjected to sweep excitations ranging from 10 Hz to 100 Hz for 2.5 sec.

From the frequency domain analysis of the response recorded from piezo sensors and accelerometer, the beam's natural frequency equipped with the dynamic shaker at the mid-span is found to be 55 Hz (Figure 3). It was also notable from Figures 3(c) and (d) that the signal to noise ratio was significantly better for the embedded piezo sensors in comparison with the surface-mounted accelerometer.

For the comparison of open-circuit voltage generated by the piezo sensors for the same assembly of the beam shaker system, the beam was excited at designated frequencies ranging from 25 Hz to 85 Hz with a step interval of 15 Hz. The shaker was then shifted to positions at a distance of $L/3$ and $L/6$ from the left support. The open-circuit voltage generated by the CVEH (curved configuration) and CVS (straight configuration) was compared for each scenario. Figure 4 (a) shows the typical response of CVEH and CVS when excited at 85 Hz at a distance of $L/3$ from the nearest support. The variation of voltage ratio (V_{CVEH}/V_{CVS}) with respect to frequency is illustrated in Figure 4 (b).

From the experimental results, it was observed that the voltage developed across CVEH is substantially higher than that of CVS in most cases. It is because of the additional strain developed due to the curved configuration

in the former one. As per the direct effect of piezoelectricity, the voltage developed across the piezoelectric materials is directly proportional to the strain experienced by them. The CVEH was found to generate 1.6 times and 1.3 times higher voltage than CVS when excited at an *L*/3 and *L*/2 distance respectively from the nearest support. The slight drop in voltage ratio while exciting at *L*/2 distance might be due to the 3-D stress effects generated by the shaker's weight, which in this case was right above the sensors. The voltage ratio had decreased to around 0.9 when the shaker was positioned closer to the support, i.e., at an *L*/6 distance from the support. Though it is not fully explainable, it is possibly due to some support effects and the generation of certain complex stress situations. However, the first two excitation positions prove the superiority of CVEH in energy harvesting.

3.2 Comparison of power generated by piezo transducers

This section deals with the comparison of power generated across CVEH and CVS under impedance matching conditions. The experimental setup consisted of a Crompton Greaves XKF5577 crude shaker connected to a speed controller and positioned at an *L*/4 distance from the nearest support. The voltage generated across the sensors as a result of the vibrations imparted by the shaker was measured using TDS 2004B oscilloscope. The crude shaker causes the beam to vibrate in a non-sinusoidal pattern, simulating a real-life situation. At the midpoint of the beam, a PCB 352C34 accelerometer with a sensitivity of 100 mV per *g* is linked to a PCB 482C Series ICP amplifier, which was then connected to the oscilloscope's third channel. An additional circuit as shown in Figure 5 was connected to the sensors for power measurement.

The voltage (V_1) generated across the sensors due to the vibrations is the input voltage to the circuit. Because of the high electrical impedance of the piezo transducer, the electric current (i) passing through the circuit will be very small, usually in the microampere range, making it almost impossible to measure. As a result, an Agilent 34411A digital multimeter was used to measure the circuit's output voltage (V_2), which was then linked to the laptop for data acquisition. The current flowing through the circuit is estimated as

$$i = V_2 \big/ R_1 \tag{1}$$

The power generated by the sensors is thus given by

$$P = i^2 \left(R_1 + R_2 \right) \tag{2}$$

According to the maximum power transfer theorem, the source impedance (or resistance) must match the load impedance (or resistance) to generate the maximum amount of power (Kaur, 2015). The impedance values of the CVEH and CVS were measured for various frequencies ranging from 25 Hz to 80 Hz with a step interval of 5 Hz using an Agilent E4980A LCR meter and their average values were 35 kΩ and 32 kΩ respectively.

Based on the principle of impedance matching and the maximum power transfer theorem, the load resistors (R_1 = 335 kΩ and R_2 = 340 kΩ) were chosen such that they are in a similar range as that of the piezo transducers. A highly unmatched system can lead to excessive loss of power and heat dissipation. It can even lead to circuit failure. Three sets of measurements were taken by varying the acceleration of the shaker to

compare the power generated across CVS and CVEH (Figures 6 and 7). From the previous section, it is clear that the voltage developed across the CVEH was higher than the CVS and therefore, the power developed across them is expected to be higher for CVEH. This is justified by the experimental results as the average power ratios (P_{CVEH}/P_{CVS}) of the three sets of measurements were about 10.36 implying that CVEH is 10 times more powerful than CVS in terms of power generation.

3.3 Potential of power storage

The energy generated from the piezo sensors due to the vibrations of the beam was stored in a 1000μF capacitor. The experimental setup is similar to that of the power measurement setup, except that the power measurement circuit was replaced by a simple full bridge rectifier circuit (Figure 8). The function of the rectifier circuit is to convert the output voltage generated by the piezo sensors in the alternating current (AC mode) to a stable power supply in the direct current (DC) mode so that it can be stored in a capacitor.

The experiment was conducted by vibrating the beam in two different accelerations provided by the shaker and the output voltage stored in the capacitor with respect to time was measured using an Agilent 34411A digital multimeter. The total energy stored in the capacitor is given by

$$E_T = \frac{1}{2} C V_c^2 \tag{3}$$

where C is the capacitance (1000 μF) and V_c is the output voltage of the rectifier circuit which is stored in the capacitor. The average power stored in the capacitor was determined as $P_{avg} = E/T_c$ where T_c is the total charging time.

The average mid-point acceleration of the beam in the two experiments was 4.89 m/s^2 and 8.84 m/s^2. The reference voltage considered for the study was 1.6 V based on the charging curve of the capacitors, and the corresponding energy harvested in the capacitors was 1.28 mJ as per Eq. (3). CVEH and CVS were charged in 236 seconds and 335 seconds, respectively, for an average mid-point acceleration of 4.89 m/s^2 and their equivalent power storage was 5.42 μW and 3.82 μW. As the average acceleration was increased to 8.84 m/s^2, the charging time was lowered to 148 and 249 seconds, respectively, and the power storage was increased to 8.65 μW and 5.14 μW. The charging curve of CVEH and CVS and their corresponding power storage are depicted in Figures 9 and 10. CVEH had harvested an average of 1.55 times higher power in each case, revealing its pre-eminence in the field of energy harvesting.

3.4 Damage detection potential

Piezoelectric sensors have established their efficacy in the field of damage detection for the past few decades. They are suitable for global vibration techniques as well as for local electromechanical impedance (EMI) techniques. However, the potential of the curved configuration of piezo sensors for damage detection is not yet analysed. The damage detection ability of CVEH (curved configuration) and CVS (straight configuration) sensors embedded inside an RC beam using the EMI technique are compared in the current section.

The experiment was conducted on the same beam installed with CVS and CVEH as mentioned in the previous section. The beam was mounted with the crude shaker, though it was not required for this part of the study.

The piezo transducers were connected to the Agilent E4980A LCR meter which was further connected to the laptop for data acquisition. Throughout the experiment, a room temperature of 29 ^{o}C was maintained, which was ensured using a La Crosse Technology WS-9006U model digital thermometer. The sensors were electrically excited by applying a harmonic electric potential across them using the LCR meter at high frequencies in sweep mode and their admittance signatures (baseline signature) were acquired. Damages were then induced in the structure by drilling 3 holes (equidistant from both CVS and CVEH) in the beam successively as shown in Figure 11 and the corresponding admittance signatures were acquired after inducing each damage. These signatures were then compared with the baseline signatures. In each stage (healthy stage and three damaged stages), the harmonic electric potential was applied across the piezo transducers in a coarser frequency range (1 kHz to 1000 kHz with a step interval of 1 kHz) as well as in a finer frequency range (100 kHz to 300 kHz with a step interval of 100 Hz).

Two signatures were obtained in each case and their correlation coefficient is calculated using the Eq. (6). The correlation between the two signatures in each case shall be closer to 1 if they are working well. Identical signatures will not be generated if there is any failure or debonding of the MFC patch leading to a decline in the value of the correlation coefficient. In this method, the Pearson correlation coefficient, a measure of the linear correlation between two samples of data is used to check the correlation between two similar signatures and is given by

$$CC = \frac{\sum_{i=1}^{n}(x_i - \bar{x})(y_i - \bar{y})}{\sqrt{\sum_{i=1}^{n}(x_i - \bar{x})^2}\sqrt{\sum_{i=1}^{n}(y_i - \bar{y})^2}} \tag{4}$$

where CC is the Pearson correlation coefficient, n is the sample size, x_i and y_i are the i^{th} value in the two signatures, and $\bar{x}$ and $\bar{y}$ represent the mean of the two signatures x and y respectively. In the experiment, a correlation coefficient greater than 0.99 was obtained in each case, thereby ensuring the proper functioning of the sensors.

To quantify the variation in signatures from the baseline signature after damage, the root mean square deviation (RMSD) value between the two was calculated using the equation

$$RMSD(\%) = \sqrt{\frac{\sum_{i=1}^{n}(x_{di} - x_{hi})^2}{\sum_{i=1}^{n} x_{hi}^2}} \times 100 \tag{5}$$

where n is the sample size, x_{di} and x_{hi} are the i^{th} value in the damaged and healthy signatures respectively.

From Figures 12 and 13, it is obvious that the deviation (leftward shift) of damaged signatures from healthy signatures was more significant in the CVEH than in the CVS. This leftward shift in the signatures represents the loss of stiffness in the structure due to the induced damage. Both conductance (real part of the admittance) and susceptance (imaginary part of the admittance) signatures corresponding to the wider range of frequencies ranging from 1 kHz to 1000 kHz were found to generate more reliable data for damage identification than the narrow range of frequencies from 100 kHz to 300 kHz. This is due to the significant

peak observed in the former range. This eminent peak in the conductance signatures between 600 kHz to 800 kHz corresponds to the resonance frequency of the piezo transducer in the thickness mode. Therefore, it is always preferable to choose the excitation frequency range that includes such peaks. Figure 14 portrays the RMSD variation of the signatures in each case.

For 1 kHz to 1000 kHz excitation, the RMSD index of the conductance and susceptance signatures was significant in identifying the first and second damages. For CVEH and CVS, the RMSD index of conductance signature after second damage was 77% and 33% respectively. However, it was decreased to 34% and 20% respectively in the case of third damage. The shift of signatures had also changed the direction after the third damage. This is due to the limitation of the EMI technique as the damage level escalates from incipient to moderate, it becomes less distinguishable, though it is highly reliable for incipient damage cases (Kaur, 2015, Shanker et al., 2011). It is also notable that in all the three damaged stages, CVEH showed a higher RMSD index than the CVS. Similarly, the RMSD variation of susceptance signatures was also maximum for the second damage with 91% and 37% respectively for CVEH and CVS and decreased afterwards.

For 100 kHz to 300 kHz excitation, there was no substantial variation in the signatures and therefore the RMSD values were less than 10% in each case. Minor variations in signatures may arise owing to external factors beyond the control. As a result, no valid conclusions can be drawn from these values. For this range of excitation, a performance comparison of CVEH and CVS for damage identification was also not possible as they do not follow a particular trend. Therefore, this frequency range was inappropriate for the current investigation.

4. FINITE ELEMENT MODELLING AND PARAMETRIC STUDY

4.1 Details of the modelling

To study the effect of various parameters of the MFC transducer in the field of energy harvesting, a 3-D model of a simply supported RC beam embedded with CVS and or CVEH is developed in COMSOL 4.4 FE software. The dimensions of the beam considered for the study were 3000 mm x 300 mm x 500 mm. The length, breadth, and depth of the beam were taken along the global X, Y, and Z directions respectively. The major properties of the RC beam and MFC patch are listed in Table 1. Concrete was considered as a linearly elastic and isotropic material and the reinforcement bars were ignored in the model. The dimensions of CVS and CVEH are the same as mentioned in section 2. Though the actual thickness of the MFC patch is 300μm, it was taken as 1mm in the model due to the difficulty in meshing the minute dimensions in COMSOL 4.4 version. As it is a comparative study between the CVS and CVEH model, the change in thickness will not affect the relative voltage generated in both cases. The CVS or CVEH whichever the case may be, were placed inside the beam so that the top surface of the CVS or CVEH coincides with that of the beam and was placed centrally with respect to the plan dimension of the beam.

The ‘Piezoelectric Devices Interface’ listed under the category of ‘Structural Mechanics’ had been utilized for the FE modelling of the patch. The interface has the ability to simulate both the direct as well as the converse piezoelectric effects by the method of piezoelectric coupling using stress or strain charge formulations. The strain charge form was considered for the current study. The poling direction of the MFC patch is normal to its surface. However, in the COMSOL 4.4 software, the poling direction is taken along the

global Z direction. For CVS, this poling direction is in agreement with the actual poling direction, whereas for CVEH, each point has a different polling direction due to its curvature as shown in Figure 15. Therefore, the study modelled curved MFC patch as a combination of 5 linear elements with the poling direction taken normal to each element by the method of coordinate transformation. The model of the RC beam and the piezo transducers are shown in Figure 16. As the MFC patch was supposed to act as an electric circuit, ground condition or electric potential equal to zero condition was applied to the top surface of the MFC patch. The bottom surface of the same was taken as terminal 1 with a terminal charge equal to zero coulombs. A dynamic load of 1kN was applied in the vertically downward direction at a point at one-fourth distance from the left end of the beam. The frequency of the load ranges from 60 Hz to 100 Hz with an interval of 5 Hz. A frequency analysis is performed in COMSOL 4.4 for various curvatures of the MFC patch and the voltage developed across the MFC patch was determined.

4.2 Validation of the FE analysis

To validate the FE analysis, the beam size was remodelled to match that of the experimental beam of an effective span of 1.3 m (refer section 2 for other properties) and an impact hammer test was conducted at one-fourth of the span. The time-domain response of the CVEH obtained through an oscilloscope was converted to the frequency domain by using Fast Fourier Transform (FFT) and was compared with the FE results. The curvature of the CVEH was taken as 60 degrees. As the frequency of the external load matches the natural frequency of the beam, it experiences maximum vibration and thus, the voltage developed across the sensors attains the peak value. The natural frequency of the simply supported beam was determined analytically as 88.8 Hz as per the Eq. (8)

$$f_n = \frac{\pi}{2}\sqrt{\frac{EI}{mL^4}} \tag{6}$$

where f_n is the natural frequency of the beam in Hz, E is the modulus of elasticity in N/m^2, I is the moment of inertia in m^4, m is mass per unit length in kg/m and L is the effective length of the beam in meters. The FE analysis and experimental analysis suggested the natural frequency of the beam as 90 Hz and 89.6 Hz respectively which was in close agreement with the analytical value and thereby validated the FE model (Figure 17).

4.3 Effect of curvature of the MFC patch

Various configurations of CVEH embedded in RC beam were developed in COMSOL 4.4 as per section 4.1 to analyse the relative piezoelectric energy harvesting capacity of each system. A sweep analysis was conducted for frequencies ranging from 70 Hz to 100 Hz with a step interval of 5 Hz. The peak voltage was obtained when excited at its natural frequency for all the curvatures or angles of bend and it matched with the theoretical natural frequency of 83 Hz based on Eq. (13). The peak voltage developed across the MFC patch was least for the CVS model. Though the peak voltage increases with the curvature of CVEH, a deviation was observed in the 170-degrees curved model. Therefore, further study was conducted to analyse the variation of peak voltage for a wide range of curvatures of CVEH by exciting the structure at its natural frequency. Results of the analysis are depicted in Figure 18.

It was observed that for very small sector angles i.e., up to 10 degrees, voltage showed a decreasing trend with the curvature. However, after 30 degrees, the curved configuration generated a higher voltage than the straight configuration. For angles of bend between 30 degrees and 120 degrees, the increase in voltage with respect to bend angle was at a slow rate whereas it has a significant effect beyond 120 degrees with a peak at 145 degrees. Therefore, a sector angle or angle of bend between 120 degrees to 180 degrees can be considered the optimum range of curvature for piezoelectric energy harvesting.

The studies were conducted on 5-element CVEH models and 145-degrees curved configuration generated 1.4 times higher voltage than the straight configuration. An increase in the number of linear elements in the curved transducer model can give a better representation of the curved patch. Hence the 11-element model and 15-element model were also developed for 145 degrees bend and a sweep analysis is performed on these models, results are plotted in Figure 19. In the voltage generated by the transducers, it was observed that the peak voltage was increasing with the increase in the number of elements considered in the model. A higher peak was observed in the 15-element model which is 1.63 times that of the CVS model. However, convergence can be observed in the results of 10 and 15-element models, pointing out that a 15-element model is a good representation of the actual system.

4.4 Effect of thickness of the MFC patch

To analyse the effect of thickness of the MFC transducer in voltage generation, FE models mentioned in the previous section were redesigned for various values of thickness of the transducer and were analysed for an excitation frequency of 85 Hz. The thickness range of the MFC patch considered for the study was 0.6 mm to 1.5 mm. A sweep analysis was also conducted for more clarity regarding the effect of thickness in voltage generation. From Figure 20, it was evident that the increase in thickness of the MFC transducer had a positive impact on increasing the voltage generation**.** This is similar to the trend of embedded CVS in RC beams as mentioned by Kaur and Bhalla, (2016).

4.5 Effect of the location of CVEH

It is necessary to find the position at which CVEH has to be placed along the depth of the beam to obtain maximum voltage. A sweep analysis was therefore conducted by varying the position of CVEH along the depth of the beam for the same load at a frequency of 85Hz. The results of the analysis are plotted in Figure 21. It was observed that the maximum voltage is generated when CVEH is placed towards the top or bottom of the beam whereas almost no voltage was generated when CVEH is at the mid-depth of the beam. This is because the strain developed in a beam under bending action is maximum at the extreme fibres and reduces linearly to zero towards the centre of the beam cross-section.

As per the direct effect of piezoelectricity, the mechanical stress or strain applied across the patch is directly proportional to the terminal voltage (Eq. (6)). Therefore, the same effect of linear reduction can be seen in the voltage generated across the MFC patch towards the mid-depth of the beam. Hence, it is suggested to embed the CVEH either towards the top or bottom surface of the beam where the strain development is maximum.

5. CONCLUSIONS

Various experimental studies followed by FE analysis have been conducted to analyse the potentiality of embedded curved configuration (CVEH) of Piezo transducers relative to its straight configuration (CVS) for energy harvesting in RC structures. The damage detection capability of curved piezo sensors over straight ones is also experimentally investigated by the method of EMI technique. The study thus opens up the door to the field of SHM for curved piezo transducers. The RC beam embedded with the piezo sensors at the mid-span is harmonically vibrated at various frequencies and the open-circuit voltage generated across them is measured. CVEH generated 1.6 times higher voltage than CVS when excited at $2l/3$ (l is the mid-span length) distance from the nearest support. The voltage ratio (V_{CVEH}/V_{CVS}) has reduced to 1.3 when the shaker is placed directly above the sensors due to the counteraction of the strain developed across the CVEH by the additional axial strain generated due to the weight of the shaker. It is also notable that a better signal to noise ratio is obtained for embedded piezo sensors in comparison to the surface-mounted accelerometer. The power generated across the piezo sensors is compared by the impedance matching method and found that the CVEH can generate an average of 10 times higher power than the CVS. The study further investigated the ability of power storage of these sensors by storing the piezoelectric energy in a 1000 μF capacitor. From the periodic vibrations of the beam, the CVEH stored 5.8 μW and 8.5 μW powers corresponding to 3.7 μW and 5 μW power of CVS for average accelerations of 4.9 m/s^2 and 8.8 m/s^2 respectively, proving that CVEH can store an average of 60% higher power than CVS.

To examine the damage detection potential of CVEH and CVS, a local vibration method known as the EMI technique is employed and obtained the baseline or healthy signatures of the RC beam in the initial stage. Damages are then induced in the beam successively and corresponding signatures are also measured. The deviation from the baseline signature provides a qualitative measure of the damage in the beam. Correlation values greater than 99% are obtained for similar signatures of both transducers in each stage pointing to the fidelity of CVS and CVEH. Higher deviation or shift in the signatures are obtained in the response of CVEH than CVS. RMSD index also showed higher values in the case of CVEH suggesting its propriety in structural health monitoring. Comparing the signatures in the range of 1 kHz to 1000 kHz and 100 kHz to 300 kHz, significant deviation or higher RMSD values are obtained in the former range. A significant peak corresponding to the resonance frequency in the thickness mode of the MFC transducer is observed in the former range and therefore higher deviations are obtained near the peak, leading to higher RMSD values. However, the latter range of frequencies is quite narrow to include such peaks and therefore the results are less reliable. Hence it is recommended to wisely choose the frequency ranges for excitation. The RMSD index of the signatures corresponding to first and second damage showed significant values, however, it decreased in the case of third damage. The shift in the signature of the third damage is in the reverse direction as that of the former ones. This is because the EMI technique is more impeccable in detecting incipient damages and is uncertain for moderate to severe damages.

A finite element analysis has been conducted using COSMOL 4.4 FE software to determine the effect of curvature, thickness and position of placement of the MFC transducer along the depth of the beam for improving the energy harvesting potential of CVEH. The actual poling direction of the curved MFC patch is normal to its curvature at each point. However, the default poling direction in COSMOL 4.4 FE software is along the global Z-direction. Hence the MFC transducer is modelled as a combination of 5-linear elements

with the polarisation direction taken normal to each element by the method of coordinate transformation. The FE analysis is validated by conducting an impact hammer test on the RC beam embedded with CVS and CVEH and matching the natural frequency of the beam from the experiment and FE analysis with the analytical value. The peak voltages are generated across the sensors when excited at their natural frequencies. On investigating the effect of the curvature of the transducer, it is noticed that an optimum bend angle between 120 degrees to 180 degrees has a significant impact on the voltage generated across the sensor, with the peak voltage obtained at 145 degrees, which is 1.4 times as that of the straight configuration. The curved MFC patch is also remodelled as a combination of 10-linear elements and 15-linear elements and witnessed a convergence in the voltage generated with the higher number of elements. The 15-element model of the curved MFC transducer generated 1.63 times higher peak voltage than the CVS for a bend angle of 145 degrees. The voltage generated across the transducers showed an increasing trend with an increase in their thickness when analysed for a thickness range of 0.6 mm to 1.5 mm which is analogous to the trend of embedded PZT based CVS in RC beam as mentioned by Kaur and Bhalla, (2016). As per the FE analysis, it is advised to place the CVEH towards the top or bottom of the beam cross-section where the beam experiences maximum strain. The direct effect of piezoelectricity states that the mechanical stress or strain applied across the piezoelectric material is directly proportional to the terminal voltage developed across them. Therefore, a linear reduction is observed in the terminal voltage as the position of the MFC patch is moved towards the centre of the cross-section, with maximum voltage at the top or bottom of the beam cross-section. The results of the experimental and numerical investigations summarise the suitability of curved piezo transducers embedded in RC structures for energy harvesting and SHM.

6. REFERENCES

1) Balguvhar, S., 2020. Piezoelectric energy harvesting through low-frequency non-sinusoidal vibrations of civil structures. Ph. D Thesis, Indian Institute of Technology Delhi, New Delhi, India
2) Baptista, F.G., Budoya, D.E., De Almeida, V.A. and Ulson, J.A.C., 2014. An experimental study on the effect of temperature on piezoelectric sensors for impedance-based structural health monitoring. *Sensors*, *14*(1), pp.1208-1227.
3) Bhalla, S. and Gupta, A.,2007. A novel vibration sensor for concrete structures. (Invention Disclosure Dt. 26 February 2007 (FT/IRR/CE/SB/2007/0570)). *Foundation for Innovation Technology and Transfer (FITT)*, IIT Delhi, Patent application no: 1011/DEL/2011, New Delhi (India).
4) Bhalla, S. and Soh, C.K., 2004. Structural health monitoring by piezo-impedance transducers. I: Modeling. *Journal of Aerospace Engineering*, *17*(4), pp.154-165.
5) COMSOL. COMSOL Multiphysics Pvt. Ltd. 2021, http://www.comsol.co.in/
6) Kaur, N. and Bhalla, S., 2014. Feasibility of energy harvesting from thin piezo patches via axial strain (d 31) actuation mode. *Journal of Civil Structural Health Monitoring*, *4*(1), pp.1-15.
7) Kaur, N. and Bhalla, S., 2015. Combined energy harvesting and structural health monitoring potential of embedded piezo-concrete vibration sensors. *Journal of Energy Engineering*, *141*(4), p.D4014001.
8) Kaur, N. and Bhalla, S., 2016. Numerical investigations on energy harvesting potential of thin PZT patches adhesively bonded on RC structures. *Sensors and Actuators A: Physical*, *241*, pp.44-59.
9) Kaur, N. and Bhalla, S.,2016. Concrete vibration energy harvester. Patent Application no: 201611014500 A, Indian Patent Office.

10) Kaur, N., 2015. Integrated structural health monitoring and energy harvesting potential of adhesively bonded thin Piezo patches operating in $d31$ mode. Ph. D Thesis, Indian Institute of Technology Delhi, New Delhi, India

11) Liang, C., Sun, F.P. and Rogers, C.A., 1997. Coupled electro-mechanical analysis of adaptive material systems-determination of the actuator power consumption and system energy transfer. *Journal of intelligent material systems and structures*, *8*(4), pp.335-343.

12) Mittal, P., 2017. Fabrication and evaluation of concrete vibration energy harvester (CVEH) using piezoelectric ceramic ring. M. Tech Thesis, Indian Institute of Technology Delhi, New Delhi.

13) PI Ceramic (2021), Product Information Catalogue, Lindenstrasse, Germany, https://www.piceramic.com/en/products

14) Shanker, R., Bhalla, S. and Gupta, A., 2010. Integration of electro-mechanical impedance and global dynamic techniques for improved structural health monitoring. *Journal of Intelligent Material Systems and Structures*, *21*(3), pp.285-295.

15) Singamsetty, S., Kaur, N. and Bhalla, S.,2014. Energy harvesting from structural vibrations using Piezo transducers: A parametric study, *3rd International Conference on Sustainable Innovative Techniques in Architecture*, Civil and Environmental Engineering (SITACEE - 2014) organized by "Krishi Sanskriti", April 26th -27th, Jawaharlal Nehru University, New Delhi, India, pp. 331-334

16) Singh, N., 2017. Fabrication and evaluation of concrete vibration energy harvester (CVEH). M. Tech Thesis, Department of Civil Engineering, Indian Institute of Technology Delhi, New Delhi, India.

17) Smart Materials (2021), https://www.smart-material.com/MFC-product-mainV2.html.

18) Sodano, H.A., Inman, D.J. and Park, G., 2005. Generation and storage of electricity from power harvesting devices. *Journal of intelligent material systems and structures*, *16*(1), pp.67-75.

19) Starner, T., 1996. Human-powered wearable computing. *IBM systems Journal*, *35*(3.4), pp.618-629.

20) Zhao, J. and You, Z., 2014. A shoe-embedded piezoelectric energy harvester for wearable sensors. *Sensors*, *14*(7), pp.12497-12510.

LIST OF FIGURES

LIST OF TABLES

FIGURES & TABLES:

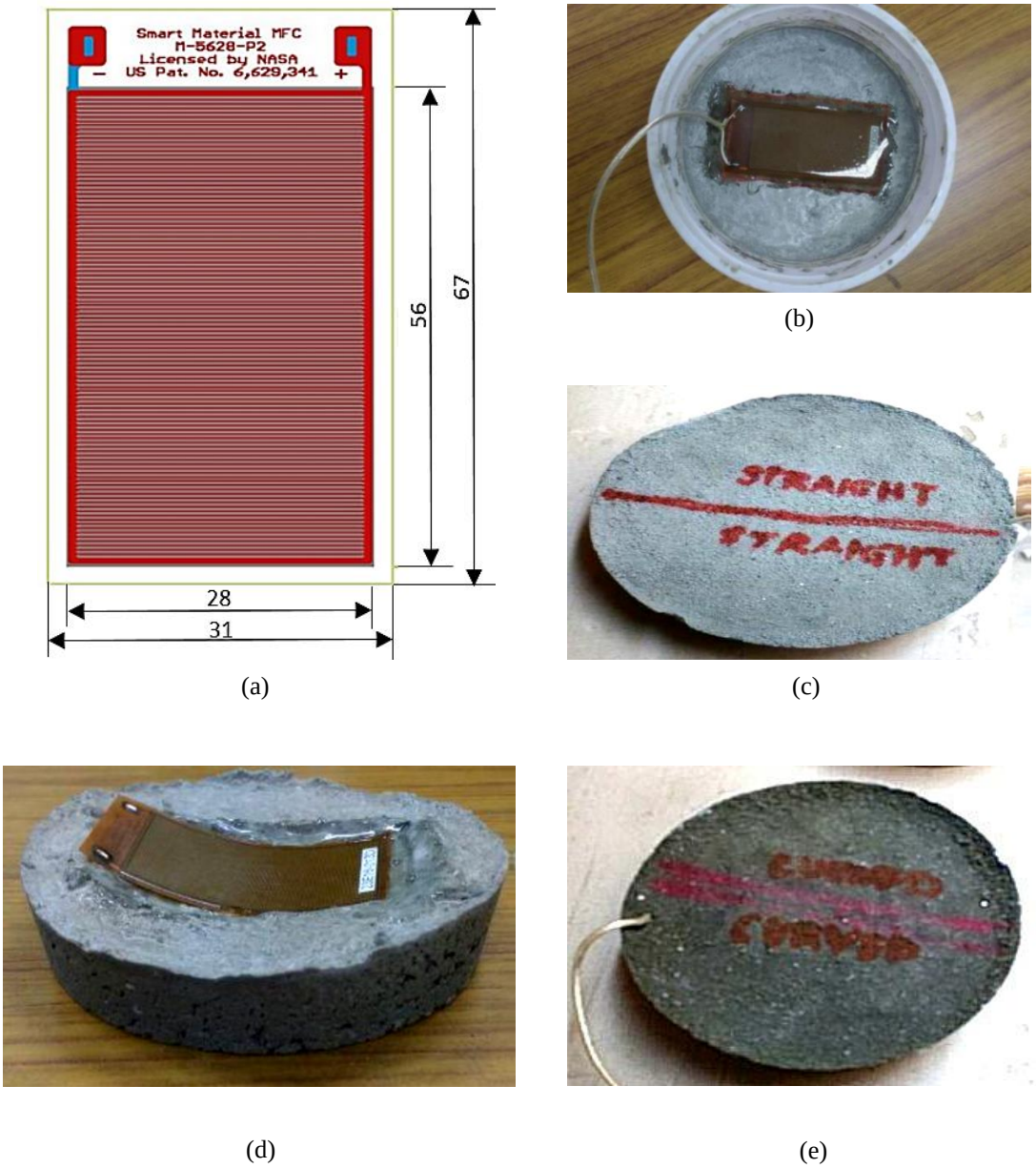

(a) (b) (c) (d) (e)

Figure 1: (a) M5628-P2 model MFC transducer (Smart Materials, 2021)
(b) Fabrication of CVS using MFC
(c) MFC based CVS
(d) Fabrication of CVEH using MFC
(e) MFC based CVEH

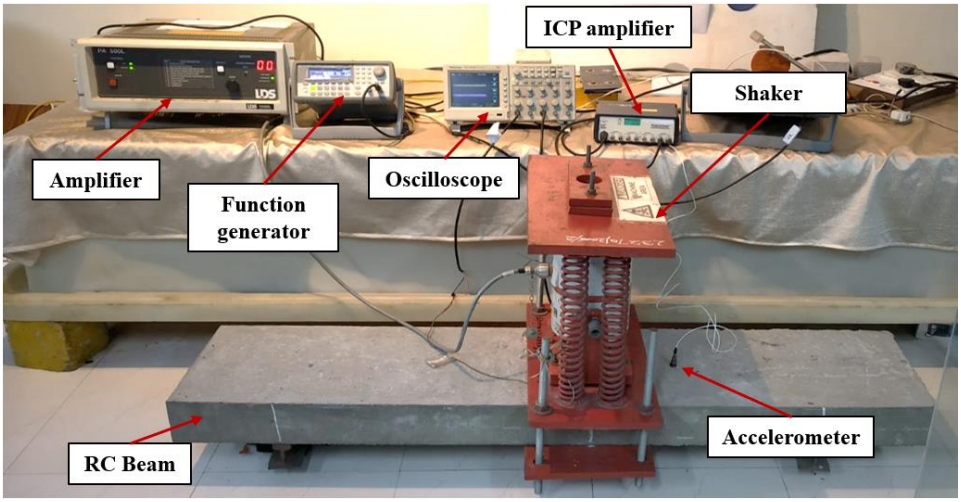

Figure 2: Experimental setup for open-circuit voltage measurement (shaker at midspan of the beam)

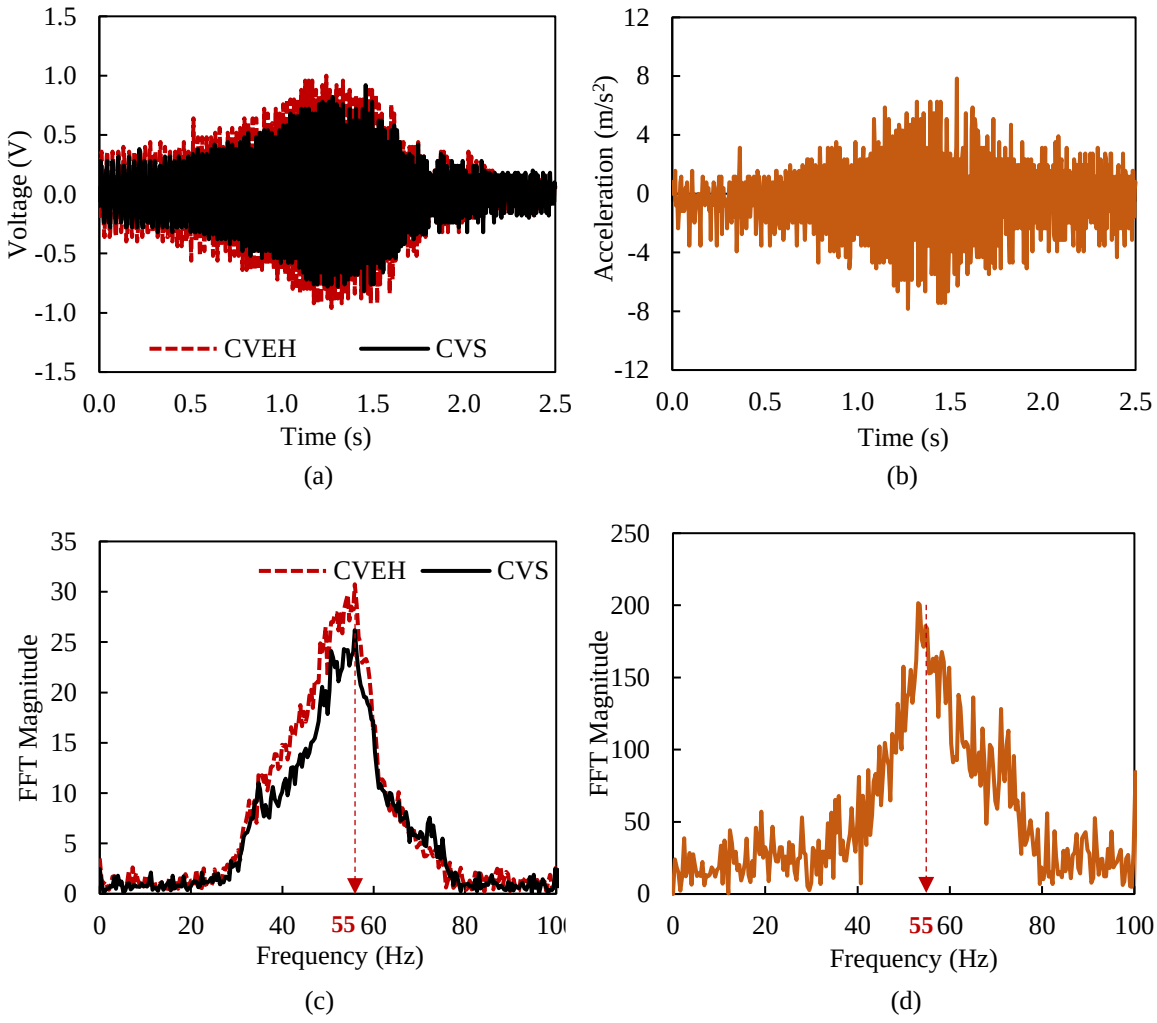

Figure 3: (a) Time-domain response of CVS and CVEH, subjected to sweep excitation

(b) Time-domain response of accelerometer, subjected to sweep excitation

(c) Frequency domain response of CVS and CVEH

(d) Frequency domain response of the accelerometer

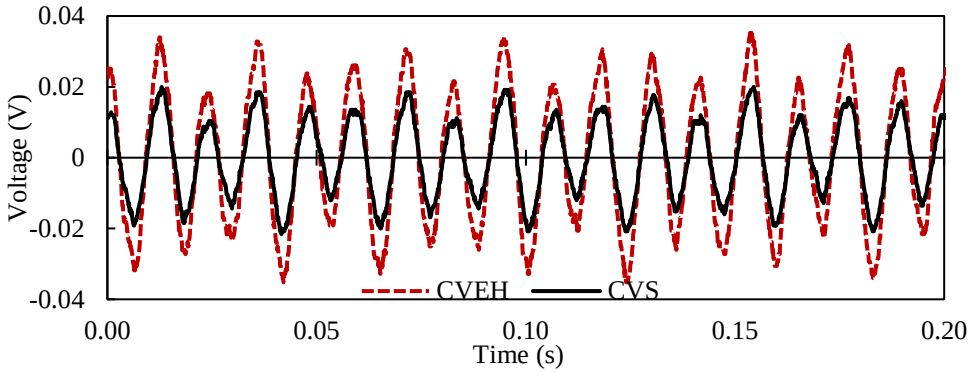

(a)

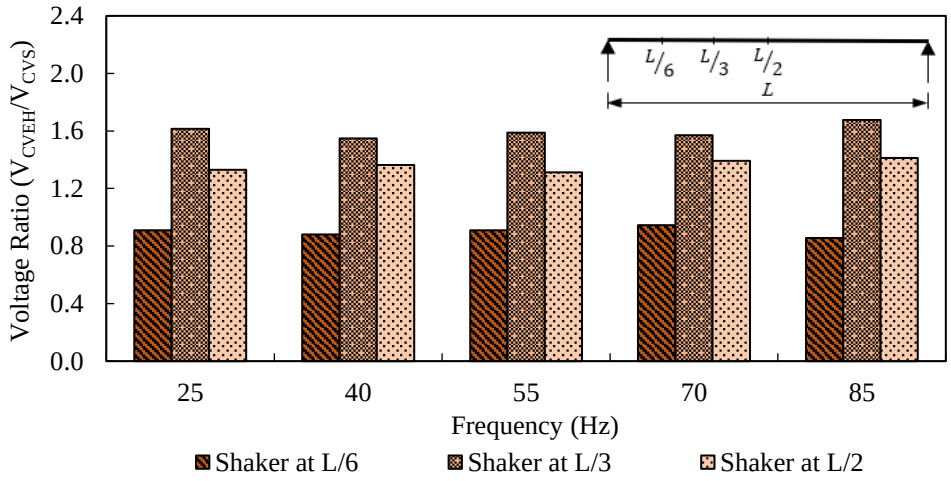

(b)

Figure 4: (a) Response of CVEH and CVS when excited at 85Hz at *L*/3 distance from the nearest support
(b) Variation of voltage ratio with respect to frequency for various positions of excitation

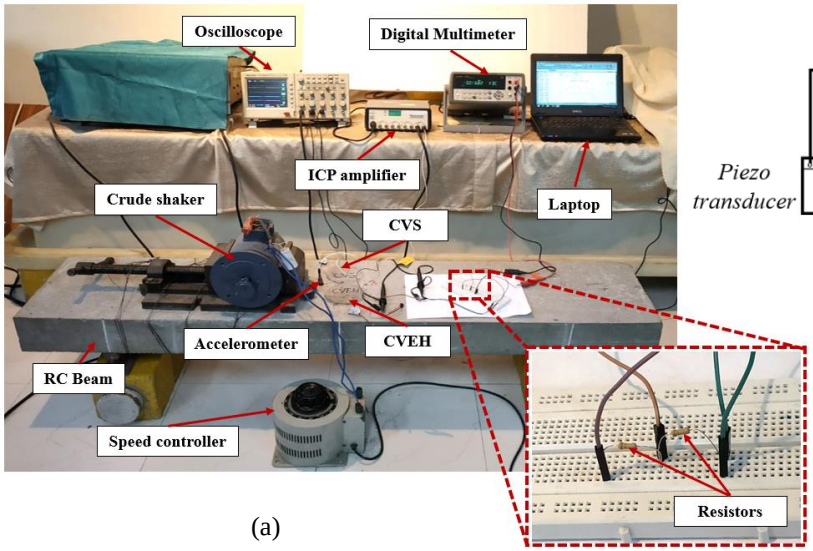

(a)

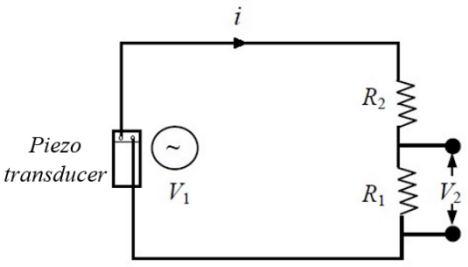

(b)

Figure 5: (a) Experimental setup for power measurement
(b) Circuit employed for power measurement

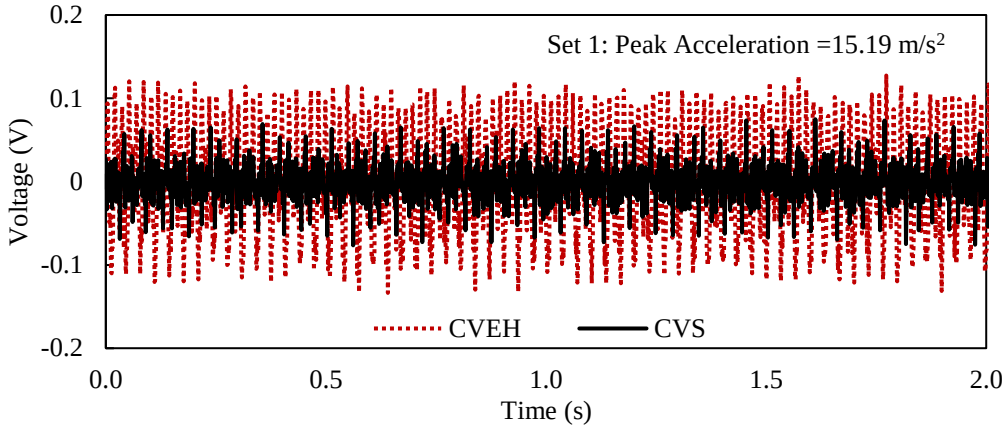

(a)

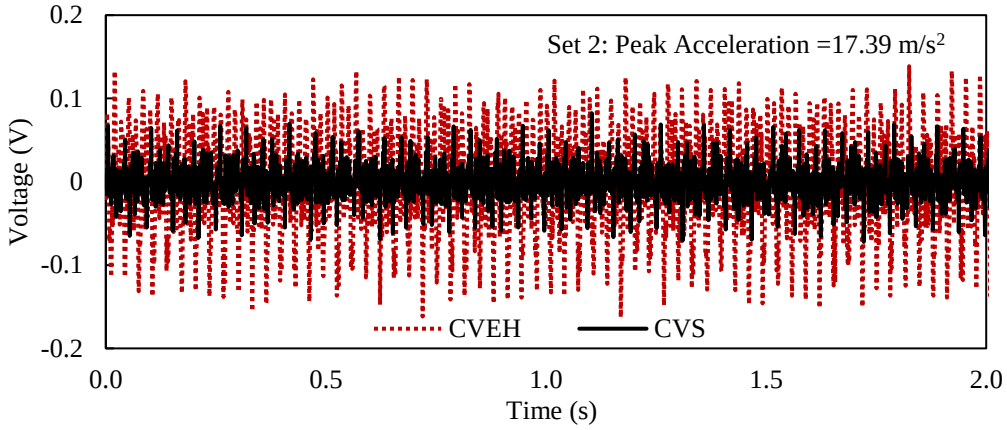

(b)

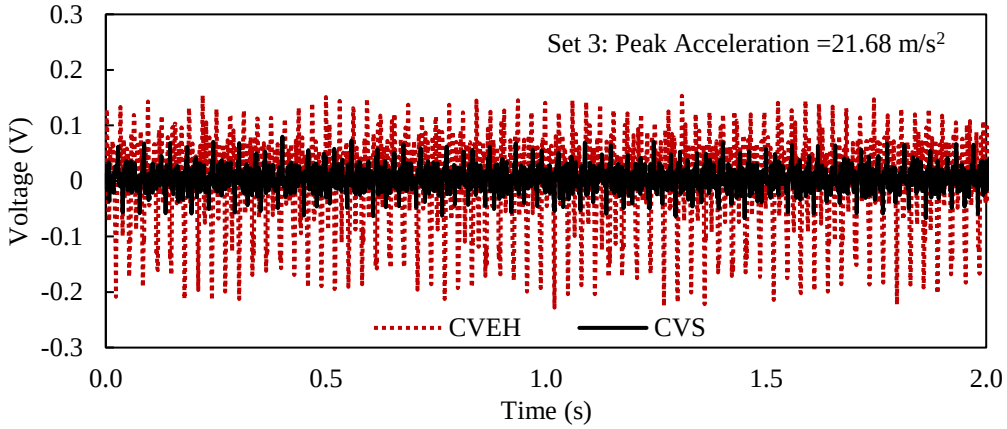

(c)

Figure 6: (a) Output voltage of the circuit for a peak acceleration of 15.19 m/s^2

(b) Output voltage of the circuit for a peak acceleration of 17.39 m/s^2

(c) Output voltage of the circuit for a peak acceleration of 21.68 m/s^2

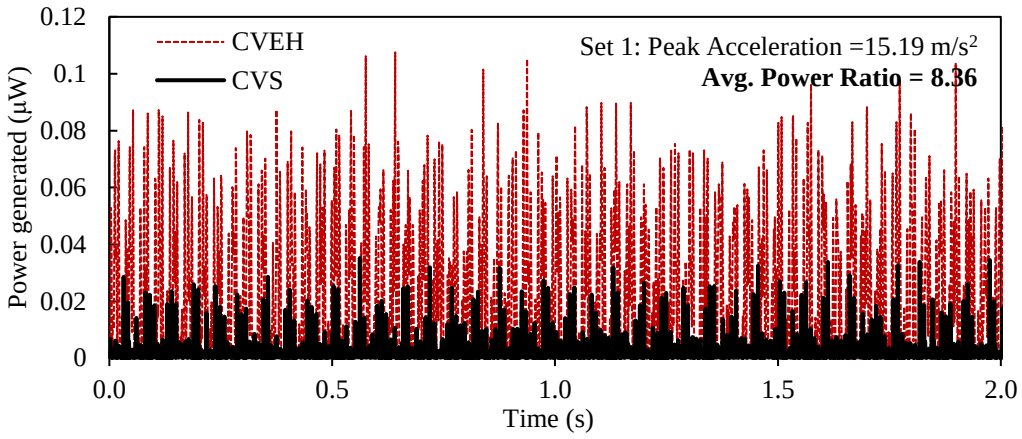

(a)

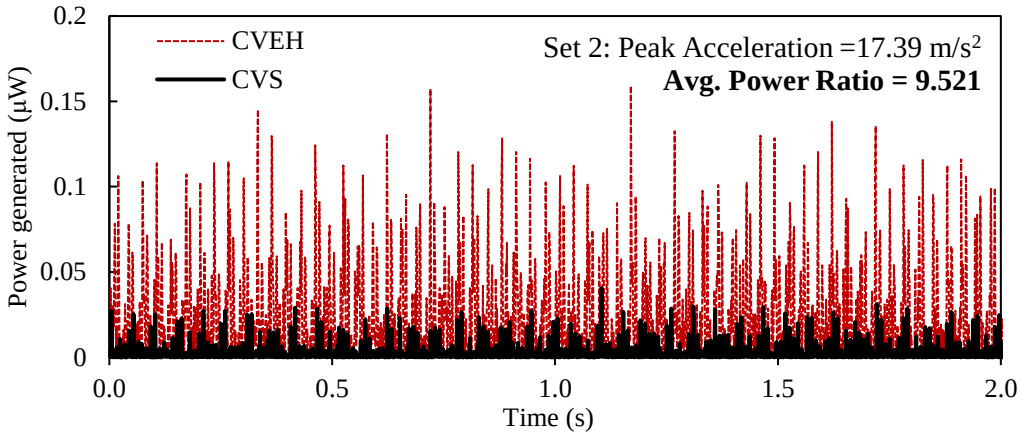

(b)

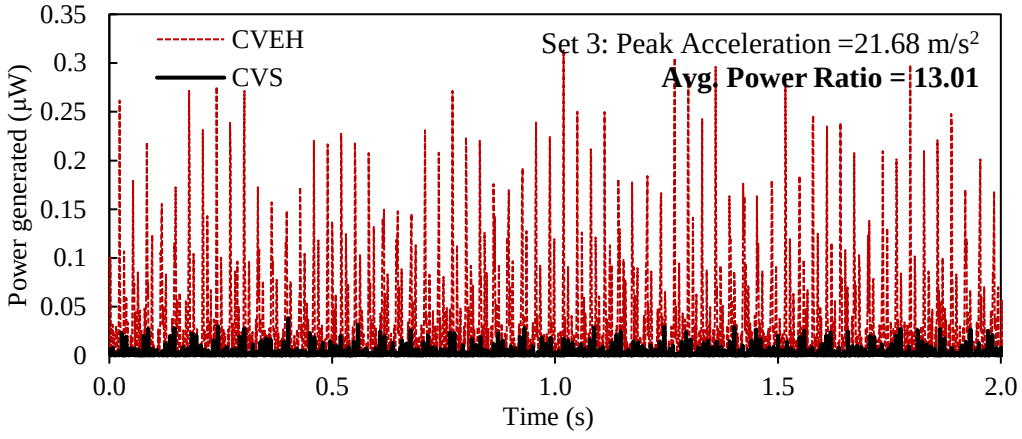

(c)

Figure 7: (a) Power developed across the sensors for a peak acceleration of 15.19 m/s^2

(b) Power developed across the sensors for a peak acceleration of 17.39 m/s^2

(c) Power developed across the sensors for a peak acceleration of 21.68 m/s^2

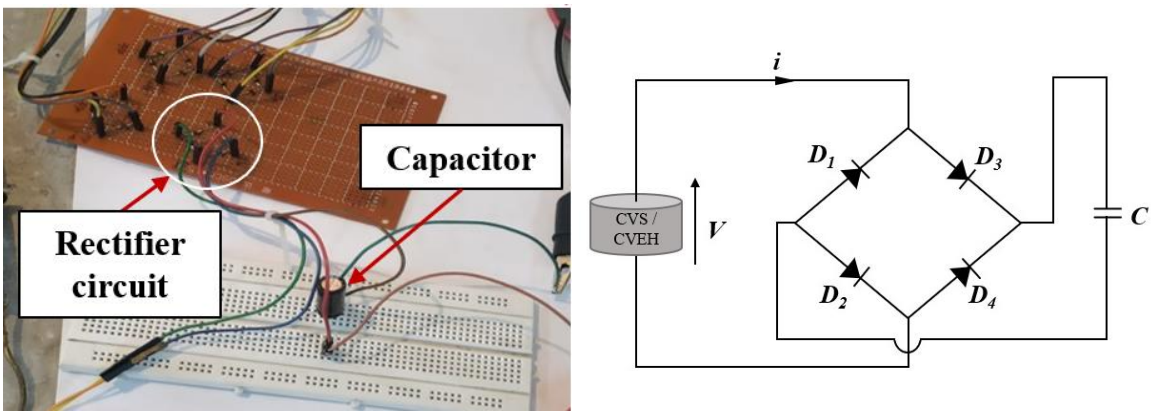

(a) (b)

Figure 8: (a) Experimental setup for power storage in a capacitor
(b) Schematic diagram of simple bridge rectifier circuit

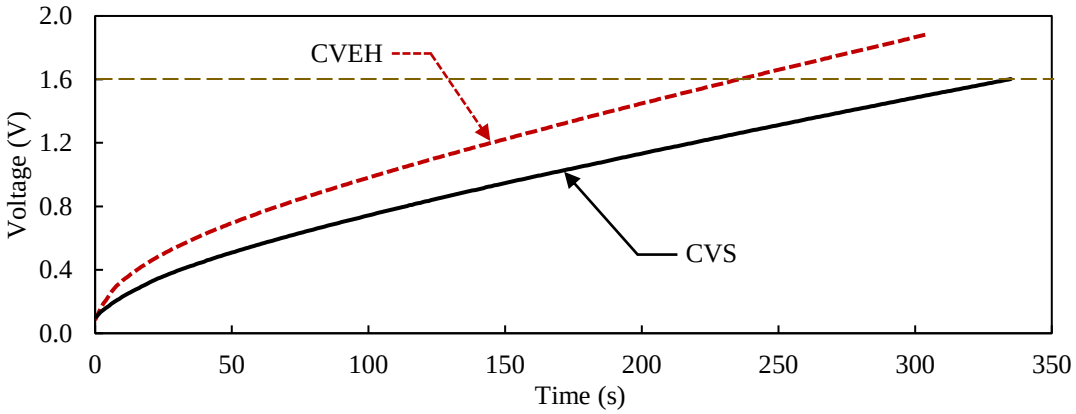

(a)

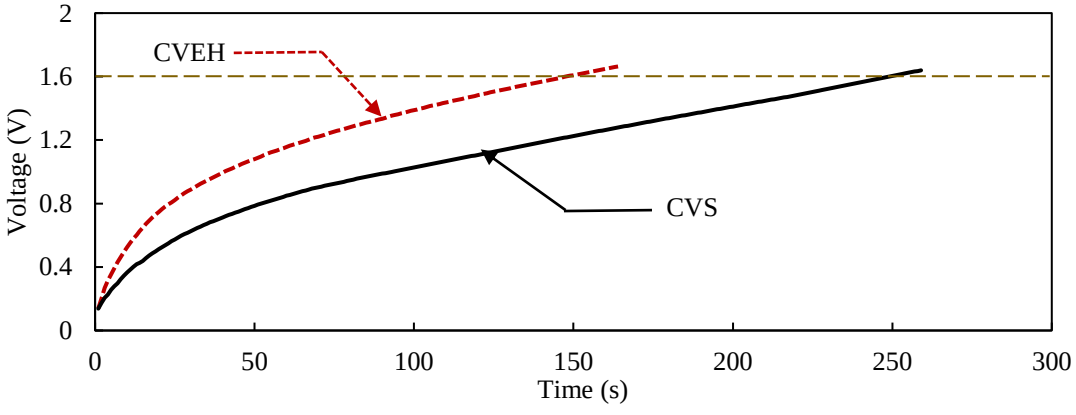

(b)

Figure 9: (a) Charging curve of the capacitor, average acceleration of the beam is 4.9 m/s^2
(b) Charging curve of the capacitor, average acceleration of the beam is 8.8 m/s^2

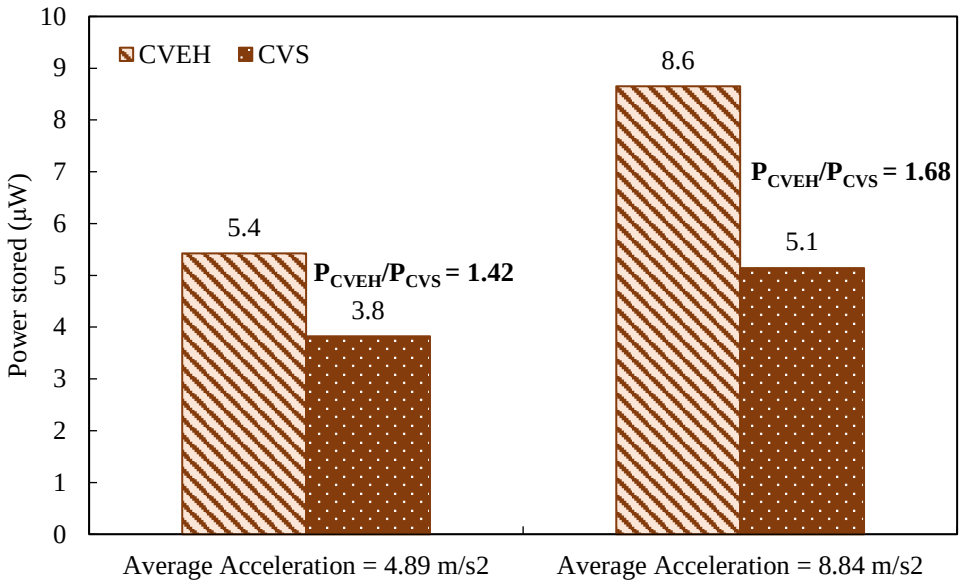

Figure 10: Histogram of average power stored in the capacitors

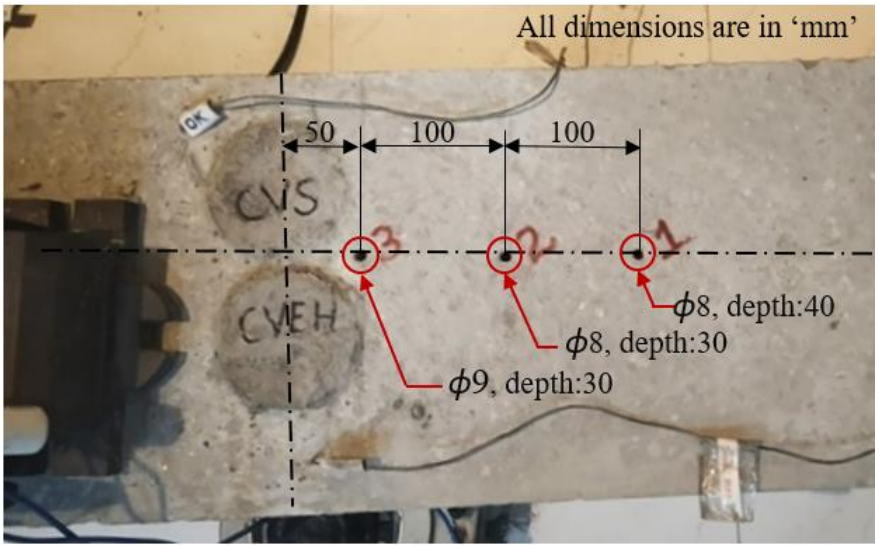

Figure 11: Damages induced in the RC beam

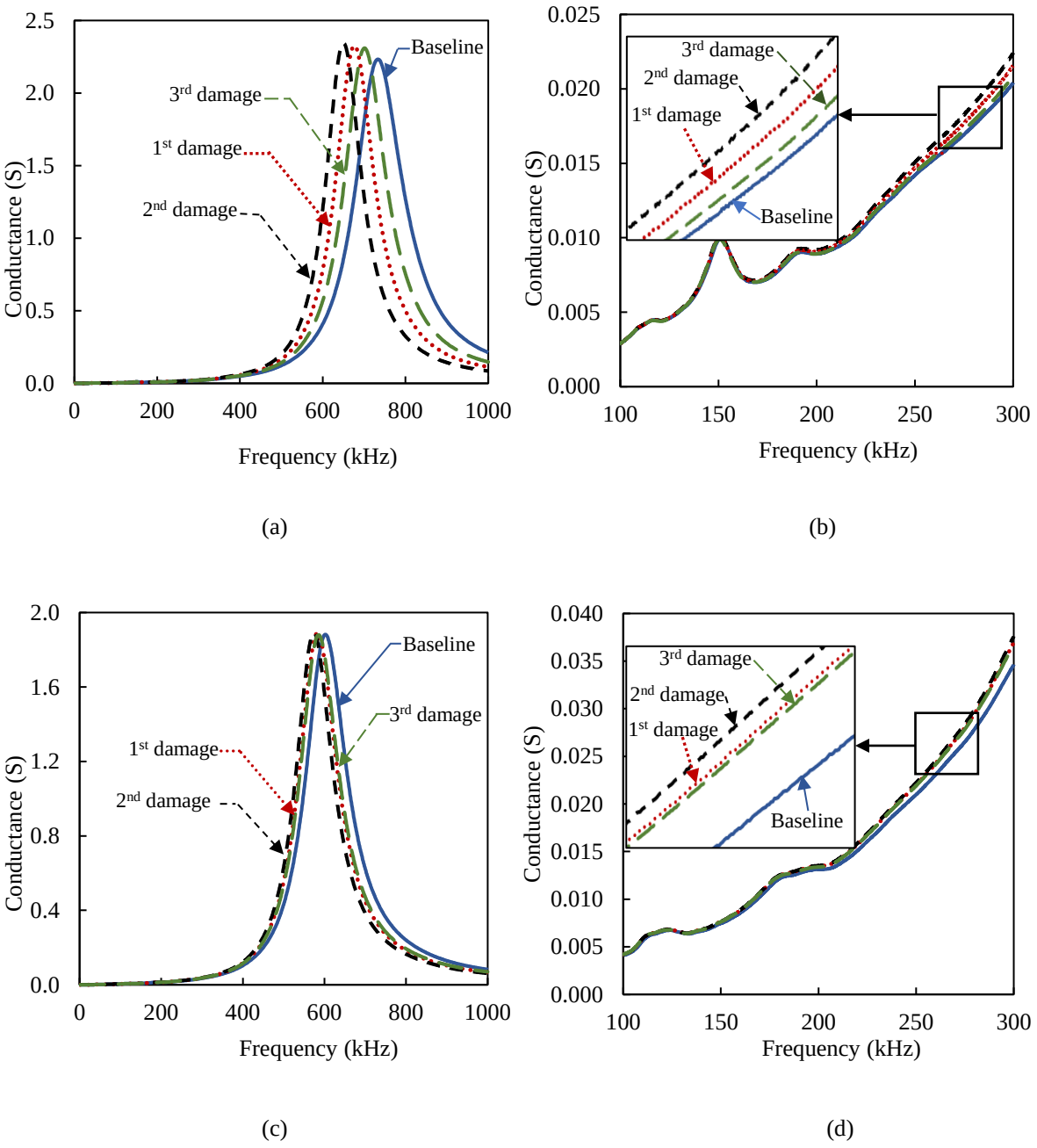

Figure 12: (a) Conductance signature of CVEH for a frequency range of 1 kHz to 1000 kHz
(b) Conductance signature of CVEH for a frequency range of 100 kHz to 300 kHz
(c) Conductance signature of CVS for a frequency range of 1 kHz to 1000 kHz
(d) Conductance signature of CVS for a frequency range of 100 kHz to 300 kHz

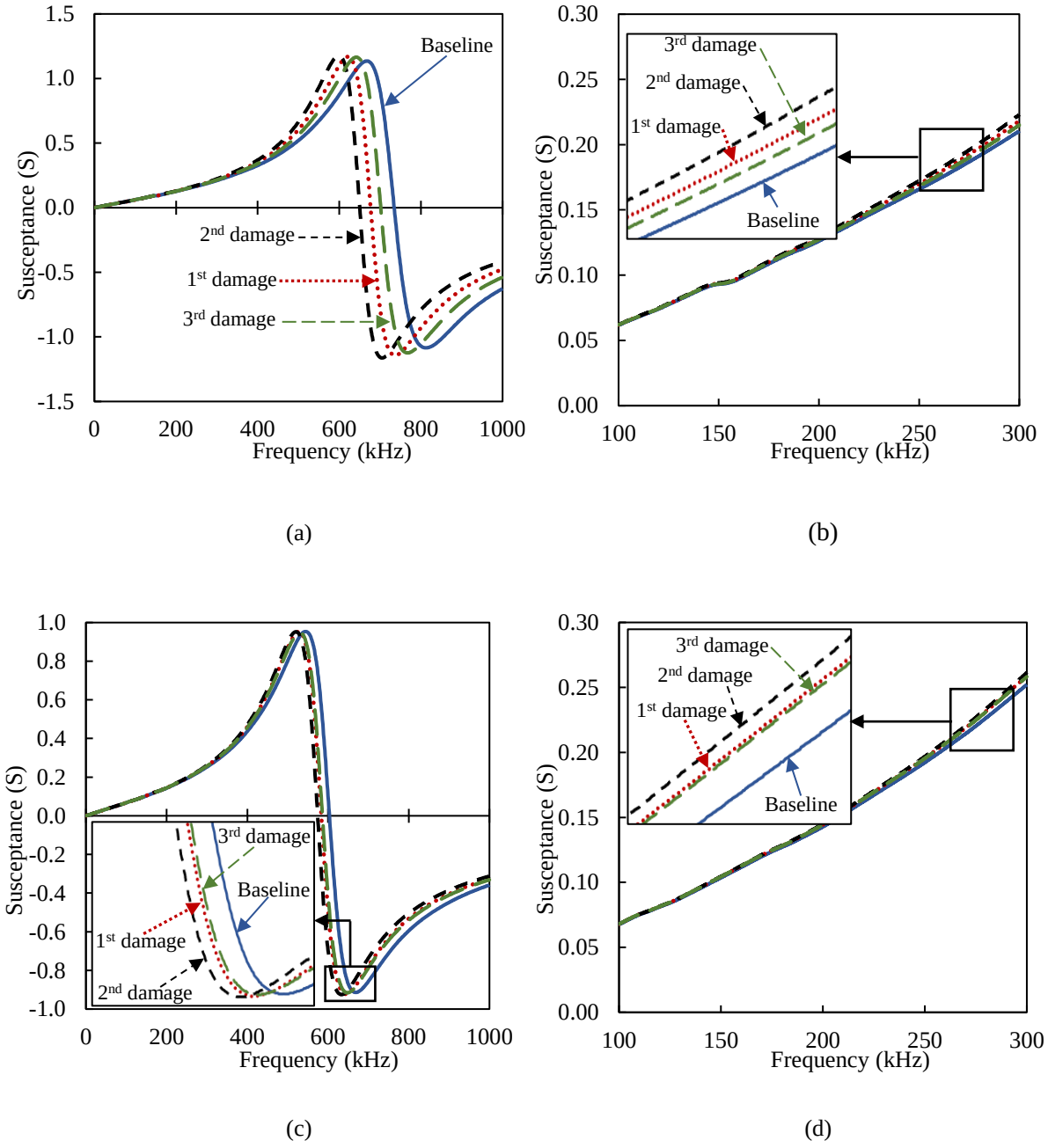

Figure 13: (a) Susceptance signature of CVEH for a frequency range of 1 kHz to 1000 kHz
(b) Susceptance signature of CVEH for a frequency range of 100 kHz to 300 kHz
(c) Susceptance signature of CVS for a frequency range of 1 kHz to 1000 kHz
(d) Susceptance signature of CVS for a frequency range of 100 kHz to 300 kHz

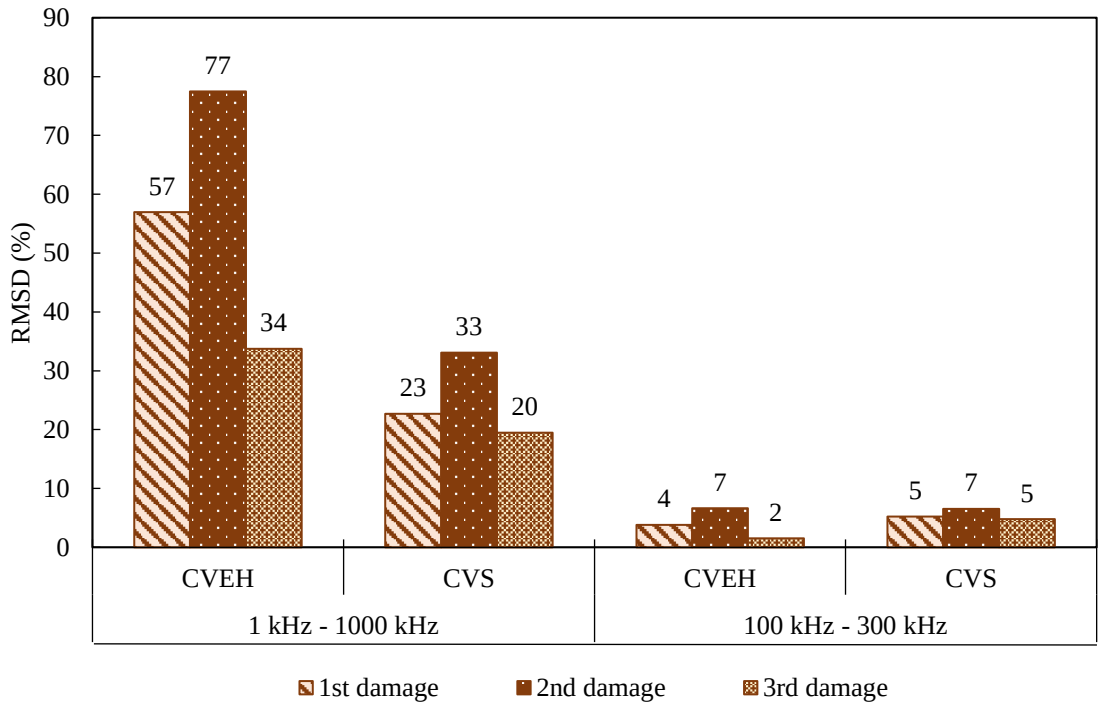

(a)

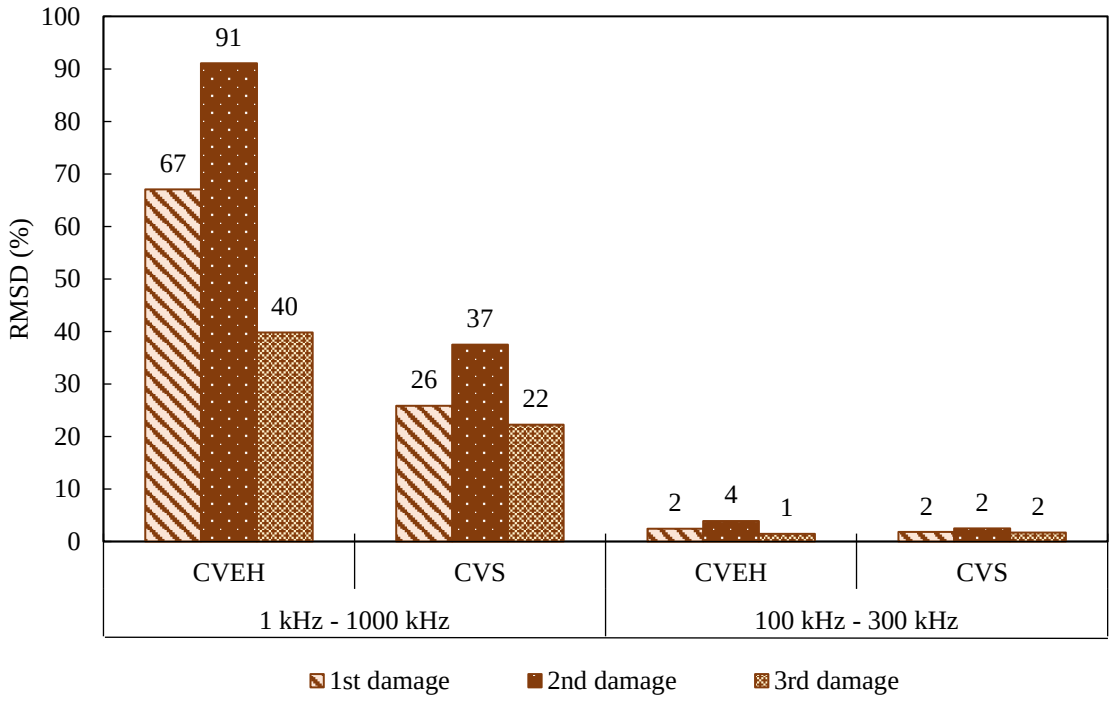

(b)

Figure 14: (a) RMSD index of conductance signatures
(b) RMSD index of susceptance signatures

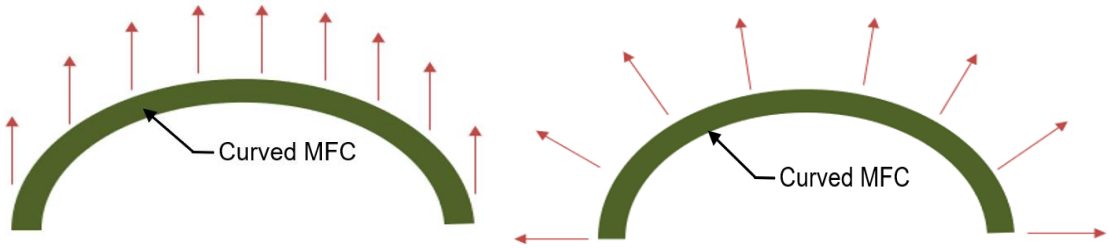

Figure 15: (a) Direction of polarisation considered in COMSOL 4.4 FE software
(b) Actual direction of polarisation

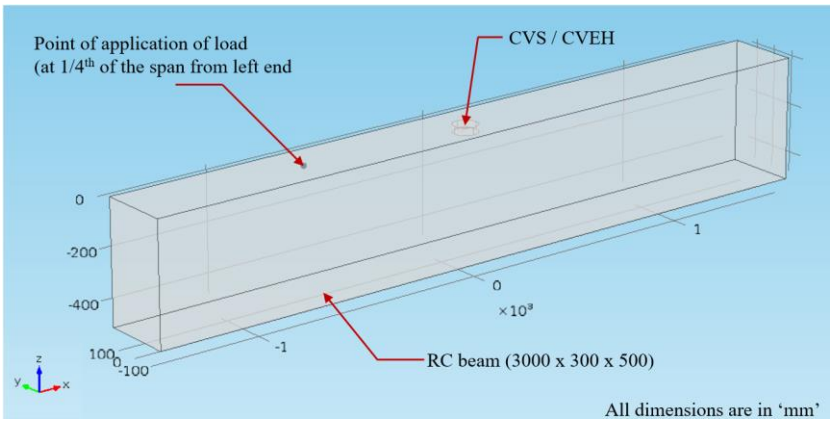

(a)

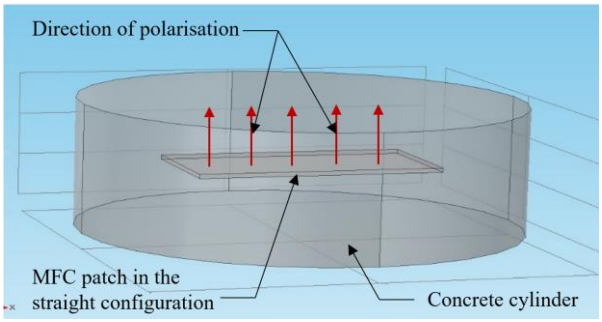

(b)

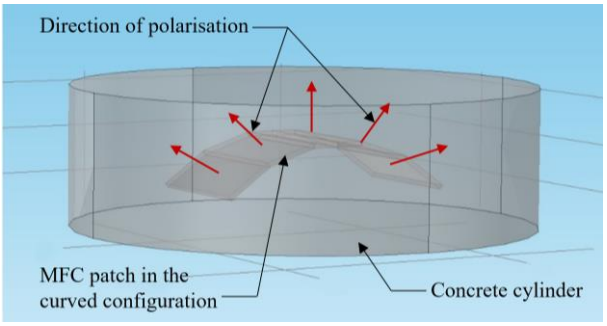

(c)

Figure 16: (a) Isometric view of the RC beam embedded with CVEH
(b) CVS model in COMSOL 4.4 FE software
(c) CVEH model in COMSOL 4.4 FE software

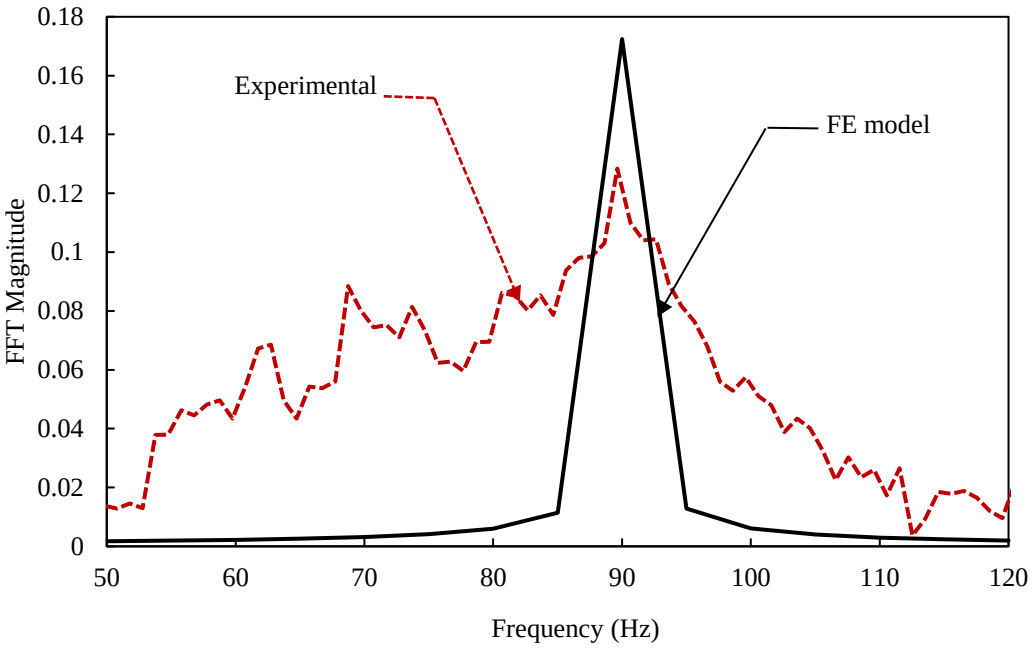

Figure 17: Impact hammer test results of experimental and FE analysis

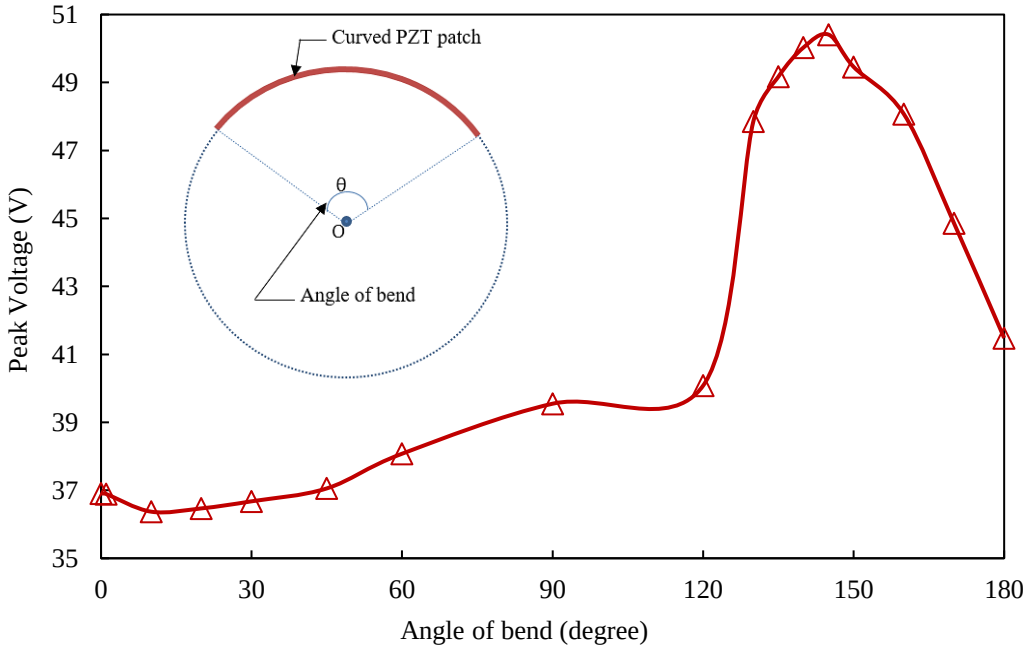

Figure 18: Variation of peak voltage with respect to the angle of bend

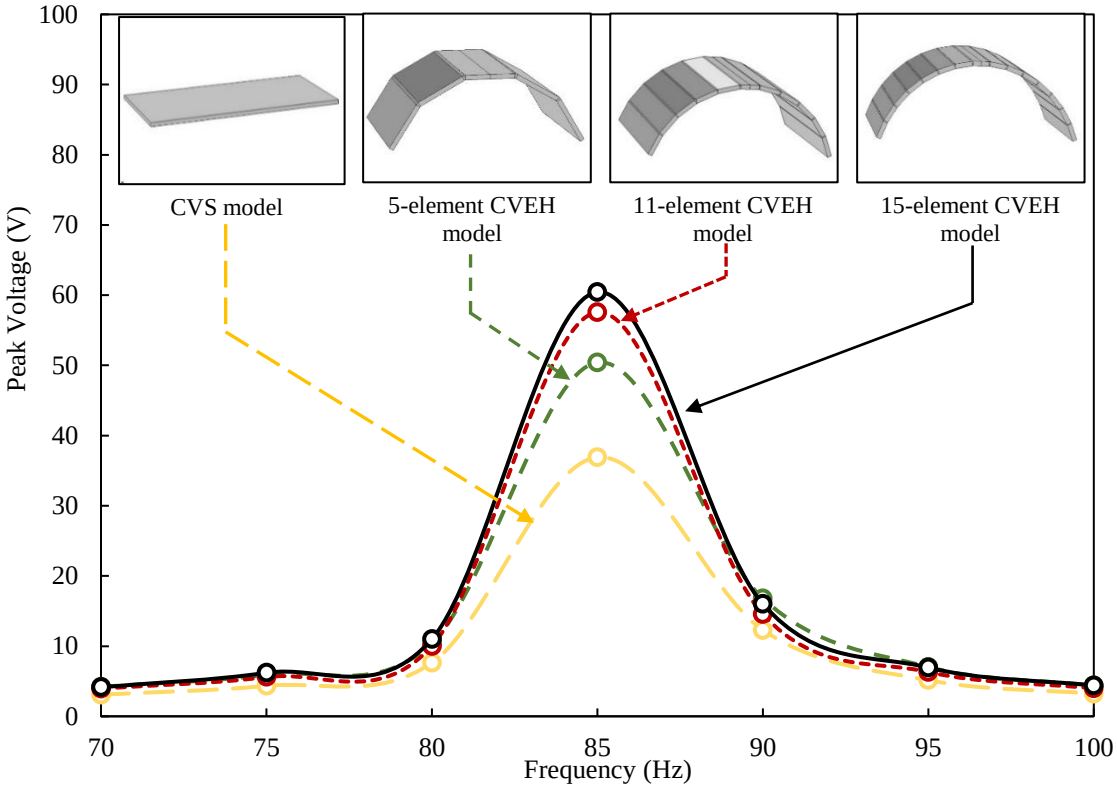

Figure 19: Voltage comparison of CVS, 5-element, 11-element and 15-element model of the curved piezo transducer (θ =145 degree)

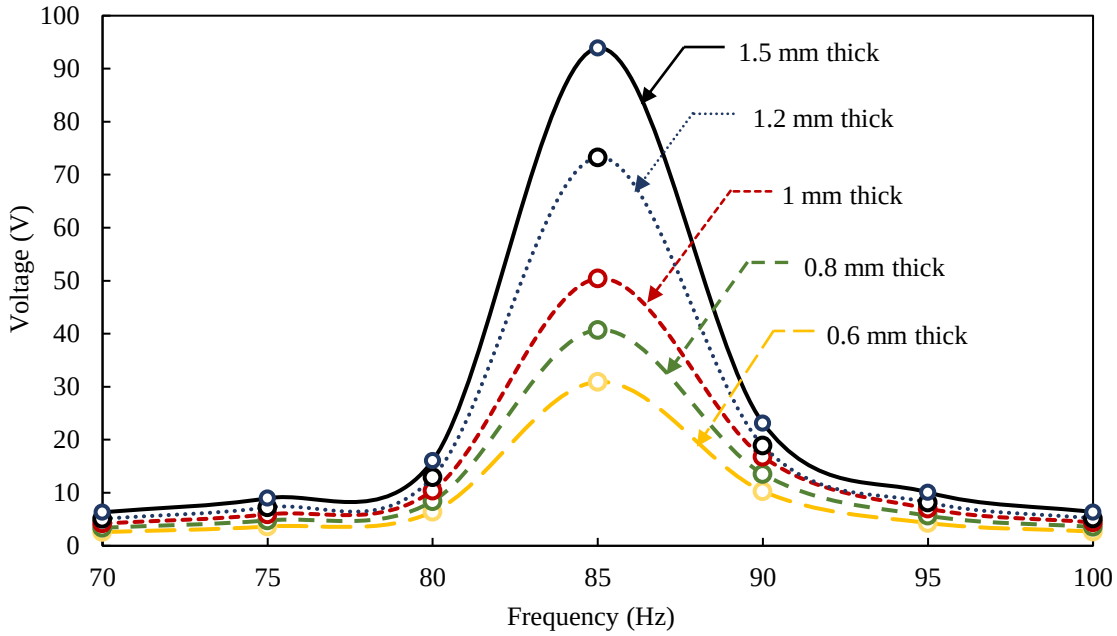

Figure 20: Voltage vs frequency plot for various thicknesses of the piezo transducer (θ =145 degree)

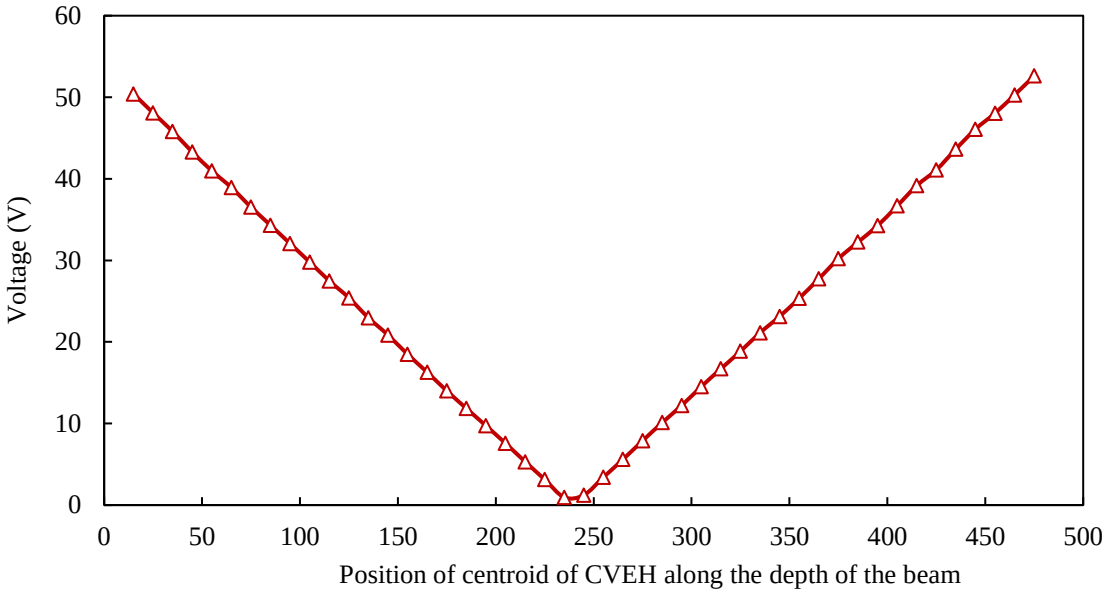

Figure 21: Variation of voltage generated for various positions of CVEH along the depth of the beam

Table 1: Properties of RC beam and piezo transducer considered for the study (Kaur, 2015 and Smart Materials, 2021)

Parameters	Beam	Piezo Transducer	Unit
Size (Plan)	3000 × 300	56 × 28	mm^2
Depth or Thickness	500	1	mm
Density	2500	5440	kg/m^3
Young's Modulus	27.3		$(\times 10^9)$ Pa
Poisson's ratio	0.3	0.3	
Compliance matrix	-	$\begin{matrix} 15 & -4.5 & -5.7 & 0 & 0 & 0 \\ 0 & 19 & -5.7 & 0 & 0 & 0 \\ 0 & 0 & 19 & 0 & 0 & 0 \\ 0 & 0 & 0 & 39 & 0 & 0 \\ 0 & 0 & 0 & 0 & 39 & 0 \\ 0 & 0 & 0 & 0 & 0 & 49.4 \end{matrix}$	$(\times 10^{-12})$ Pa^{-1}
Coupling matrix or piezoelectric strain coefficients	-	$\begin{matrix} 0 & 0 & 0 & 0 & 0 & 0 \\ 0 & 0 & 0 & 0 & 0 & 0 \\ 2.1 & 2.1 & 0 & 0 & 0 & 0 \end{matrix}$	$(\times 10^{-10})$ C/N
Relative permittivity	-	$\begin{matrix} 1977.4 & 0 & 0 \\ 0 & 1977.4 & 0 \\ 0 & 0 & 2395.5 \end{matrix}$	-
Dielectric loss factor	-	0.02	-
Compliance Matrix loss factor	-	0.02	

ALEENA V K

vkaleena@gmail.com

PROFILE SUMMARY

- Currently pursuing ***M.Tech in Structural Engineering*** from ***IIT Delhi*** and holding the ***topmost position*** among all 2020 entry M. Tech (Structures) full-time students in the Civil Engineering Department, IIT Delhi.
- Dynamic and determined Civil Engineer with ***2 years of experience*** in the construction and management field. Proficient in ***Project Coordination, Planning and MIS***.
- Possess a great interest in the ***analysis and design of civil engineering structures***.

WORK EXPERIENCE

SENIOR ENGINEER (PLANNING DEPARTMENT)

L&T CONSTRUCTION
Erode Water Supply Project
July, 2017 – April, 2019

Responsibilities:

- In-charge of ***Management Information System (MIS)***.
- Preparation of ***Work Breakdown Structure (WBS), Project Scheduling, Monitoring*** and ***Control***.
- Involved in ***Rate Analysis, Budgeting, Estimation, Quantity Surveying, Work Order Management*** and ***Client Management***.
- Collaboratively developed the overall **Project *Procurement Strategy*** with the Planning Manager.
- Had exposure in ***QA & QC, EHS and Cluster Coordination***.

EDUCATIONAL QUALIFICATIONS

2020-2022 M.Tech., Structural Engineering
Indian Institute of Technology (IIT) Delhi, India
CGPA: 9.38 (as of 3rd semester)

2013-2017 B.Tech., Civil Engineering
National Institute of Technology (NIT) Calicut, India
CGPA: 9.05

SOFTWARE SKILLS

- AutoCAD
- COMSOL
- STAAD Pro
- MS Project
- MATLAB
- C & C++

ACADEMIC ENDEAVOURS

M.Tech Thesis: Experimental & Numerical Investigations on Efficacy of Singly Curved Thin Piezo Transducers for Energy Harvesting & Structural Health Monitoring (SHM)

Description:

- Experimental investigations were conducted to analyse the voltage, power and energy generated and harvested by the singly curved thin piezo transducers relative to their straight configuration. The research also analysed their efficacy for the first time in the field of ***SHM*** by the method of ***Electro-Mechanical Impedance (EMI)*** technique.
- 3D modelling and ***finite element analysis (FEA)*** of the curved piezo transducers were performed to analyse the influence of various parameters such as its thickness, curvature, the position of placement etc for ***energy harvesting***.

B.Tech Thesis: Precipitation Downscaling Using Hybrid Wavelet Neural Network Models

Description:

- An ***Artificial Neural Network (ANN)*** model and ***Hybrid Wavelet ANN*** model were developed and trained to predict the monthly precipitation and their performance was compared.
- Using the better network, the monthly precipitation of Chaliyar river basin was projected by the method of ***Statistical Downscaling***.

INTERNSHIP DETAILS

DMRC, Kochi unit

- Familiarized with the methodology and technology used in ***Heavy Civil Engineering*** and various stages of ***Metro Rail*** construction at Kochi.

ACHIEVEMENTS

- Secured ***first prize*** in the ***Cost-Effective House Design*** competition conducted in NIT Calicut in the year 2017.
- One of the ***top five students (Rank 4)*** of the Civil Engineering Department of NIT Calicut based on academic performance in the year 2017.
- One among the ***top 1%*** students of Kerala based on the Higher Secondary Examination conducted by the Kerala State Board in the year 2013.
- Actively participated in various dance, drama and literary competitions held at the school, district and state levels.